Hepatic miR-20b promotes nonalcoholic fatty liver disease by suppressing PPARα

Yo Han Lee[1,5], Hyun-Jun Jang[1,5], Sounkou Kim[1,5], Sun Sil Choi[1], Keon Woo Khim[1], Hye-Jin Eom[1], Jimin Hyun[1], Kyeong Jin Shin[1], Young Chan Chae[1], Hongtae Kim[1], Jiyoung Park[1], Neung Hwa Park[2], Chang-Yun Woo[3], Chung Hwan Hong[4], Eun Hee Koh[3], Dougu Nam[1,*], Jang Hyun Choi[1,*]

[1]Department of Biological Sciences, Ulsan National Institute of Science and Technology (UNIST), Ulsan, 44919, Republic of Korea

[2]Department of Internal Medicine, University of Ulsan College of Medicine, Ulsan University Hospital, Ulsan, 44033, Republic of Korea

[3]Department of Internal Medicine, Asan Medical Center, University of Ulsan College of Medicine, Seoul, 05505, Republic of Korea

[4]Department of Medical Science, Asan Medical Center, University of Ulsan College of Medicine, Seoul, 05505, Republic of Korea.

[5]These authors contributed equally to this work.

[*]**Corresponding Author**

Dougu Nam, Department of Biological Sciences, Ulsan National Institute of Science and Technology (UNIST), Ulsan, Republic of Korea. Tel.: +82 52 217 2525; Fax: +82 52 217 2639

E-mail: dougnam@unist.ac.kr (D. Nam)

Jang Hyun Choi, Department of Biological Sciences, Ulsan National Institute of Science and Technology (UNIST), Ulsan, Republic of Korea. Tel.: +82 52 217 2543; Fax: +82 52 217 3219

E-mail: janghchoi@unist.ac.kr (J.H. Choi)

Abstract

Background:

Non-alcoholic fatty liver disease (NAFLD) is associated with hepatic metabolic reprogramming that leads to excessive lipid accumulation and imbalances in lipid metabolism in the liver. Although nuclear receptors (NRs) play a crucial role in hepatic metabolic reprogramming, the underlying mechanisms of NR regulation in NAFLD remain largely unclear.

Methods:

Using network analysis and RNA-seq to determine the correlation between NRs and microRNA in NAFLD patients, we revealed that miR-20b specifically targets PPARα. miR-20b mimic and anti-miR-20b were administered to hepatocytes as well as high fat diet (HFD)- or methionine-deficient diet (MCD)-fed mice to verify the specific function of miR-20b in NAFLD. We tested the inhibition of the therapeutic effect of a PPARα agonist, fenofibrate, by miR-20b.

Results:

We revealed that miR-20b specifically targets PPARα through miRNA regulatory network analysis of nuclear receptor genes in NAFLD. The expression of miR-20b was upregulated in free fatty acid (FA)-treated hepatocytes and the livers of both obesity-induced mice and NAFLD patients. Overexpression of miR-20b significantly increased hepatic lipid accumulation and triglyceride levels. Furthermore, miR-20b significantly reduced FA oxidation and mitochondrial biogenesis by targeting PPARα. In miR-20b-introduced mice, the effect of fenofibrate to ameliorate hepatic steatosis was significantly suppressed. Finally, inhibition of miR-20b significantly increased FA oxidation and uptake, resulting in improved insulin sensitivity and a decrease in NAFLD progression.

Conclusions:

Taken together, our results demonstrate that the novel miR-20b targets PPARα, plays a significant role in hepatic lipid metabolism, and present an opportunity for the development of novel therapeutics for NAFLD.

Funding:

This research was funded by Korea Mouse Phenotyping Project (2016M3A9D5A01952411), the National Research Foundation of Korea (NRF) grant funded by the Korea government (2020R1F1A1061267, 2018R1A5A1024340), the Future-leading Project Research Fund (1.210034.01) of UNIST and the National Research Foundation of Korea (NRF) grant funded by the Korea government (2020R1I1A1A01074940).

Introduction

Obesity has emerged as a host of metabolic disorders, such as non-alcoholic fatty liver disease (NAFLD). Many reports have demonstrated that 90% of obese patients in the United States have NAFLD ranging from hepatic steatosis to much more severe forms of non-alcoholic steatohepatitis (NASH), which can induce fibrosis, cirrhosis, and hepatocellular carcinoma (HCC)(Corey & Kaplan, 2014). NAFLD is associated with hepatic metabolic reprogramming that leads to excessive lipid accumulation and imbalances in lipid metabolism in the liver(de Alwis & Day, 2008). Hepatic lipid homeostasis is appropriately described as a complex machinery involving signaling and transcriptional pathways, as well as targeted genes associated with fatty acid (FA) oxidation and lipogenesis(Fabbrini, Sullivan, & Klein, 2010). Although the pathogenesis of NAFLD has been widely studied for years, the molecular mechanisms underlying its complicated disorder are still being investigated.

Nuclear receptors (NRs) are a superfamily of ligand-activated transcription factors that regulate biological homeostasis(McKenna et al., 2009). Recent evidence suggests that NRs are key regulators in the progression of diverse hepatic diseases associated with glucose and lipid metabolism, inflammation, bile acid homeostasis, fibrosis, and cancer development in the liver(Lopez-Velazquez, Carrillo-Cordova, Chavez-Tapia, Uribe, & Mendez-Sanchez, 2012). Among them, growing evidence suggests a link between PPARα and obesity-induced NAFLD. Hepatic PPARα plays an important role in energy homeostasis by regulating the expression of genes required for FA uptake, FA oxidation, and triglyceride (TG) hydrolysis in the liver(Chakravarthy et al., 2005). The decreased expression of PPARα is significantly associated with severity in NAFLD patients(Francque et al., 2015). Therefore, understanding the molecular mechanism underlying PPARα regulation is critical for understanding the pathogenesis of NAFLD.

MicroRNAs (miRNAs) are short, non-coding RNA molecules with a length of 18-25 nucleotides that play an important role in regulating the expression of target genes in a post-transcriptional manner by targeting base-pairing with the 3'-UTR of specific target mRNAs, inhibiting translation, or mRNA degradation(Bartel, 2004). These miRNAs contribute to the regulation of a wide variety of cellular functions and metabolic homeostasis, including fatty acid metabolism. Recent studies have suggested that miRNAs significantly regulate the pathogenesis of NAFLD by targeting the nuclear receptors(Lopez-Sanchez, Dominguez-Perez, Uribe, Chavez-Tapia, & Nuno-Lambarri, 2021). Previous report has demonstrated that miR-20b, a member of the miR-17 family, presents in the circulating plasma of NAFLD patients and has been highlighted as a novel biomarker of NAFLD and type 2 diabetes mellitus (T2DM) for the diagnosis and risk estimation of NAFLD(Ye et al., 2018). However, the mechanisms underlying the involvement of miR-20b in the occurrence and progression of NAFLD remain unknown. In this study, we analyzed the regulatory networks of miRNAs for NR genes and RNA-seq data in NAFLD patients, which prioritized miR-20b as a key regulator of NAFLD. miR-20b suppressed FA β-oxidation and FA uptake, which led to the regulation of mitochondrial biogenesis in both liver cells and tissues by targeting PPARα. Furthermore, we confirmed that the inhibition of miR-20b ameliorates NAFLD progression. These results suggest that miR-20b plays a critical role in regulating lipid metabolism in the liver and may provide a promising target for therapeutic strategies in the development of NAFLD.

Results

miR-20b significantly increases in the livers of dietary obese mice and human.

We constructed a regulatory network of NRs that were differentially expressed in NAFLD patients(Hoang et al., 2019) and microRNA targeting NRs based on miRNA target prediction(Agarwal, Bell, Nam, & Bartel, 2015), to identify the correlation between NR and microRNA in the development of NAFLD. As shown in Figure 1A, the top ten miRNAs were found to be highly correlated with the modulation of NR expression in NAFLD. To further prioritize key miRNAs, we assessed the expression levels of miRNAs in NAFLD patients compared to those in normal individuals using public GSE data (GSE40744). Among the selected miRNAs, miR-20b expression was predominantly increased in NAFLD patients compared to that in normal individuals (adjusted *p*-value = 0.008) (Figure 1B). Next, to validate the importance of miR-20b in NAFLD, we assessed the expression of

miR-20b in histological NASH, simple steatosis, and normal patient samples (Figure 1C, Figure 1-figure supplement 1). The expression of miR-20b was significantly increased in simple steatosis and NASH compared to that in normal individuals, and the extent of increase in NASH was higher than that in simple steatosis.

miR-20b expression was increased in both oleic acid (OA)-treated HepG2 and Huh-7 cells (Figure 1D, E). Moreover, the expression of miR-20b was significantly upregulated in the fatty livers of high-fat diet (HFD)-fed mice, *ob/ob* mice, and methionine-deficient diet (MCD)-fed mice compared to that in the liver of normal chow diet (NCD)-fed wild mice (Figure 1F-H). Together, our results indicate that miR-20b expression is increased in NAFLD and is highly associated with the regulation of NRs in NAFLD.

PPARα is a direct target of miR-20b.

Next, we characterized the physiological roles of miR-20b in NAFLD. Oil Red O staining showed that miR-20b expression increased intracellular lipid content, and this lipid accumulation was increased with OA treatment in HepG2 cells (Figure 2A). As expected, overexpression of miR-20b significantly upregulated TG content and cholesterol in OA-treated HepG2 cells (Figure 2B, C). To further investigate the functions and targets of miR-20b, HepG2 cells were transfected with miR-20b and two separate RNA-Seq libraries of non-targeting control (miR-NC) and forced miR-20b expression (miR-20b) were constructed. The six RNA-seq samples were clearly separated between the forced miR-20b expression and control conditions, implying a significant impact on gene expression in HepG2 cells (Figure 2D, Figure 2-figure supplement 1A). The NR metapathway was detected as the most significant pathways (adjusted *p*-value = 2.47-E8) by the gene-set enrichment analysis (GSEA) (Subramanian et al., 2005), indicating that NRs and related genes are the major targets of miR-20b (Figure 2E, F). The heatmap of RNA-seq data for the NR transcription pathway is shown in Figure 2G. Five NRs (*PPARA*, *RORA*, *RORC*, *THRB,* and *NRBP1*) were downregulated (adjusted *p*-value ≤ 0.05), and *PPARA* was the most significantly downregulated NR (adjusted *p*-value = 3.25-E5). Furthermore, GSEA showed that PPARA pathways and PPAR signaling pathways were significantly decreased in miR-20b overexpressed cells (Figure 2-figure supplement 1B, C). We validated the expression of these NRs and the *PPARA*, *RORC*, *THRB*, and *NRBP1* expression was

decreased by miR-20b in human liver cells and mouse primary hepatocytes. Consistent with the RNA-seq data, the expression change of *PPARA* at both the protein and mRNA levels with miR-20b transfection was the most distinct compared to the control (Figure 2H, I). Moreover, among candidate targets, only *PPARA* was selected as an overlapped predicted target of miR-20b between various miRNA target prediction programs, including miRDB, picTAR, TargetSCAN, and miRmap (Figure 2J, Figure 2-figure supplement 2). Notably, the 3'-UTR of *PPARA* mRNA includes miR-20b binding sites that are well conserved between humans and mice, suggesting that miR-20b may have a direct inhibitory effect on PPARα expression (Figure 2K). Using a luciferase reporter construct including the 3'-UTR of *PPARA*, we revealed that miR-20b suppressed the luciferase activity in both HepG2 and Huh-7 cells in a dose-dependent manner. Furthermore, we built the mutant construct of the predicted miR-20b binding sites within the 3'-UTR of *PPARA*; the inhibitory effect of miR-20b on luciferase activity was completely blunted (Figure 2L, M). Taken together, these results indicate that miR-20b inhibits the expression of PPARα by interacting with its 3'-UTR.

miR-20b regulates fatty acid metabolism.

Since PPARα, the target of miR-20b, is a master regulator of lipid metabolism such as FA utilization and oxidation, and decreased in diverse diet-induced NAFLD conditions (Figure 3-figure supplement 1), we investigated the effects of miR-20b on lipid metabolism to reveal the functional contribution of increased miR-20b to NAFLD. The mRNA levels of genes involved in FA β-oxidation and FA uptake, including *CPT1A, ACOX1, CD36,* and *FABP1*, were decreased by overexpression of miR-20b compared to the control in HepG2 cells and primary hepatocytes (Figure 3A-C and Figure 3-figure supplement 2A-F), whereas the genes associated with lipogenesis and ketogenesis were not affected by miR-20b (Figure 3D, Figure 3-figure supplement 2G and Figure 3-figure supplement 3A,B). miR-20b overexpressed HepG2 cells showed reduced levels of palmitoyl-carnitine, a substrate of β-oxidation, and acetyl-CoA, a product of β-oxidation. Subsequently, TCA cycle intermediate levels, including citrate and succinate, also decreased (Figure 3E).

Enforced expression of miR-20b in HepG2 cells under both basal and OA treatments decreased the expression of *PPARGC1A* and *SIRT1*, which are involved in mitochondrial biogenesis (Figure 3F). The copy number of two mtDNA genes, *VIPR1* and *MT-ATP6*, was decreased by miR-20b overexpression following OA treatment (Figure 3G). Consistently, mitochondrial function that was

analyzed *via* OCR (oxygen consumption rate) was reduced by miR-20b under both basal and OA treatment conditions compared to the control (Figure 3H). In particular, the basal respiration and maximal respiratory capacity were significantly suppressed by miR-20b (Figure 3I). Furthermore, the level of ATP production, FA uptake, and FA oxidation was reduced in miR-20b overexpressed cells compared with that in the control under both basal and OA-treated conditions (Figure 3J-L).

To further clarify the role of miR-20b in hepatic steatosis, miR-20b inhibitor (anti-miR-20b), which silences miR-20b, was delivered into HepG2 cells and primary hepatocytes with OA treatment (Figure 3M, Figure 3-figure supplement 4G). Oil red O staining showed that anti-miR-20b remarkably decreased intracellular lipid accumulation upon OA treatment (Figure 3-figure supplement 4G A, *D*). As expected, miR-20b inhibition reduced the levels of TG and cholesterol both under basal and OA conditions compared to the control (Figure 3-figure supplement 4G B, C, E, and F). Lipid consumption-associated genes, not lipogenic genes, were significantly upregulated in miR-20b inhibited HepG2 cells and primary hepatocytes compared to those in the control under both basal and OA conditions (Figure 3N-P and Figure 3-figure supplement 4H-J). Inhibition of miR-20b increased the levels of palmitoyl-carnitine, acetyl-CoA, and TCA cycle intermediates (Figure 3Q), whereas ketogenesis was not affected (Figure 3-figure supplement 4C and D). Furthermore, the expression of mitochondrial biogenesis genes (Figure 3R) and the copy number of mitochondrial DNA genes were increased in both basal and OA conditions (Figure 3S). Consequently, anti-miR-20b treatment significantly upregulated the mitochondrial activity, FA uptake, and FA oxidation (Figure 3T-X). Taken together, these results demonstrated that miR-20b contributes to hepatic steatosis by controlling lipid oxidation and mitochondrial function through changes in gene expression, further contributing to the progression of NAFLD.

miR-20b promotes hepatic steatosis in HFD-fed mice

To confirm the *in vivo* roles of miR-20b in obesity model mice, we introduced miR-20b using an adenovirus-associated vector (AAV), referred to as AAV-miR-20b, into C57BL/6 mice that had been fed a normal chow diet (NCD) or a high-fat diet (HFD). Administration of AAV-miR-20b led to high expression levels of miR-20b in the livers of NCD- and HFD-fed mice compared to AAV-Control injection (Figure 4A). However, the expression level of miR-20b was not changed in peripheral tissues

including white and brown adipose tissues except in muscle (Katayama et al., 2019) (Figure 4-figure supplement 1). Consequently, AAV-miR-20b injected mice exhibited a reduction in the PPARα protein levels compared with AAV-Control injected mice on both NCD and HFD (Figure 4B).

Alterations in body weight were not detected in NCD-fed mice after AAV-miR-20b administration; however, AAV-miR-20b led to a significant increase in the body weight of HFD-induced obese mice (Figure 4C). The ratio of fat mass to body weight in AAV-miR-20b administration HFD-fed mice was higher than that in AAV-Control treated mice (Figure 4D and Figure 4-figure supplement 2); however, the ratio of lean mass to body weight showed no significant differences (Figure 4E). Consistently, AAV-miR-20b administration increased liver weight and steatosis in HFD-fed mice (Figure 4F, G). The hepatic TG level, serum activities of aspartate aminotransferase (AST) and alanine aminotransferase (ALT), markers of liver injury, were significantly increased with AAV-miR-20b administration compared with AAV-Control administration in HFD-fed mice (Figure 4H-J).

Additionally, we observed that delivery of AAV-miR-20b to HFD-fed mice significantly impaired glucose tolerance and insulin sensitivity compared to the AAV-Control (Figure 4K, L). Fasting glucose, insulin, and homeostasis model assessment of insulin resistance (HOMA-IR) levels were also increased in AAV-miR-20b administrated HFD-fed mice (Figure 4M-O). We observed that genes involved in FA β-oxidation and FA uptake pathways were downregulated by AAV-miR-20b compared to AAV-Control in both NCD- and HFD-fed mice, whereas lipogenesis genes were not altered in AAV-miR-20b administrated mice (Figure 4P-R). These results suggest that miR-20b could aggravate NAFLD by dysregulating lipid metabolism in a HFD-induced obesity model.

Inhibition of miR-20b alleviates hepatic steatosis in HFD-fed mice.

Next, we introduced anti-miR-20b into HFD-fed mice. Administration of AAV-anti-miR-20b led to decrease of miR-20b in the livers of NCD- and HFD-fed mice compared to AAV-Control injection (Figure 5A). AAV-anti-miR-20b significantly increased PPARα expression in the livers of both NCD- and HFD-fed mice (Figure 5B). Administration of AAV-anti-miR-20b in HFD-fed mice reduced the body weight compared to that of AAV-Control administrated mice (Figure 5C). We further determined that alterations in body weight were highly associated with fat mass loss (Figure 5D and Figure 5-figure supplement 1). While the ratio of lean mass to body weight of AAV-anti-miR-20b administrated HFD-fed mice was increased, the lean mass was comparable to that of the control (Figure 5E). We

next observed that AAV-anti-miR-20b administration reduced liver weight and hepatic steatosis in HFD-fed mice than in AAV-Control mice (Figure 5F). H&E and Oil Red O staining demonstrated that delivery of AAV-anti-miR-20b significantly attenuated the size and number of lipid droplets in the liver compared to AAV-Control administration in HFD-fed mice (Figure 5G). In accordance with histological changes, metabolic parameters were reduced in AAV-anti-miR-20b administrated mice compared with the AAV-Control administrated mice (Figure 5H-J). Furthermore, AAV-anti-miR-20b significantly improved glucose tolerance (Figure 5K) and insulin sensitivity (Figure 5L) compared to the AAV-Control in HFD-fed mice. Consistently, we determined that both fasting glucose and fasting insulin levels were decreased by AAV-anti-miR-20b (Figure 5M-O). Delivery of AAV-anti-miR-20b increased the expression of genes associated with FA β-oxidation and FA uptake compared with the administration of AAV-Control (Figure 5P-R). Together, these results suggest that suppression of miR-20b could ameliorate NAFLD by recovering lipid metabolism in a HFD-induced obesity model.

The effects of miR-20b are mediated by PPARα.

Next, we confirmed that the regulation of FA β-oxidation and mitochondrial function by miR-20b is primarily mediated through the reduction of PPARα. Transfection of miR-20b into HepG2 cells reduced the expression and activity of PPARα, but co-transfected PPARα expression vector restored them (Figure 6A, B). Furthermore, the decreased expression of genes involved in lipid metabolism, such as FA β-oxidation and FA uptake by miR-20b, was significantly restored by the forced expression of PPARα (Figure 6C-E). Next, we tested whether the effect of anti-miR-20b was inhibited by the suppression of PPARα. The increased expression and activity of PPARα by anti-miR-20b was reduced by siRNA targeting PPARα (siPPARA) (Figure 6F, G). The increased expression of genes by anti-miR-20b was also suppressed by siPPARA (Figure 6H-J). In addition, fenofibrate, a PPARα agonist, increased the expression of PPARα and its transcriptional activity in HepG2 cells transfected with miR-20b, but could not restore as much on its own effects (Figure 6K, L). Interestingly, fenofibrate treatment increased the expression of genes involved in FA β-oxidation and FA uptake which are regulated by PPARα, but could not overcome the inhibitory effect of miR-20b (Figure 6M-O). Taken together, these results indicate that the contribution of miR-20b to hepatic steatosis is mediated by direct inhibition of PPARα and is important for the treatment of NAFLD.

The effects of fenofibrate are limited in miR-20b-introduced mice.

Next, we tested whether NAFLD treatment with fenofibrate was affected by miR-20b expression *in vivo*. Administration of AAV-miR-20b led to elevated hepatic levels of miR-20b compared to AAV-Control injection in HFD-fed mice, and the level was slightly decreased by fenofibrate treatment (Figure 7A). Interestingly, we observed that administration of AAV-Control with fenofibrate increased the level of PPARα; however, fenofibrate could not restore the reduced PPARα expression by AAV-miR-20b (Figure 7B). Administration of fenofibrate reduced the body and liver weights of AAV-Control injected mice; however, AAV-miR-20b injected mice exhibited no significant differences by fenofibrate (Figure 7C, F). The ratio of fat to body weight also displayed no alterations between AAV-miR-20b and AAV-miR-20b with fenofibrate (Figure 7D). While the ratio of lean mass to body weight was increased by fenofibrate in AAV-miR-20b injected mice, the lean mass was comparable (Figure 7E). H&E staining, Oil Red O staining, and hepatic TG levels demonstrated that fenofibrate significantly attenuated lipid accumulation in the liver of HFD-fed mice, but the effect of fenofibrate was suppressed by AAV-miR-20b (Figure 7G, H). Serum AST and ALT levels were decreased by fenofibrate, but this benefit was did not detected in AAV-miR-20b injected mice (Figure 7I, J). We further observed that blood glucose tolerance and insulin sensitivity were improved by fenofibrate; however, AAV-miR-20b offset the improvement by fenofibrate (Figure 7K, L). Fasting glucose, fasting insulin, and HOMA-IR levels were markedly decreased by fenofibrate in HFD-fed mice (Figure 7M-O). In AAV-miR-20b injected mice, fenofibrate did not reduce fasting insulin levels, but decreased fasting glucose and HOMA-IR levels. Fenofibrate also did not restore the suppressed expression of genes regulating FA β-oxidation in AAV-miR-20b-injected mice (Figure 7P-R). Taken together, the effect of fenofibrate to ameliorate NAFLD-like symptoms was limited in AAV-miR-20b administrated HFD-fed mice because of the targeting PPARα by miR-20b.

miR-20b promotes liver inflammation and fibrosis in MCD-Fed Mice.

We further demonstrated that RNA-seq data have a significant correlation of fold change values with previously published RNA-seq data under both NASH and liver fibrosis conditions within the NR transcription(Hoang et al., 2019) (Figure 8A, B). This implies that miR-20b is able to set up an NR transcription program similar to that of NASH and liver fibrosis. To test this hypothesis, AAV-Control or AAV-anti-miR-20b was administered to C57BL/6 mice placed on a methionine/choline-deficient diet

(MCD), which is the most widely used diet to induce NAFLD/NASH. Administration of AAV-anti-miR-20b led to decrease of miR-20b in the livers of NCD- and MCD-fed mice compared to AAV-Control injection (Figure 8C). We observed that the expression of PPARα was increased in MCD-fed mice and administration of AAV-anti-miR-20b displayed an elevation of PPARα, both at the mRNA and protein levels (Figure 8D, E). We next observed that AAV-anti-miR-20b administration significantly reduced hepatic steatosis in MCD-fed mice than in AAV-Control mice (Figure 8F). Liver sections clearly showed a decrease in both lipid accumulation and fibrosis with AAV-anti-miR-20b administration in MCD-fed mice (Figure 8G). Consistently, AAV-anti-miR-20b administration decreased the levels of hepatic TG, AST, and ALT activity compared to AAV-Control injection (Figure 8H-J). Moreover, AAV-anti-miR-20b significantly reduced the expression of genes related to hepatic inflammation, including *Tnf, Ccl2, Il6,* and *Il1b* (Figure 8K), and fibrosis, including the NASH-relevant genes, such as *Acta2, Col1a1, Col3a1, Fn, Timp1*, and *Vim* (Figure 8L), in MCD-fed mice. Taken together, these results indicate that miR-20b plays an important role in the development of fibrosis, inflammation, and hepatic steatosis in NAFLD progression.

Discussion

Obesity has been widely demonstrated to be central to the pathogenesis of NAFLD. Among other peripheral tissues, the liver plays a dominant role in the regulation of lipid homeostasis(Pawlak, Lefebvre, & Staels, 2015). Although abnormal regulation of metabolic homeostasis in the liver has been recognized in diabetes and NAFLD, the underlying molecular mechanisms remain to be elucidated. Growing evidence has demonstrated that miR-20b levels are significantly upregulated in the plasma miRNA profiles of NAFLD patients(Jin et al., 2012). Moreover, plasma miR-20b levels were highly elevated in T2DM/NAFLD patients compared to those in T2DM patients(Ye et al., 2018). However, the molecular mechanism through which miR-20b regulates NAFLD progression remains unknown. In this study, we demonstrated that miR-20b promotes NAFLD progression by modulating lipid metabolism, including FA β-oxidation and FA uptake, as well as ATP production by mitochondrial biogenesis. Our data clearly showed the regulatory mechanism of PPARα by miR-20b, and miR-20b may serve as a novel biological marker in NAFLD.

A previous study demonstrated that upregulated miR-20b levels in obesity-induced metabolic disorders such as T2DM were considered to prevent several targets, such as STAT3, CD36, and

PTEN, which are involved in glucose and lipid homeostasis. The miR-20b/STAT axis, which is involved in the insulin signaling pathway, alters glycogen synthesis in human skeletal muscle cells(Katayama et al., 2019). Moreover, miR-20b directly targets PTEN involved in PI3K/Akt/mTOR signaling pathway that modulates glucose metabolism in gastric cells(Streleckiene et al., 2020). Hosui et al. (2017) proposed a model in which the fatty acid transporter CD36 is also a potential target of miR-20b, which crucially regulates hepatic lipid metabolism in STAT5 KO mice models. But, it has been reported that CD36 and FABP1 are direct PPARα target genes(Rakhshandehroo, Knoch, Muller, & Kersten, 2010). In this study, we observed that miR-20b downregulated PPARα and suppressed the expression of CD36 and FABP1. Thus, PPARα is the primary target of miR-20b in regulating hepatic lipid metabolism.

Decreased PPARα is contributed to development of NAFLD(Francque et al., 2015). A few miRNAs were reported to regulate PPARα expression in NAFLD. miR-34a targets PPARα and SIRT1, associating with FA oxidation and cholesterol synthesis. However the effect of miR-34a on inflammation and fibrosis is not clear(Ding et al., 2015). miR-21 also decreases the expression of PPARα in NASH, however, activated PPARα by miR-21 suppression reduces inflammation, liver injury, and fibrosis without improvement in FA β-oxidation and lipid accumulation(Loyer et al., 2016). In the present study, we demonstrate the novel miRNA which has different mode of action. miR-20b showed the improved effects on FA oxidation, steatosis, inflammation, and fibrosis in HFD- or MCD-fed mice. How these miRNAs targeting PPARα have different regulatory mechanisms should be further studied.

Recent reports suggest that some transcription factors regulate metabolic homeostasis by directly mediating the expression of miRNAs(Yang & Wang, 2011). E2F1, which is a member of the E2F transcription factor family, regulates myoblast differentiation and proliferation *via* the auto-regulatory feedback loop between E2F1 and miR-20b in muscle(Luo, Li, Yi, Nie, & Zhang, 2016). Both the hepatic expression and activity of E2F1 are increased during obesity. E2F1 deficiency protects against obesity- and diabetes-induced liver steatosis in mouse models(Zhang et al., 2014). Additionally, E2F1 induced chronic inflammation and hepatic lipid metabolism during NAFLD development(Denechaud et al., 2016). Consistent with these results, we observed that the expression of E2F1 was significantly increased in the fatty liver of both mice and humans, and its expression was positively correlated with that of miR-20b (Figure 9). These results suggest that E2F1 may be an

upstream regulator of miR-20b in the liver, and this upregulation of miR-20b regulates lipid metabolism in the pathogenesis of NAFLD.

NAFLD patients can develop NASH, which is characterized by hepatic steatosis complicated by chronic hepatocellular damage and severe inflammation with fibrosis, potentially developing into cirrhosis and HCC(Corey & Kaplan, 2014). This indicates that suppression of NAFLD progression is the primary option for preventing the development of HCC. Recent reports suggest that PPARα KO mice fed an MCD developed much more severe NASH than wild-type mice, and the expression of PPARα in HCC tissue was significantly lower than that in normal liver tissue(Montagner et al., 2016). PPARα activation contributes to the inhibition of HCC cell proliferation Thus, hepatic PPARα plays a crucial role in tumorigenesis in the liver(Lefebvre, Chinetti, Fruchart, & Staels, 2006). Interestingly, it has been reported that upregulated miR-20b highly regulates cancer cell proliferation and promotes proliferation of H22 hepatocellular carcinoma cells (Peng et al., 2019; Xia et al., 2020). Thus, plasma miR-20b can be a promising target in liver cancer development. Indeed, we observed that the level of miR-20b was increased in NAFLD patients, but even robustly increased in the NASH stage. Furthermore, we observed that the hepatic function of miR-20b dramatically regulates the genes involved in inflammation and fibrosis by directly repressing PPARα in MCD-fed mice. Thus, our study strongly suggested that miR-20b regulates the pathogenesis of NAFLD, but might also be relevant in the development of severe stages of liver fibrosis and even in HCC.

Our present results strongly suggest that miR-20b may be a druggable target in NAFLD patients. Fenofibrates, PPARα agonists, are widely used in clinical trials for the treatment of NAFLD patients. Administration of fenofibrate significantly increases the expression of PPARα and its activity, thereby improving NAFLD by activating FA β-oxidation and inhibiting inflammation(Valasek, Clarke, & Repa, 2007). However, chronic fenofibrate administration causes various side effects and efficiency problems. Growing evidence suggests that long-term treatment with fenofibrate induces HCC in NAFLD patients(Gonzalez & Shah, 2008). Therefore, multiple reports suggest that the combination therapy of fenofibrates with various agents is very encouraging as a more effective and safe treatment option for improving NAFLD(Athyros, Papageorgiou, Athyrou, Demitriadis, & Kontopoulos, 2002; Farnier et al., 2005). Our results suggest that administration of fenofibrate does not effectively improve lipid accumulation and lipid metabolism when miR-20b is overexpressed. Thus, these

findings suggest that targeting miR-20b may be a novel therapeutic strategy for the treatment of NAFLD.

Materials and Methods

Cell Culture

Human liver cells, HepG2 and Huh-7 cells were purchased from American Type Culture Collection (ATCC, Manassas, VA) and cultured in Dulbecco's Modified Eagle's Medium (DMEM) containing 10 % fetal bovine serum (Gibco, BRL, Grand Island, NY) and 1 % penicillin/streptomycin (ThermoFisher Scientific, Waltham, MA). miRNAs and siRNA were obtained from GenePharma (Shanghai, China). The miRNAs and siRNA used in this study are listed in the table below. HepG2 and Huh-7 cells were transfected with miRNA or siRNA using Lipofectamine^{TM} RNAiMAX transfection reagent (ThermoFisher Scientific) according to the manufacturer's instructions and following experiments were performed 48 h after transfection. For intracellular lipid accumulation, cells were cultured in a medium with the addition of 1 mmol/L sodium oleic acid for 24 h and then cells were harvested for further analysis. Images of cells stained with Oil Red O were obtained with EVOS FL (Thermo Fisher Scientific).

Name	Sequence
miR-NC	UCACAACCUCCUAGAAAGAGUAGA
miR-20b (Mimic)	CAAAGUGCUCAUAGUGCAGGUAG
anti-miR-20b (Inhibitor)	CUACCUGCACUAUGAGCACUUUG
siPPARA	CGGCGAGGATAGTTCTGGAAGCTTT

Human patients

Human liver tissue samples of 13 patients were acquired from the BioResource Center (BRC) of Asan Medical Center, Seoul, Republic of Korea. The process of 13 human tissue samples was officially approved by the Institutional Review Board of Asan Medical Center (IRB approval number: 2018-1512). Human liver tissues were obtained from 5 control individuals, 4 simple steatosis patients (fatty liver), and 4 non-alcoholic steatohepatitis (NASH) patients. Histologically normal liver, simple steatosis and NASH samples dissected adjacent to the tumor but beyond the observed aberrations are indicated as control normal liver samples, simple steatosis, and NASH samples, respectively(Aran et al., 2017). In addition, all patients diagnosed with alcoholic liver disease, viral infected hepatitis and toxic hepatitis were excluded.

411

412 **Library preparation for transcriptome sequencing**

413 RNA-seq was performed on triplicate sample from HepG2 cell with or without overexpression of
414 miR-20b. Total RNA was isolated using the RNeasy mini kit (Qiagen, Hilden, Germany) according to
415 the manufacturer's instructions. Library prep and RNA-seq were performed by Novogene (Hong
416 Kong). A total amount of 1 μg RNA per sample was used as input material for the RNA sample
417 preparations. Sequencing libraries were generated using NEBNext® UltraTM RNA Library Prep Kit for
418 Illumina® (NEB, Ipswich, MA) following manufacturer's recommendations and index codes were
419 added to attribute sequences to each sample. PCR products were purified (AMPure XP system,
420 Beckman Coulter Life Sciences, Indianapolis, IN) and library quality was assessed on the Agilent
421 Bioanalyzer 2100 system (Agilent Technologies, Inc., Santa Clara, CA). The clustering of the index-
422 coded samples was performed on a cBot Cluster Generation System using PE Cluster Kit cBot-HS
423 (Illumina, San Diego, CA) according to the manufacturer's instructions. After cluster generation, the
424 library preparations were sequenced on an Illumina platform (NovaSeq 6000 PE150) and paired-end
425 reads were generated.

426

427 **miRNA regulatory network analysis of nuclear receptor genes**

428 The RNA-seq fold change data for 16,010 genes were obtained from the Supplementary file 1 of a
429 previous work (Hoang et al., 2019). The miRNA target genes that shared evolutionarily conserved
430 binding sites for 353 miRNAs (≥ 10 genes) were downloaded from TargetScan database (Ver.7.2)
431 (Agarwal et al., 2015). We used the 50 genes that belonged to the nuclear receptor transcription
432 pathway in REACTOME database (Jassal et al., 2020) (Liberzon et al., 2015) to analyze how miRNAs
433 regulate the transcription of NR genes. Among them 17 genes were significantly downregulated in
434 NASH patients (adjusted *p*-value < 0.1). The enrichment of these downregulated NR genes in the
435 targets of the 353 miRNAs were assessed using hypergeometric distribution. The *p*-value of a miRNA
436 is given as follows:

$$p - \text{value (miRNA)} = \sum_{i=0}^{M \wedge D} \frac{\binom{D}{i}\binom{N-D}{M-i}}{\binom{N}{M}}$$

where *N* is the total number of genes analyzed, *M* is the number of candidate target genes of the miRNA, *D* is the downregulated NR genes, and *O* is the observed overlap between miRNA targets and the downregulated NR genes.

The miRNAs whose target genes were enriched in the downregulated NR genes with adjusted *p*-value $\leq$ 0.05 were used to construct the regulatory networks of the NR transcription pathway (Figure 1A).

Differential expression and gene-set enrichment analysis (GSEA)

The differential expression analysis of RNA-seq data were performed using limma package(Ritchie et al., 2015) where moderated *t*-test was applied for voom-transformed read counts. The resulting fold-change values between the test and control conditions were used for the pathway analysis. The preranked GSEA (R package)(Subramanian et al., 2005) was used for the pathway analysis of gene sets from WikiPathway(Martens et al., 2021), REACTOME(Jassal et al., 2020), KEGG(Kanehisa, Furumichi, Tanabe, Sato, & Morishima, 2017) databases (MSigDB) and the enrichment score plots.

Immunoblotting

Supernatants containing protein contents were determined by Bradford Protein Assay (Bio-Rad Laboratories, Hercules, CA). Proteins were immunoblotted with anti-PPARα (ab24509, Abcam, Cambridge, MA) and anti-HSP90 (4877S, Cell Signaling Technology, Danvers, MA).

Quantitative PCR

Total mRNAs were isolated using TRIzol reagent purchased from Thermo Fisher Scientific. Reverse-transcription of the RNA was performed with ABI Reverse Transcription Kit (Thermo Fisher Scientific). Quantitative PCR was performed using 7900HT Fast Real-Time PCR System (Life Technologies, Carlsbad, CA) following the manufacturer's instructions. Relative mRNA expression levels of each gene were normalized to TATA-binding protein TBP. The mtDNA copy number was evaluated based on the ratio of mtDNA to nuclear DNA by quantitative PCR. The mtDNA was quantified based on the mitochondrial gene, *VIPR1*, and *MT-ATP6*, respectively. The relative amounts

of mtDNA were normalized to nuclear DNA, *B2M*. The primer pairs used in this study are listed in the table below.

	Sequences of the primers for qPCR	
Human Gene	**Forward primer**	**Reverse primer**
miR-20b	GCAAAGTGCTCATAGTGCAGGTAG	TCGCACTTGTCATACACCAG
U6	CTCGCTTCGGCAGCACA	AACGCTTCACGAATTTGCGT
PPARA	GCTATCATTACGGAGTCCACG	TCGCACTTGTCATACACCAG
CPT1A	AGGCGACATCAATCCGAAC	AAAGGCTACGAATGGGAAGG
ACOX1	CCACGTATGACCCTGAAACC	TCCATAGCATTTCCCCTTAGTG
SREBF1	CAACACAGCAACCAGAAACTC	CTCCACCTCAGTCTTCACG
FASN	CAAGCTGAAGGACCTGTCTAG	CGGAGTGAATCTGGGTTGATG
CD36	GCCAGGTATTGCAGTTCTTTTC	TGTCTGGGTTTTCAACTGGAG
FABP1	GCAGAGCCAGGAAAACTTTG	AGCGGTGATGGTGAACTTG
PPARGC1A	ACCAAACCCACAGAGAACAG	GGGTCAGAGGAAGAGATAAAGTTG
SIRT1	CCCTCAAAGTAAGACCAGTAGC	CACAGTCTCCAAGAAGCTCTAC
VIPR1	CTCCACCATTAGCACCCAAAGCTAAG	GATATTGATTTCACGGAGGATGGTGGTC
MT-ATP6	AACGAAAATCTGTTCGCTTCAT	ATGTGTTGTCGTGCAGGTAGAG
HMGCL	GAGTTTTCAGAGGTTTGACGC	CAAGAGCACAGGAGACGTAC
ACAT1	CGGGCTAACTGATGTCTACAA	CAAATTTCCCAGCTTCCCATG
ACAT2	CCCAGAACAGGACAGAGAATG	AGCTTGGACATGGCTTCTATG
RORA	GGTGATGCTTTTGTTCTTACTGG	TGTCTCCACAGATCTTGCATG
RORC	TGGTGCTGGTTAGGATGTG	GGAGTGGGAGAAGTCAAAGATG
THRB	CATCAAAACTGTCACCGAAGC	TCCAAGTCAACCTTTCCACC
NRBP1	GTTCCACCCAGCATTGTTTG	CAGGGATTTCAGCCAGTACG
NAGK	TATTTCCAGGTGCCAGATCG	CTGAAGATATAGCGGGAAAGGG
USP46	ATACACCAAGCTGTCTTACCG	ATATAATGCCCACGATTAGGACC
ITGB8	CGTCTCATCTCGCTCTTGATAG	TTCTCTGAAAGTTGGCCTAGTG
BMPR2	GGCTGACTGGAAATAGACTGG	CACAGTCCCTCAAGTTCACAG
ZNFX1	CCGAGGATTGTCATAGTGGAAG	AGATCATACACGTTGGCACTG
EPHA5	AGATTGAGGCAGTGAATGGAG	GCCAAGACAAAGAGATGCTG
E2F1	TCTCCGAGGACACTGACAG	ATCACCATAACCATCTGCTCTG
TBP	CCACTCACAGACTCTCACAAC	CTGCGGTACAATCCCAGAACT
B2M	TGCTGTCTCCATGTTTGATGTATCT	TCTCTGCTCCCCACCTCTAAGT

	Sequences of the primers for qPCR	
Mouse Gene	**Forward primer**	**Reverse primer**
miR-20b	GCAAAGTGCTCATAGTGCAGGTAG	TCGCACTTGTCATACACCAG
U6	CTCGCTTCGGCAGCACA	AACGCTTCACGAATTTGCGT
Ppara	TCAGGGTACCACTACGGAGT	CTTGGCATTCTTCCAAAGCG
Cpt1a	AGTTCCATGACCCATCTCTGTC	TTCTTCTTCCAGAGTGCAGC
Acox1	TAACTTCCTCACTCGAAGCCA	AGTTCCATGACCCATCTCTGTC
Srebf1	GGAGCCATGGATTGCACATT	CTTCCAGAGAGGAGGCCAG
Fasn	GGAGGTGGTGATAGCCGGTAT	TGGGTAATCCATAGAGCCCAG
Cd36	GCGACATGATTAATGGCACAG	GATCCGAACACAGCGTAGATAG
Fabp1	TCTCCGGCAAGTACCAATTG	TTGATGTCCTTCCCTTTCTGG
Tnf	CCCTCACACTCAGATCATCTTCT	GCTACGACGTGGGCTACAG
Ccl2	TTAAAAACCTGGATCGGAACCAA	GTTCACCGTAAGCCCAATTT
Il6	TAGTCCTTCCTACCCCAATTTCC	TTGGTCCTTAGCCACTCCTTC
Il1b	GCACTACAGGCTCCGAGATGAAC	TTGTCGTTGCTTGGTTCTCCTTGT
Acta2	GTGAAGAGGAAGACAGCACAG	GCCCATTCCAACCATTACTCC
Col1a1	CATAAAGGGTCATCGTGGCT	TTGAGTCCGTCTTTGCCAG
Col3a1	GAAGTCTCTGAAGCTGATGGG	TTGCCTTGCGTGTTTGATATTC

Fn	CTTTGGCAGTGGTCATTTCAG	ATTCTCCCTTTCCATTCCCG
Timp1	CTCAAAGACCTATAGTGCTGGC	CAAAGTGACGGCTCTGGTAG
Vim	CGTCCACACGCACCTACAG	GGGGGATGAGGAATAGAGGCT
E2f1	TGCAGAACAGATGGTCATAGTG	GGGCACAGGAAAACATCAATG
Tbp	ACCCTTCACCAATGACTCCTATG	TGACTGCAGCAAATCGCTTGG

Cellular Oxygen Consumption Rate (OCR)

OCR of HepG2 cells were analyzed by Seahorse XF24 extracellular flux analyzer (Seahorse Bioscience, North Billerica, MA) following the manufacturer's instruction. The results were normalized with the protein quantity of each corresponding well.

Measurement of FA β-oxidation and uptake

FA β-oxidation were measured by the conversion of [9,10-^{3}H(N)]-Palmitic Acid (PerkinElmer, Waltham, MA) to $^{3}H_2O$. Cells were incubated with 1.25 mCi/L [9,10-^{3}H(N)]-Palmitic Acid with cold palmitic acid in a final concentration of 200μM for 4 hours. After incubation, medium were recovered and precipitated with an equal volume of 10 % tricholoroacetic acid. The supernatant was transferred to new- and capless-microtube and the capless-tube was inserted into D.W-added Scintillation tube and incubated at 60 °C for 12 h. The capless tube was removed from scintillation tube and measured the CPMA with scincillation counter oil using Tri-carb 2910TR liquid scintillation counter (PerkinElmer).

For FA uptake measurement, cells were incubated with 0.5 μCi/L [9,10-^{3}H(N)]-Palmitic Acid with cold palmitic acid in a final concentration of 200μM for 2 hours. Uptake was stopped by addition of 200 μM phloretin in 0.1 % BSA and lysed in 0.1 N NaOH / 0.03 % SDS buffer. The radioactivity of each lysate was counted using Tri-carb 2910TR liquid scintillation counter. The β-oxidation and uptake was normalized to lysate protein concentration determined by BSA assay.

Metabolites assay

HepG2 cells were transfected with miR-20b, anti-miR-20b, or miR-NC, respectively. After 48 h, HepG2 cells (20,000 cells per well) were seeded in 96-well MitoPlate S-1 plates and examined in mitochondrial metabolites activity following the manufacturer's instructions (Biolog, Hayward, CA).

Mice

All animal experiments were performed according to procedures approved by the Ulsan National Institute of Science and Technology's Institutional Animal Care and Use Committee (UNISTIACUC-19-04). Mice were maintained in a specific pathogen–free animal facility under a 12-h light/dark cycle at a temperature of 21°C and allowed free access to water and food. Seven-week-old male C57BL/6J mice (DBL, Chungbuk, Republic of Korea) were fed a HFD (60% kcal fat, D12492, Research Diets Inc., New Brunswick, NJ) for 12 weeks or a MCD (A02082002BR, Research Diets Inc., New Brunswick, NJ, USA) for 4 weeks. Fenofibrate (100 mg/kg, sc-204751, Santa Cruz biotechnology, Dallas, TX) was administered orally for 4 weeks before mice were sacrificed.

Hepatocyte isolation

Briefly, mice were anesthetized with isoflurane, and 24-gauge needle was inserted into the portal vein. Then the inferior vena cava was cut, and the mouse liver was perfused sequentially with solution I (142 μM NaCl, 6.7 μM KCl, 10 μM HEPES, and 2.5 mM EGTA), and solution II (66.7 mM NaCl, 6.7 mM KCl, 50mM HEPES, 4.8 mM $CaCl_2 \cdot 2H_2O$, and 0.01 % Type IV collagenase (Sigma- Aldrich, St. Louis, MO)). After digestion, the liver was disrupted over a 70-μm cell strainer, and cell suspension was spun at 50 x g for 5min at 4 °C. The supernatant was gently aspirated and the cells were resuspended in M199 with EBSS (M199/EBSS) medium and gently mixed with equal volume of Percoll working solution (48.6 % Percoll). The cell suspension was spun at 100 x g for 5 min at 4 °C, and the pellet washed once with M199/EBSS. After viable cells were counted with trypan blue, the isolated hepatocytes were seed in M199/EBSS medium supplemented with 10 % FBS, 1 % penicillin/streptomycin, and 10 nM dexamethasone.

Production of AAV

The miR-20b and anti-miR-20b were cloned into the pOTTC385-pAAV CMV-IE IRES EGFP vector (Addgene plasmid # 102936)(Nelson et al., 2019) and co-transfected with pAAV-DJ vector and pAAV-Helper vector into HEK 293T cells to generate recombinant adeno-associated virus expressing miR-20b or anti-miR-20b according to the manufacturer's protocol (Cell Biolabs, San Diego, CA). The AAVs were purified with AAVpro® Purification Kit (Takara Bio, Shiga, Japan). After feeding HFD for 8 weeks, purified AAV-miR-20b, AAV-anti-miR-20b, or AAV-Control (1 X 10^{10} PFU) was injected into

mice *via* tail-vein. AAV-Control or AAV-anti-miR-20b was injected into mice *via* tail-vein before the initiation of MCD diet.

Metabolic analysis

Mice were fasted overnight (18 h) before intraperitoneal injection of D-glucose (2 g/kg body weight) for glucose tolerance test. For insulin tolerance test, mice were fasted for 4 h before intraperitoneal injection of insulin (0.75 U/kg body weight). Every glucose was examined with tail-vein blood at indicated intervals after injection using a glucometer. For analyzing metabolic parameters, insulin (90080, Crystal Chem, Elk Grove Village, IL), ALT (K752, Biovision Inc., Milpitas, CA), AST (K753, Biovision Inc.), cholesterol (K603, BioVision Inc.), and TG (10010303, Cayman Chemical, Ann Arbor, MI) were determined. Body composition of mice was measured using an EchoMRI100V, quantitative nuclear resonance system (Echo Medical Systems, Houston, TX).

Histological analysis

Liver tissues were isolated from mice and immediately fixed with 4% formalin (Sigma- Aldrich, St. Louis, MO). Histological changes of lipid droplets were examined by H&E staining and Oil Red O staining. As counterstain, Mayer's hematoxylin was used for every slide. Liver fibrosis was further examined by Sirius red with liver section. Images were obtained with Olympus BX53 microscope and DP26 camera.

Statistical analysis

All data are represented as mean ± SEM. Statistically significant differences were assessed by the Student's t-test. Statistical analyses were performed using Microsoft Excel or GraphPad Prism 9. All of the significance are expressed as $^{*}P < 0.05$, $^{**}P < 0.01$, $^{***}P < 0.001$, $^{\#}P < 0.05$, $^{\#\#}P < 0.01$, $^{\#\#\#}P < 0.001$, $^{\$}P < 0.05$, $^{\$\$}P < 0.01$, and $^{\$\$\$}P < 0.001$.

Data Availability

The data sets generated and analyzed during the current study are available from the corresponding author upon reasonable request. The RNA-Seq data have been deposited at the Gene Expression Omnibus (GEO) website: https://www.ncbi.nlm.nih.gov/geo/query/acc.cgi?acc=GSE168484

(accession number GSE168484). Source data files are provided for Figure 1, Figure 2, Figure 2-figure supplement 2, Figure 3, Figure 3-figure supplement 1, Figure 3-figure supplement 2, Figure 3-figure supplement 3, Figure 3-figure supplement 4, Figure 4, Figure 4-figure supplement 1, Figure 5, Figure 6, Figure 7, Figure 8, and Figure 9.

Acknowledgments

This research was funded by Korea Mouse Phenotyping Project (2016M3A9D5A01952411), the National Research Foundation of Korea (NRF) grant funded by the Korea government (2020R1F1A1061267, 2018R1A5A1024340), the Future-leading Project Research Fund (1.210034.01) of UNIST to J.H.C. and the National Research Foundation of Korea (NRF) grant funded by the Korea government (2020R1I1A1A01074940) to H-J.J.

Competing Interest Statement

No conflicts of interest relevant to this manuscript.

References

Agarwal, V., Bell, G. W., Nam, J. W., & Bartel, D. P. (2015). Predicting effective microRNA target sites in mammalian mRNAs. *Elife, 4*. doi:10.7554/eLife.05005

Aran, D., Camarda, R., Odegaard, J., Paik, H., Oskotsky, B., Krings, G., . . . Butte, A. J. (2017). Comprehensive analysis of normal adjacent to tumor transcriptomes. *Nat Commun, 8*(1), 1077. doi:10.1038/s41467-017-01027-z

Athyros, V. G., Papageorgiou, A. A., Athyrou, V. V., Demitriadis, D. S., & Kontopoulos, A. G. (2002). Atorvastatin and micronized fenofibrate alone and in combination in type 2 diabetes with combined hyperlipidemia. *Diabetes Care, 25*(7), 1198-1202. doi:10.2337/diacare.25.7.1198

Bartel, D. P. (2004). MicroRNAs: genomics, biogenesis, mechanism, and function. *Cell, 116*(2), 281-297. doi:10.1016/s0092-8674(04)00045-5

Chakravarthy, M. V., Pan, Z., Zhu, Y., Tordjman, K., Schneider, J. G., Coleman, T., . . . Semenkovich, C. F. (2005). "New" hepatic fat activates PPARalpha to maintain glucose, lipid, and cholesterol homeostasis. *Cell Metab, 1*(5), 309-322. doi:10.1016/j.cmet.2005.04.002

Corey, K. E., & Kaplan, L. M. (2014). Obesity and liver disease: the epidemic of the twenty-first century. *Clin Liver Dis, 18*(1), 1-18. doi:10.1016/j.cld.2013.09.019

584 de Alwis, N. M., & Day, C. P. (2008). Non-alcoholic fatty liver disease: the mist gradually clears. *J*
585 *Hepatol, 48 Suppl 1*, S104-112. doi:10.1016/j.jhep.2008.01.009
586 Denechaud, P. D., Lopez-Mejia, I. C., Giralt, A., Lai, Q., Blanchet, E., Delacuisine, B., . . . Fajas, L.
587 (2016). E2F1 mediates sustained lipogenesis and contributes to hepatic steatosis. *J Clin*
588 *Invest, 126*(1), 137-150. doi:10.1172/JCI81542
589 Ding, J., Li, M., Wan, X., Jin, X., Chen, S., Yu, C., & Li, Y. (2015). Effect of miR-34a in regulating
590 steatosis by targeting PPARalpha expression in nonalcoholic fatty liver disease. *Sci Rep, 5*,
591 13729. doi:10.1038/srep13729
592 Fabbrini, E., Sullivan, S., & Klein, S. (2010). Obesity and nonalcoholic fatty liver disease:
593 biochemical, metabolic, and clinical implications. *Hepatology, 51*(2), 679-689.
594 doi:10.1002/hep.23280
595 Farnier, M., Freeman, M. W., Macdonell, G., Perevozskaya, I., Davies, M. J., Mitchel, Y. B., . . .
596 Ezetimibe Study, G. (2005). Efficacy and safety of the coadministration of ezetimibe with
597 fenofibrate in patients with mixed hyperlipidaemia. *Eur Heart J, 26*(9), 897-905.
598 doi:10.1093/eurheartj/ehi231
599 Francque, S., Verrijken, A., Caron, S., Prawitt, J., Paumelle, R., Derudas, B., . . . Staels, B. (2015).
600 PPARalpha gene expression correlates with severity and histological treatment response in
601 patients with non-alcoholic steatohepatitis. *J Hepatol, 63*(1), 164-173.
602 doi:10.1016/j.jhep.2015.02.019
603 Gonzalez, F. J., & Shah, Y. M. (2008). PPARalpha: mechanism of species differences and
604 hepatocarcinogenesis of peroxisome proliferators. *Toxicology, 246*(1), 2-8.
605 doi:10.1016/j.tox.2007.09.030
606 Hoang, S. A., Oseini, A., Feaver, R. E., Cole, B. K., Asgharpour, A., Vincent, R., . . . Sanyal, A. J. (2019).
607 Gene Expression Predicts Histological Severity and Reveals Distinct Molecular Profiles of
608 Nonalcoholic Fatty Liver Disease. *Sci Rep, 9*(1), 12541. doi:10.1038/s41598-019-48746-5
609 Hosui, A., Tatsumi, T., Hikita, H., Saito, Y., Hiramatsu, N., Tsujii, M., . . . Takehara, T. (2017). Signal
610 transducer and activator of transcription 5 plays a crucial role in hepatic lipid metabolism
611 through regulation of CD36 expression. *Hepatol Res, 47*(8), 813-825.
612 doi:10.1111/hepr.12816
613 Jassal, B., Matthews, L., Viteri, G., Gong, C., Lorente, P., Fabregat, A., . . . D'Eustachio, P. (2020). The
614 reactome pathway knowledgebase. *Nucleic Acids Res, 48*(D1), D498-D503.
615 doi:10.1093/nar/gkz1031
616 Jin, X., Chen, Y. P., Kong, M., Zheng, L., Yang, Y. D., & Li, Y. M. (2012). Transition from hepatic
617 steatosis to steatohepatitis: unique microRNA patterns and potential downstream
618 functions and pathways. *J Gastroenterol Hepatol, 27*(2), 331-340. doi:10.1111/j.1440-
619 1746.2011.06864.x
620 Kanehisa, M., Furumichi, M., Tanabe, M., Sato, Y., & Morishima, K. (2017). KEGG: new perspectives
621 on genomes, pathways, diseases and drugs. *Nucleic Acids Res, 45*(D1), D353-D361.
622 doi:10.1093/nar/gkw1092

623 Katayama, M., Wiklander, O. P. B., Fritz, T., Caidahl, K., El-Andaloussi, S., Zierath, J. R., & Krook, A.
624 (2019). Circulating Exosomal miR-20b-5p Is Elevated in Type 2 Diabetes and Could Impair
625 Insulin Action in Human Skeletal Muscle. *Diabetes, 68*(3), 515-526. doi:10.2337/db18-0470
626 Lefebvre, P., Chinetti, G., Fruchart, J. C., & Staels, B. (2006). Sorting out the roles of PPAR alpha in
627 energy metabolism and vascular homeostasis. *J Clin Invest, 116*(3), 571-580.
628 doi:10.1172/JCI27989
629 Liberzon, A., Birger, C., Thorvaldsdottir, H., Ghandi, M., Mesirov, J. P., & Tamayo, P. (2015). The
630 Molecular Signatures Database (MSigDB) hallmark gene set collection. *Cell Syst, 1*(6), 417-
631 425. doi:10.1016/j.cels.2015.12.004
632 Lopez-Sanchez, G. N., Dominguez-Perez, M., Uribe, M., Chavez-Tapia, N. C., & Nuno-Lambarri, N.
633 (2021). Non-alcoholic fatty liver disease and microRNAs expression, how it affects the
634 development and progression of the disease. *Ann Hepatol, 21*, 100212.
635 doi:10.1016/j.aohep.2020.04.012
636 Lopez-Velazquez, J. A., Carrillo-Cordova, L. D., Chavez-Tapia, N. C., Uribe, M., & Mendez-Sanchez,
637 N. (2012). Nuclear receptors in nonalcoholic Fatty liver disease. *J Lipids, 2012*, 139875.
638 doi:10.1155/2012/139875
639 Loyer, X., Paradis, V., Henique, C., Vion, A. C., Colnot, N., Guerin, C. L., . . . Rautou, P. E. (2016). Liver
640 microRNA-21 is overexpressed in non-alcoholic steatohepatitis and contributes to the
641 disease in experimental models by inhibiting PPARalpha expression. *Gut, 65*(11), 1882-
642 1894. doi:10.1136/gutjnl-2014-308883
643 Luo, W., Li, G., Yi, Z., Nie, Q., & Zhang, X. (2016). E2F1-miR-20a-5p/20b-5p auto-regulatory
644 feedback loop involved in myoblast proliferation and differentiation. *Sci Rep, 6*, 27904.
645 doi:10.1038/srep27904
646 Martens, M., Ammar, A., Riutta, A., Waagmeester, A., Slenter, D. N., Hanspers, K., . . . Kutmon, M.
647 (2021). WikiPathways: connecting communities. *Nucleic Acids Res, 49*(D1), D613-D621.
648 doi:10.1093/nar/gkaa1024
649 McKenna, N. J., Cooney, A. J., DeMayo, F. J., Downes, M., Glass, C. K., Lanz, R. B., . . . O'Malley, B.
650 W. (2009). Minireview: Evolution of NURSA, the Nuclear Receptor Signaling Atlas. *Mol*
651 *Endocrinol, 23*(6), 740-746. doi:10.1210/me.2009-0135
652 Montagner, A., Polizzi, A., Fouche, E., Ducheix, S., Lippi, Y., Lasserre, F., . . . Guillou, H. (2016). Liver
653 PPARalpha is crucial for whole-body fatty acid homeostasis and is protective against
654 NAFLD. *Gut, 65*(7), 1202-1214. doi:10.1136/gutjnl-2015-310798
655 Nelson, B. S., Fulenwider, H. D., Nennig, S. E., Smith, B. M., Sequeira, M. K., Chimberoff, S. H., . . .
656 Schank, J. R. (2019). Escalated Alcohol Self-Administration and Sensitivity to Yohimbine-
657 Induced Reinstatement in Alcohol Preferring Rats: Potential Role of Neurokinin-1
658 Receptors in the Amygdala. *Neuroscience, 413*, 77-85.
659 doi:10.1016/j.neuroscience.2019.06.023

660 Pawlak, M., Lefebvre, P., & Staels, B. (2015). Molecular mechanism of PPARalpha action and its
661 impact on lipid metabolism, inflammation and fibrosis in non-alcoholic fatty liver disease. *J*
662 *Hepatol, 62*(3), 720-733. doi:10.1016/j.jhep.2014.10.039
663 Peng, L., Li, S., Li, Y., Wan, M., Fang, X., Zhao, Y., . . . Xuan, Y. (2019). Regulation of BTG3 by
664 microRNA-20b-5p in non-small cell lung cancer. *Oncol Lett, 18*(1), 137-144.
665 doi:10.3892/ol.2019.10333
666 Rakhshandehroo, M., Knoch, B., Muller, M., & Kersten, S. (2010). Peroxisome proliferator-activated
667 receptor alpha target genes. *PPAR Res, 2010*. doi:10.1155/2010/612089
668 Ritchie, M. E., Phipson, B., Wu, D., Hu, Y., Law, C. W., Shi, W., & Smyth, G. K. (2015). limma powers
669 differential expression analyses for RNA-sequencing and microarray studies. *Nucleic Acids*
670 *Res, 43*(7), e47. doi:10.1093/nar/gkv007
671 Streleckiene, G., Inciuraite, R., Juzenas, S., Salteniene, V., Steponaitiene, R., Gyvyte, U., . . .
672 Skieceviciene, J. (2020). miR-20b and miR-451a Are Involved in Gastric Carcinogenesis
673 through the PI3K/AKT/mTOR Signaling Pathway: Data from Gastric Cancer Patients, Cell
674 Lines and Ins-Gas Mouse Model. *Int J Mol Sci, 21*(3). doi:10.3390/ijms21030877
675 Subramanian, A., Tamayo, P., Mootha, V. K., Mukherjee, S., Ebert, B. L., Gillette, M. A., . . . Mesirov,
676 J. P. (2005). Gene set enrichment analysis: a knowledge-based approach for interpreting
677 genome-wide expression profiles. *Proc Natl Acad Sci U S A, 102*(43), 15545-15550.
678 doi:10.1073/pnas.0506580102
679 Valasek, M. A., Clarke, S. L., & Repa, J. J. (2007). Fenofibrate reduces intestinal cholesterol
680 absorption via PPARalpha-dependent modulation of NPC1L1 expression in mouse. *J Lipid*
681 *Res, 48*(12), 2725-2735. doi:10.1194/jlr.M700345-JLR200
682 Xia, L., Li, F., Qiu, J., Feng, Z., Xu, Z., Chen, Z., & Sun, J. (2020). Oncogenic miR-20b-5p contributes
683 to malignant behaviors of breast cancer stem cells by bidirectionally regulating CCND1
684 and E2F1. *BMC Cancer, 20*(1), 949. doi:10.1186/s12885-020-07395-y
685 Yang, Z., & Wang, L. (2011). Regulation of microRNA expression and function by nuclear receptor
686 signaling. *Cell Biosci, 1*(1), 31. doi:10.1186/2045-3701-1-31
687 Ye, D., Zhang, T., Lou, G., Xu, W., Dong, F., Chen, G., & Liu, Y. (2018). Plasma miR-17, miR-20a,
688 miR-20b and miR-122 as potential biomarkers for diagnosis of NAFLD in type 2 diabetes
689 mellitus patients. *Life Sci, 208*, 201-207. doi:10.1016/j.lfs.2018.07.029
690 Zhang, Y., Xu, N., Xu, J., Kong, B., Copple, B., Guo, G. L., & Wang, L. (2014). E2F1 is a novel
691 fibrogenic gene that regulates cholestatic liver fibrosis through the Egr-1/SHP/EID1
692 network. *Hepatology, 60*(3), 919-930. doi:10.1002/hep.27121
693

694

Figures and Tables

Figure 1. miR-20b significantly increases in the livers of dietary obese mice and human.

A

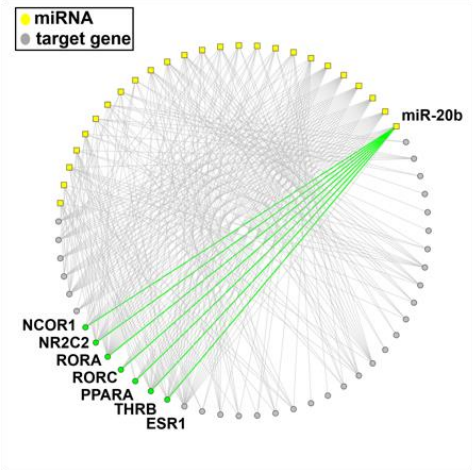

Rank	microRNA	adjusted *p*-value
1	hsa-miR-129	0.0120
2	hsa-miR-219a	0.0158
3	hsa-miR-4782	0.0158
4	hsa-miR-6766	0.0158
5	hsa-miR-20b	0.0474
6	hsa-miR-20a	0.0474
7	hsa-miR-106a	0.0474
8	hsa-miR-106b	0.0474
9	hsa-miR-17	0.0474
10	hsa-miR-519d	0.0474

B

microRNA	Fold change	adjusted *p*-value
hsa-miR-20b	1.226639893	0.0080
hsa-miR-106a	1.078651094	0.0894
hsa-miR-129	1.031414803	0.3217
hsa-miR-106b	0.982514098	0.3020
hsa-miR-519d	0.935426862	0.1644
hsa-miR-17	0.923967423	0.0079
hsa-miR-219a	0.919478183	0.0504
hsa-miR-20a	0.553090004	0.0002

C

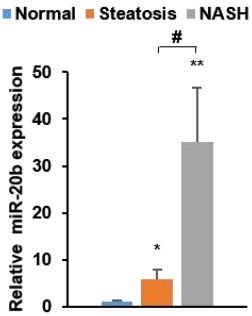

D

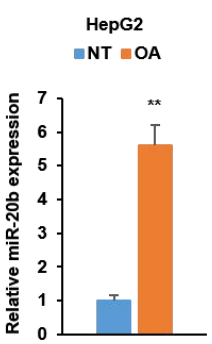

E

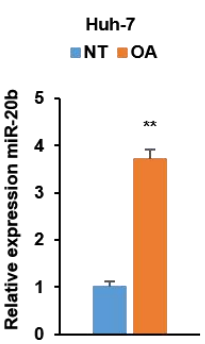

F

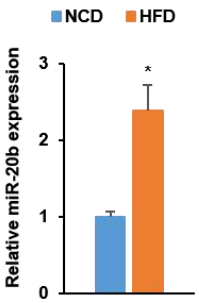

G

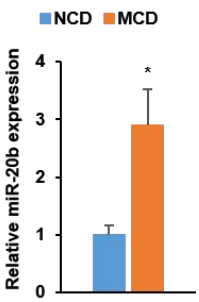

H

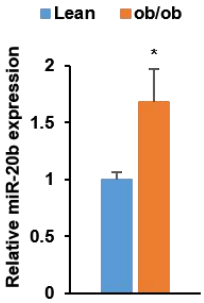

FIGURE 1. miR-20b significantly increases in the livers of dietary obese mice and human.

The miRNA-target genes network was constructed using public hepatic NR transcriptome data from NAFLD patients (A). The ranked candidates were examined in NAFLD patients compared to normal individuals using public GSE data (GSE40744) (B). The expression of miR-20b was measured in indicated condition by quantitative RT-PCR (*C-H*). Hepatic miR-20b levels of steatosis or NASH patients were normalized to those of normal individuals. $^{*}P < 0.05$ and $^{**}P < 0.01$ *vs* normal individuals. $^{\#}P < 0.05$ *vs* steatosis patients (C). miR-20b levels from HepG2 cells (D) and Huh-7 cells (E) treated with OA for 24 h were normalized to no treatment (NT). Hepatic miR-20b levels from C57BL/6J mice fed a HFD (F), or MCD (G) were normalized to NCD. Hepatic miR-20b levels from leptin-deficient *ob/ob* mice were normalized to lean wild mice (H). Values represent means ± SEM (n = 3-5). $^{*}P < 0.05$, $^{**}P < 0.01$ *vs* NT in cells or NCD-fed mice.

Figure 1-figure supplement 1. Clinical characteristics of patients with control individuals (N=5), steatosis (steatosis > 50%, N=4) and NASH patients (N=4).

Patients	Normal					Steatosis				NASH			
Age (years)	54	45	41	59	58	58	72	54	70	61	67	71	68
Gender	F	M	F	M	M	M	M	F	M	M	M	M	F
Weight (kg)	60.5	67	66.15	73.75	51.1	59.1	70.1	54.91	62.5	73.5	58.7	58.7	65.16
BMI	26.39	22.65	24.33	27.22	18.2	23.92	25.29	21.97	22.98	24.7	21.02	23.5	27.34
AST (IU/L)	26	13	26	28	18	20	23	28	20	31	58	20	64
ALT (IU/L)	30	38	20	28	20	33	23	9	16	35	32	21	31
GGT (IU/L)	30	N/A	33	31	26	26	34	11	38	110	136	37	158
ALP (IU/L)	47	60	73	74	93	62	70	63	68	99	77	63	88
Billirubin (mg/dL)	0.9	0.9	1.1	1.1	0.7	0.6	1	0.7	0.4	0.7	0.5	0.5	0.9
INR	0.97	1.06	1	1.03	0.97	1	0.93	1.07	1	1.01	0.97	1.09	1
Total Cholesterol (mg/dL)	203	88	179	162	178	171	115	169	148	238	161	260	258

Figure 2. PPARα is a direct target of miR-20b.

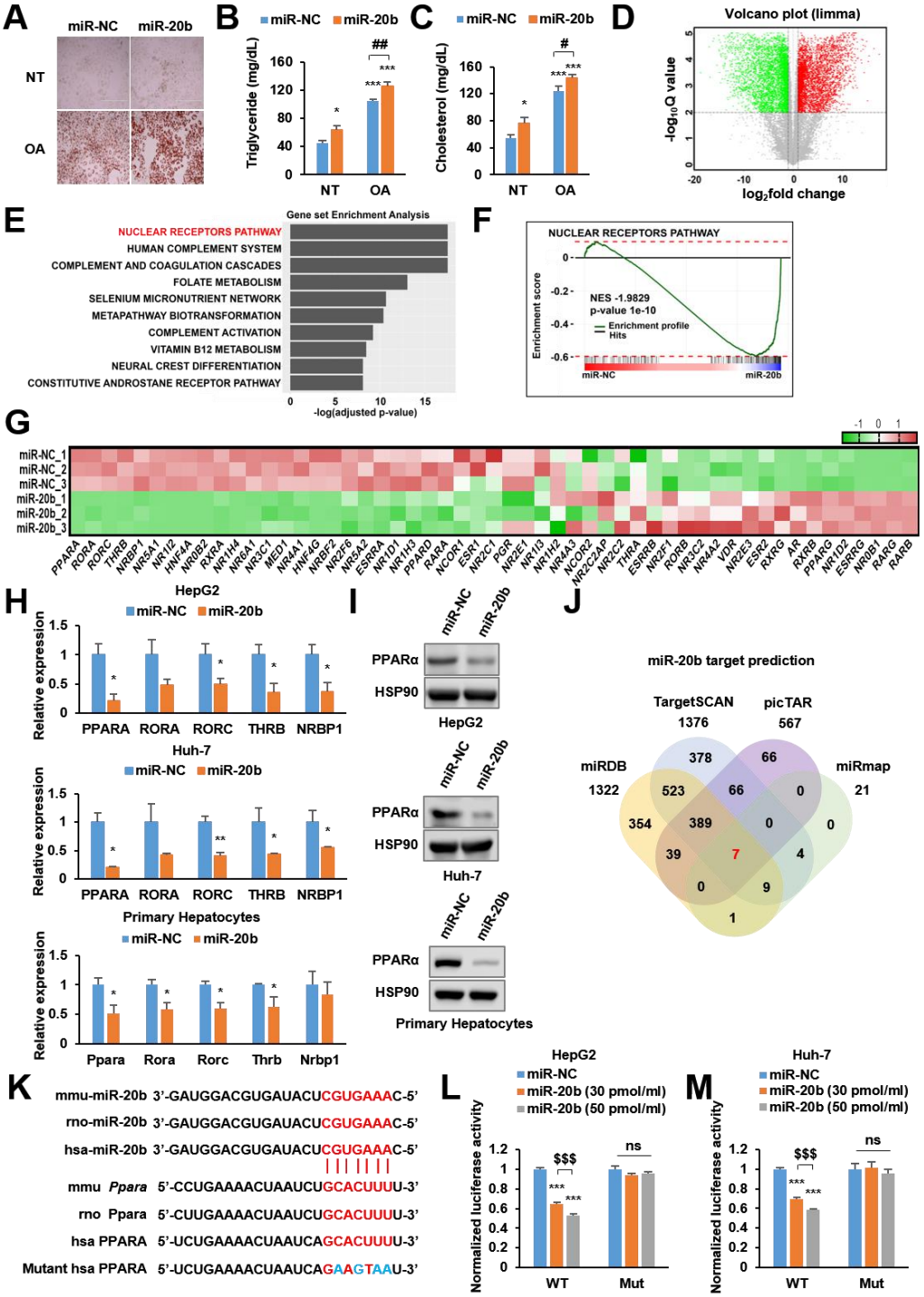

FIGURE 2. PPARα is a direct target of miR-20b.

Overexpressed miR-20b induces hepatic steatosis in HepG2 cells treated with OA (1 mM). Oil Red O staining showed intracellular lipid accumulation in HepG2 cells. Scale bar is 400 μm (A). TG (B) and Cholesterol levels (C) were examined in OA-treated HepG2 cells transfected with miR-NC or miR-20b. RNA-seq was performed on sample from HepG2 cell with or without overexpression of miR-20b.Volcano plot of the gene expressions (log_2 fold change) compared to the negative control from RNA-seq analysis (D). Top ranked GSEA in overexpressed miR-20b compared to miR-NC in HepG2 cells (E). The primary ranked enrichment plot of nuclear receptors pathway (F). Heatmap of the genes in NR pathway upon miR-20b overexpression compared to control (G). Expression of primary ranked nuclear receptors pathway genes from RNA-seq analysis in HepG2 cells, Huh-7 cells, and primary hepatocytes transfected with miR-20b were normalized to each cells transfected with miR-NC (H). Western blot analysis of PPARα on miR-NC or miR-20b transfected cells (I). Venn diagram of predicted targets for miR-20b in four major database system (J). Graphic image of the conserved binding motifs of miR-20b within 3'-UTR mRNA of PPARA (K). Luciferase activities of miR-20b-transfected HepG2 cells and Huh-7 cells containing the luciferase reporter DNA constructs for wild-type or mutated 3'-UTR of *PPARA* were normalized to those or miR-NC-transfected cells (L, M). Values represent means ± SEM (n = 3). $^{*}P < 0.05$, $^{**}P < 0.01$, $^{***}P < 0.001$ *vs* miR-NC. $^{\#}P < 0.05$, $^{\#\#}P < 0.01$ *vs* miR-NC + OA. $^{\$\$\$}P < 0.001$ *vs* miR-20b (30 pmol/ml).

Figure 2-figure supplement 1. Analysis of PPARα related pathway in RNA-seq of miR-20b overexpressed HepG2 cells.

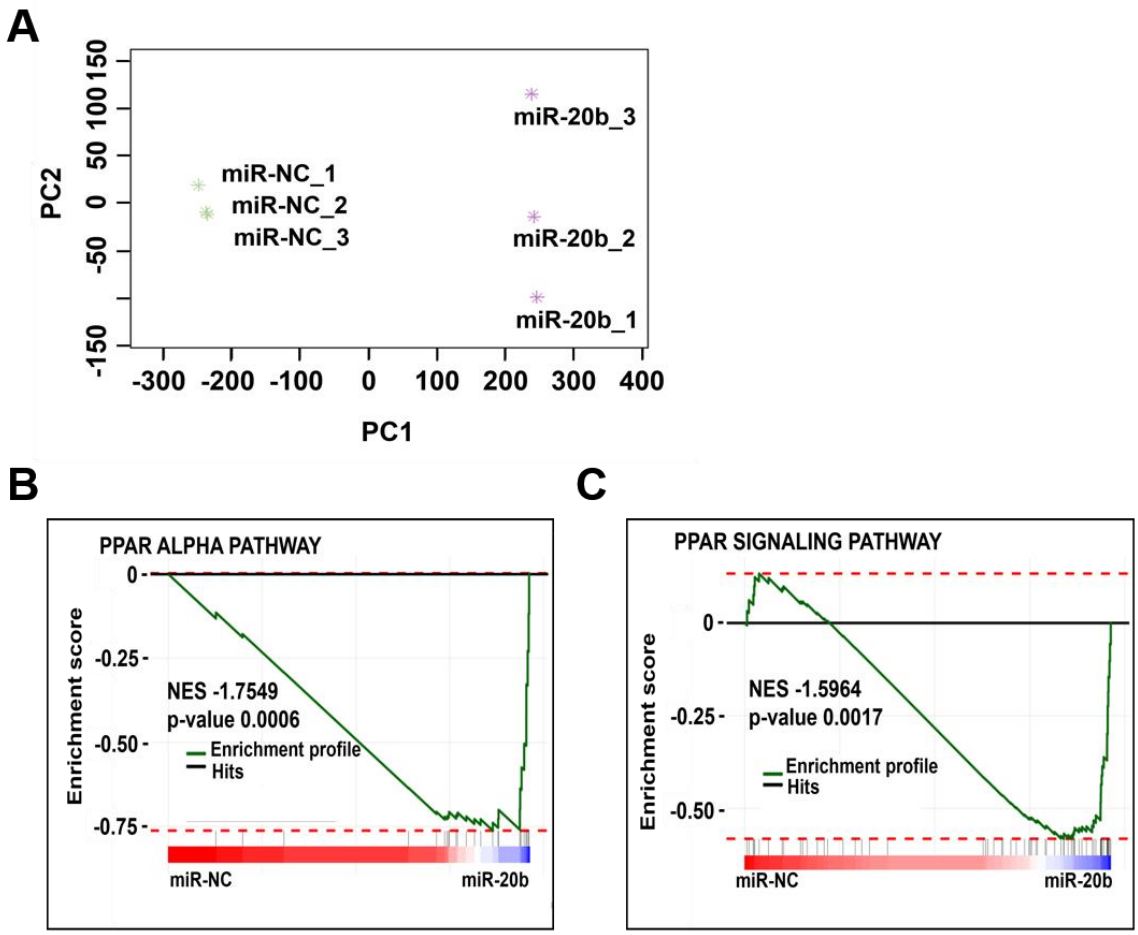

Figure 2-figure supplement 1. Analysis of PPARα related pathway in RNA-seq of miR-20b overexpressed HepG2 cells.

HepG2 cells were transfected either with miR-NC or miR-20b and analyzed by RNA-seq. Analysis of the miR-20b compared to the negative control (n = 3) *via* PCA plot from RNA-seq data (A). Gene set enrichment pathway analysis of PPARα-related pathways, including PPARA pathway and PPAR signaling pathway in overexpressed miR-20b compared to miR-NC (B, C).

Figure 2-figure supplement 2. PPARα is the primary target of the overlapped candidates.

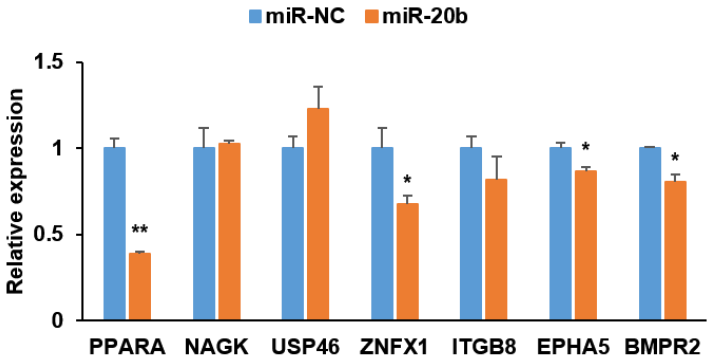

739

740 **Figure 2-figure supplement 2. PPARα is the primary target of the overlapped candidates.**

741 The seven predicted miR-20b targets were overlapped (PPARA, NAGK, USP46, ZNFX1, ITGB8,
742 EPHA5, BMPR2). HepG2 cells were transfected with miR-NC or miR-20b and the expression of
743 seven predicted miR-20b targets were measured by quantitative RT-PCR. Relative values are
744 normalized to miR-NC. Values represent means ± SEM (n = 3). *P < 0.05, **P < 0.01 vs miR-NC.

Figure 3. miR-20b regulates fatty acid metabolism.

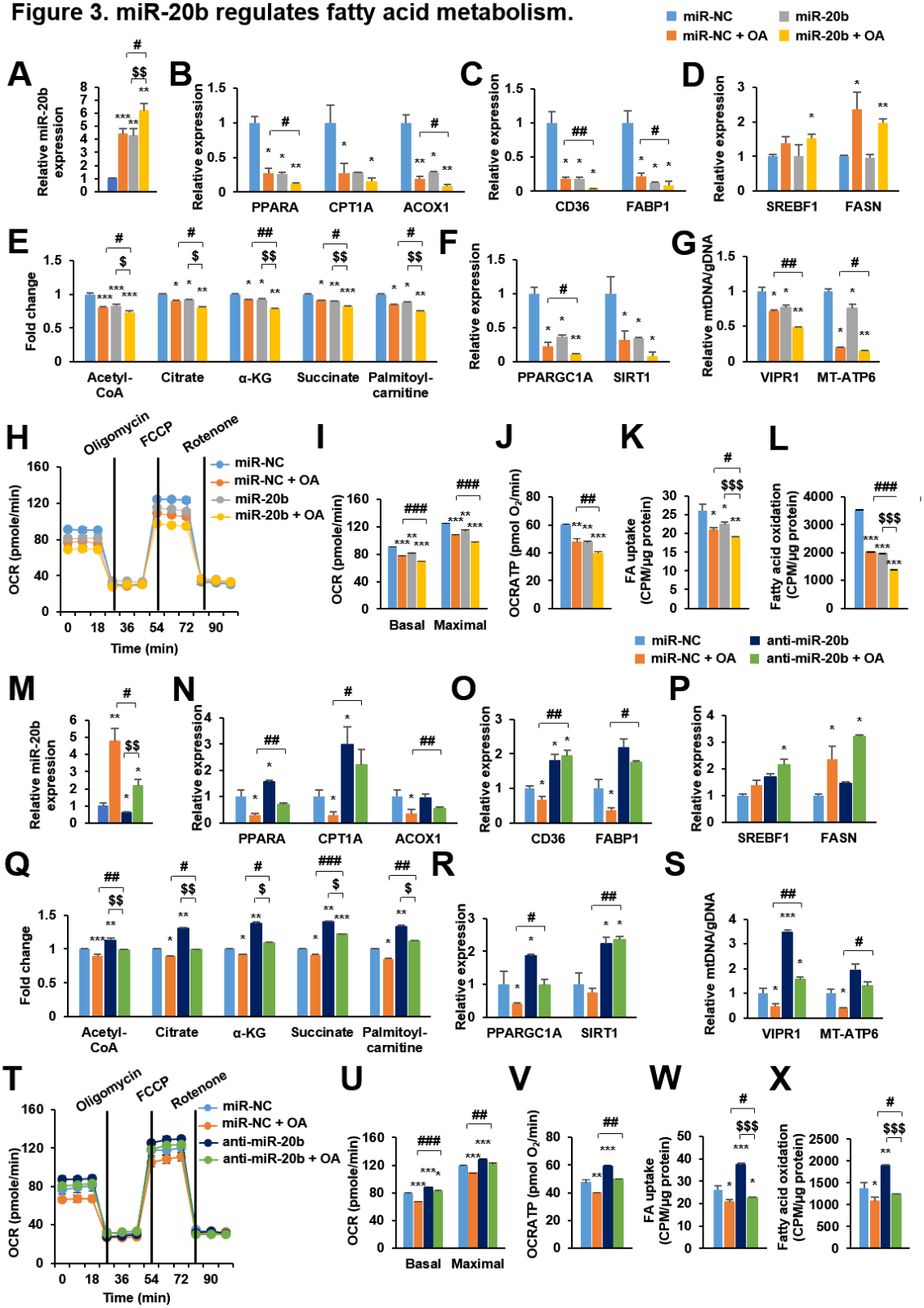

745

746

FIGURE 3. miR-20b regulates fatty acid metabolism.

HepG2 cells were transfected with miR-20b or anti-miR-20b and treated with OA for 24 h. The expression of miR-20b (A, M) and genes related to FA β-oxidation (B, N), FA uptake (C, O), and lipogenesis (D, P) were measured by quantitative RT-PCR. Representative mitochondrial metabolites were measured in HepG2 cells (E, Q). The expression of genes related to mitochondrial biogenesis (F, R) were measured by quantitative RT-PCR. The mitochondrial copy of VIPR1 and MT-ATP6 were determined (G, S). OCR (H, T), basal and maximal OCR (I, U), and ATP levels (J, V) were measured in HepG2 cells. FA uptake (K, W) and β-oxidation (L, X) activity were measured using [9,10-^{3}H(N)]-Palmitic Acid and normalized to the total protein content. Relative values are normalized to miR-NC. Values represent means ± SEM (n = 3-5). **P* < 0.05, ***P* < 0.01, ****P* < 0.001 *vs* miR-NC. $^{\#}$*P* < 0.05, $^{\#\#}$*P* < 0.01, $^{\#\#\#}$*P* < 0.001 *vs* miR-20b or anti-miR-20b, respectively. $^{\$}$*P* < 0.05, $^{\$\$}$*P* < 0.01, $^{\$\$\$}$*P* <0.001 *vs* miR-NC + OA.

Figure 3-figure supplement 1. The expression of PPARα is regulated both in human and mice.

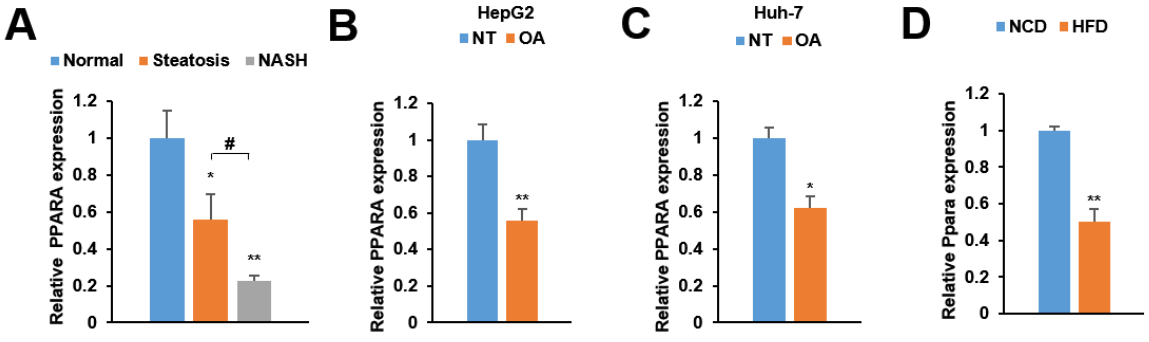

Figure 3-figure supplement 1. The expression of PPARα is regulated both in human and mice.

The expression of PPARα was measured in human patients, mice liver tissues, HepG2, and Huh-7 cells by quantitative RT-PCR. Hepatic PPARA expression levels of steatosis or NASH patients were normalized to those of normal individuals. **P* < 0.05 and ***P* < 0.01 vs normal individuals. $^{\#}P$ < 0.05 vs steatosis patients (A). PPARA expression levels from HepG2 cells (B) and Huh-7 cells (C) treated with OA for 24 h were normalized to no treatment (NT). Hepatic Ppara expression levels from C57BL/6J mice fed a HFD (D) were normalized to NCD. Values represent means ± SEM (n = 3-5). **P* < 0.05, ***P* < 0.01 vs NT in cells or NCD-fed mice.

Figure 3-figure supplement 2. miR-20b induces hepatic steatosis in primary hepatocytes

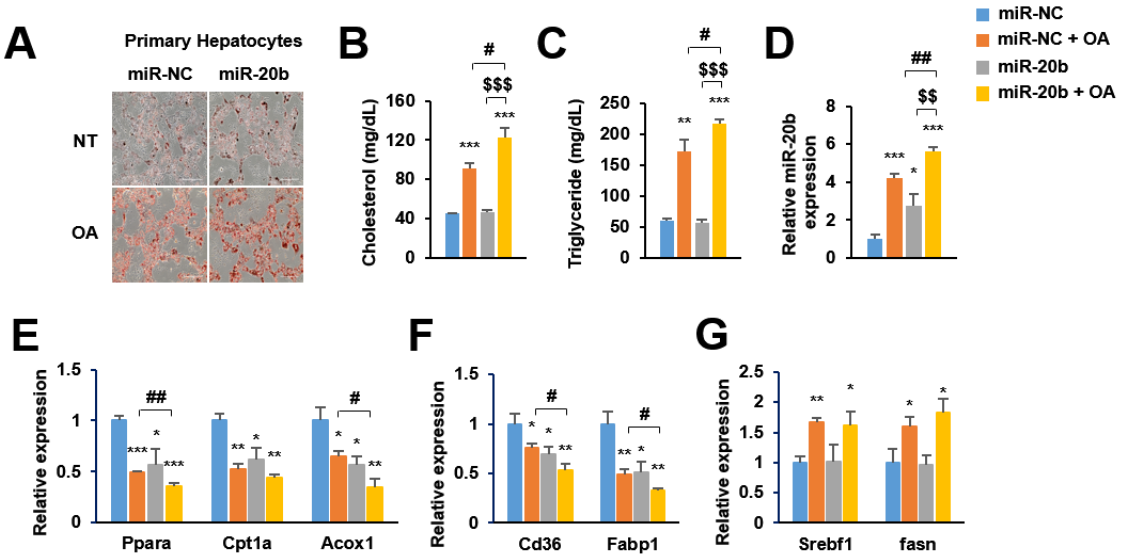

768

769 **Figure 3-figure supplement 2. miR-20b induces hepatic steatosis in primary hepatocytes.**

770 Primary hepatocytes were transfected with miR-NC or miR-20b, subsequently treated with OA (1
771 mM). Representative Oil Red O staining revealed intracellular lipid accumulation (A). The level of
772 triglyceride (B) and cholesterol (C) were analyzed. The expression of miR-20b (D) and genes related
773 to FA β-oxidation (E), FA uptake (F), and lipogenesis (G) were measured by quantitative RT-PCR.
774 Values represent means ± SEM (n = 3). **P* < 0.05, ***P* < 0.01, ****P* < 0.001 vs miR-NC. $^{\#}$*P* < 0.05,
775 $^{\#\#}$*P* < 0.01, *vs* miR-NC + OA. $^{\$\$}$*P* < 0.01, $^{\$\$\$}$*P* < 0.001, *vs* miR-20b.

Figure 3-figure supplement 3. Ketogenesis is not regulated by miR-20b in HepG2 cells.

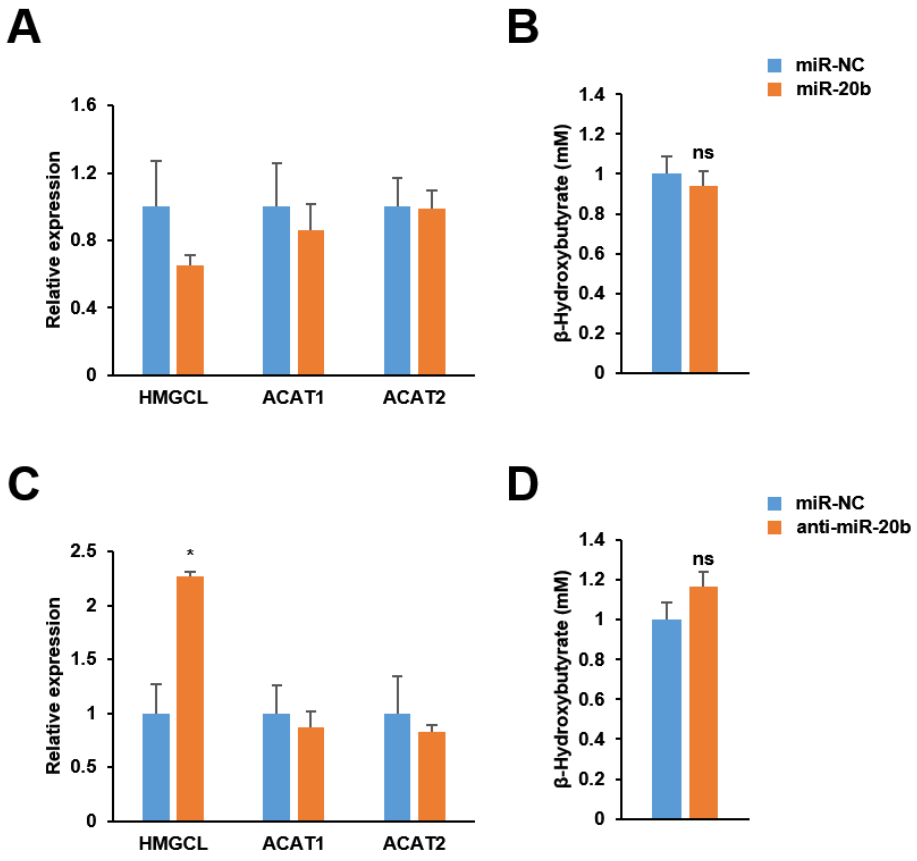

Figure 3-figure supplement 3. Ketogenesis is not affected by miR-20b in HepG2 cells.

HepG2 cells were transfected with miR-20b, anti-miR-20b, or miR-NC as control. Genes involved in ketogenesis- *HMGCL, ACAT1 and ACAT2*- were measured by quantitative RT-PCR. Relative values are normalized to miR-NC (A, C). The concentration of β-hydroxybutyrate which generated by ketogenesis was examined in HepG2 cells using β-hydroxybutyrate assay kit (ab83390, abcam) (B, D). Values represent means ± SEM (n = 3). **P* < 0.05, ***P* < 0.01, ****P* < 0.001 *vs* miR-NC.

Figure 3-figure supplement 4. Inhibition of miR-20b alleviates hepatic steatosis in HepG2 cells.

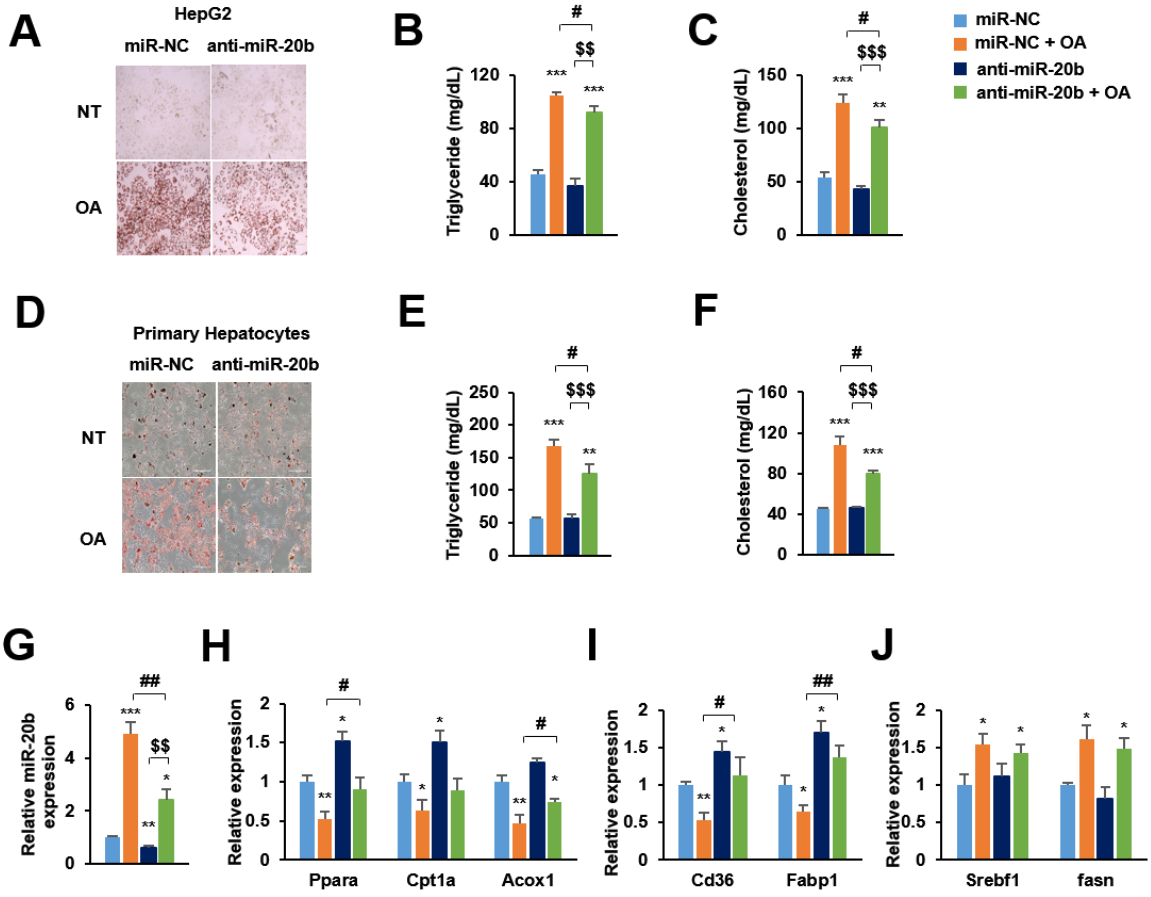

Figure 3-figure supplement 4. Inhibition of miR-20b alleviates hepatic steatosis in HepG2 cells.

HepG2 cells and primary hepatocytes were transfected with miR-NC or anti-miR-20b, subsequently treated with OA (1 mM). Representative Oil Red O staining revealed intracellular lipid accumulation (A and *D*). The level of triglyceride (*B* and *E*) and cholesterol (C and *F*) were analyzed. The expression of miR-20b (*G*) and genes related to FA β-oxidation (*H*), FA uptake (*I*), and lipogenesis (*J*) were measured by quantitative RT-PCR. Values represent means ± SEM (n = 3). **P* < 0.05, ***P* < 0.01, ****P* < 0.001 vs miR-NC. $^{\#}P < 0.05$, $^{\#\#}P < 0.01$ *vs* miR-NC+OA. $^{\$\$}P < 0.01$, $^{\$\$\$}P < 0.001$ vs anti-miR-20b.

Figure 4. miR-20b promotes hepatic steatosis in HFD-fed mice

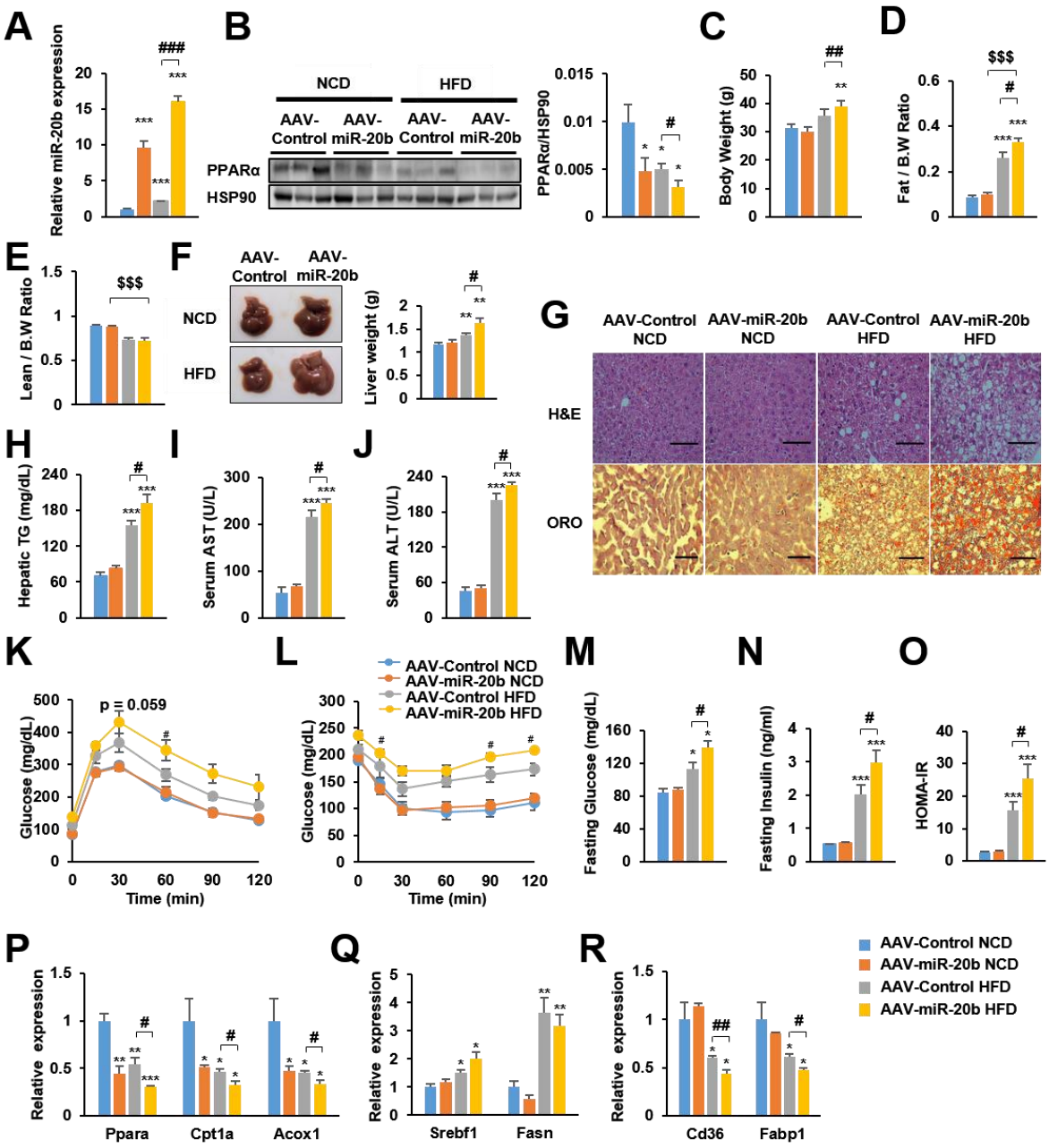

FIGURE 4. miR-20b promotes hepatic steatosis in HFD-fed mice

C57BL/6J mice were fed a NCD or a HFD for 12 weeks with administration of indicated AAV (n = 5 per group). Hepatic expression of miR-20b (A) and PPARα (B), body weight (C), the ratio of fat mass to body weight (D), the ratio of lean mass to body weight (E), representative images of liver and liver weight (F), representative images of H&E staining and Oil Red O staining of liver slides (G), hepatic TG (H), serum AST (I), and serum ALT (J), glucose tolerance (K), insulin tolerance (L), fasting glucose (M), fasting insulin (N), and HOMA-IR (O) were analyzed in indicated mice. Genes related to FA β-oxidation (P), lipogenesis (Q) and FA uptake (R) were determined by quantitative RT-PCR. Relative values are normalized to AAV-Control NCD. Values represent means ± SEM (n = 5). **P* < 0.05, ***P* < 0.01, ****P* < 0.001 *vs* AAV-Control NCD. $^{\#}P < 0.05$, $^{\#\#}P < 0.01$, $^{\#\#\#}P < 0.001$ *vs* AAV-Control HFD. $^{\$\$\$}P < 0.001$ *vs* AAV-miR-20b NCD. Scale bar is 100μm

Figure 4-figure supplement 1. The expression of miR-20b in peripheral tissues.

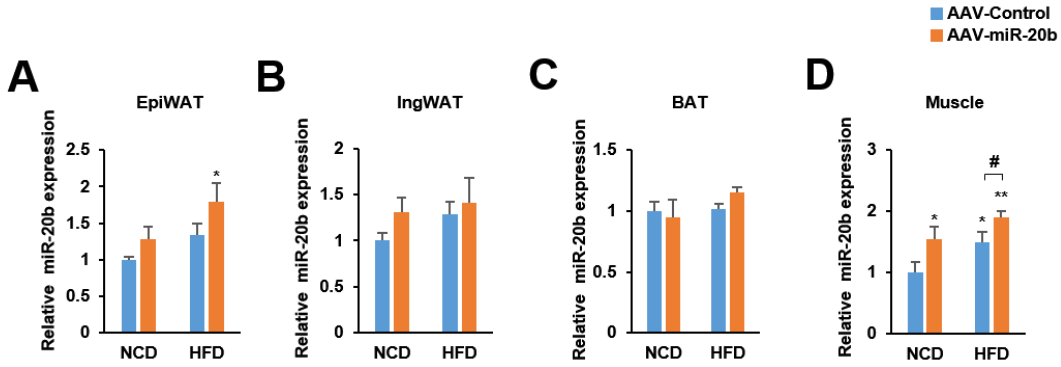

Figure 4-figure supplement 1. The expression of miR-20b in peripheral tissues.

C57BL/6J fed on normal chow diet (NCD, n = 5 per group) or high fat diet (HFD, n = 5 per group) for 12 weeks with administered of indicated AAV. All tissues were harvested at the same time. Quantitative RT-PCR analysis of miR-20b expression in epididymal white adipose tissue (a), inguinal white adipose tissue (b), brown adipose tissue (c), and muscle (d) in AAV-Control or AAV-miR-20b injected mice. Relative values are normalized to AAV-Control. Values represent means ± SEM (n = 5). **P* < 0.05, ***P* < 0.01 *vs* AAV-Control NCD. $^{\#}$*P* < 0.05 *vs* AAV-Control HFD.

Figure 4-figure supplement 2. The weight of peripheral tissues with AAV-miR-20b

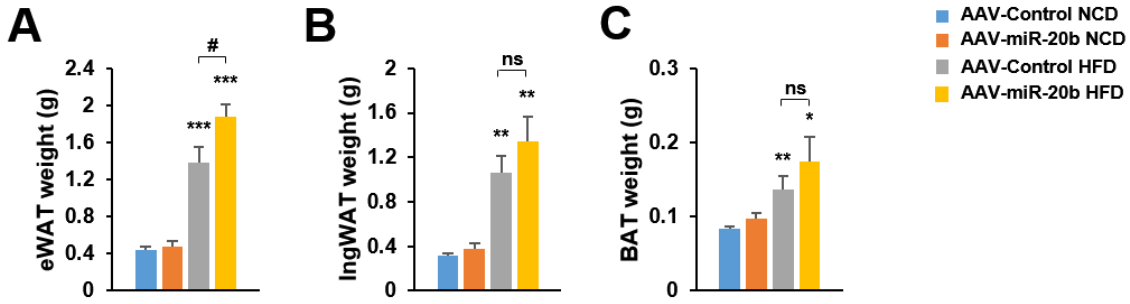

Figure 4-figure supplement 2. The weight of peripheral tissues with AAV-miR-20b.

C57BL/6J fed on normal chow diet (NCD, n = 5 per group) or high fat diet (HFD, n = 5 per group) for 12 weeks with administration of indicated AAV. All tissues were harvested at the same time. Wet weight of epididymal white adipose tissue (A), inguinal white adipose tissue (B), and brown adipose tissue (C) in AAV-Control or AAV-miR-20b injected mice. Values represent means ± SEM (n = 5). ns, not significant. **P* < 0.05, ***P* < 0.01, ****P* < 0.01 *vs* AAV-Control NCD. $^{\#}$*P* < 0.05 *vs* AAV-Control HFD.

Figure 5. Inhibition of miR-20b alleviates hepatic steatosis in HFD-fed mice.

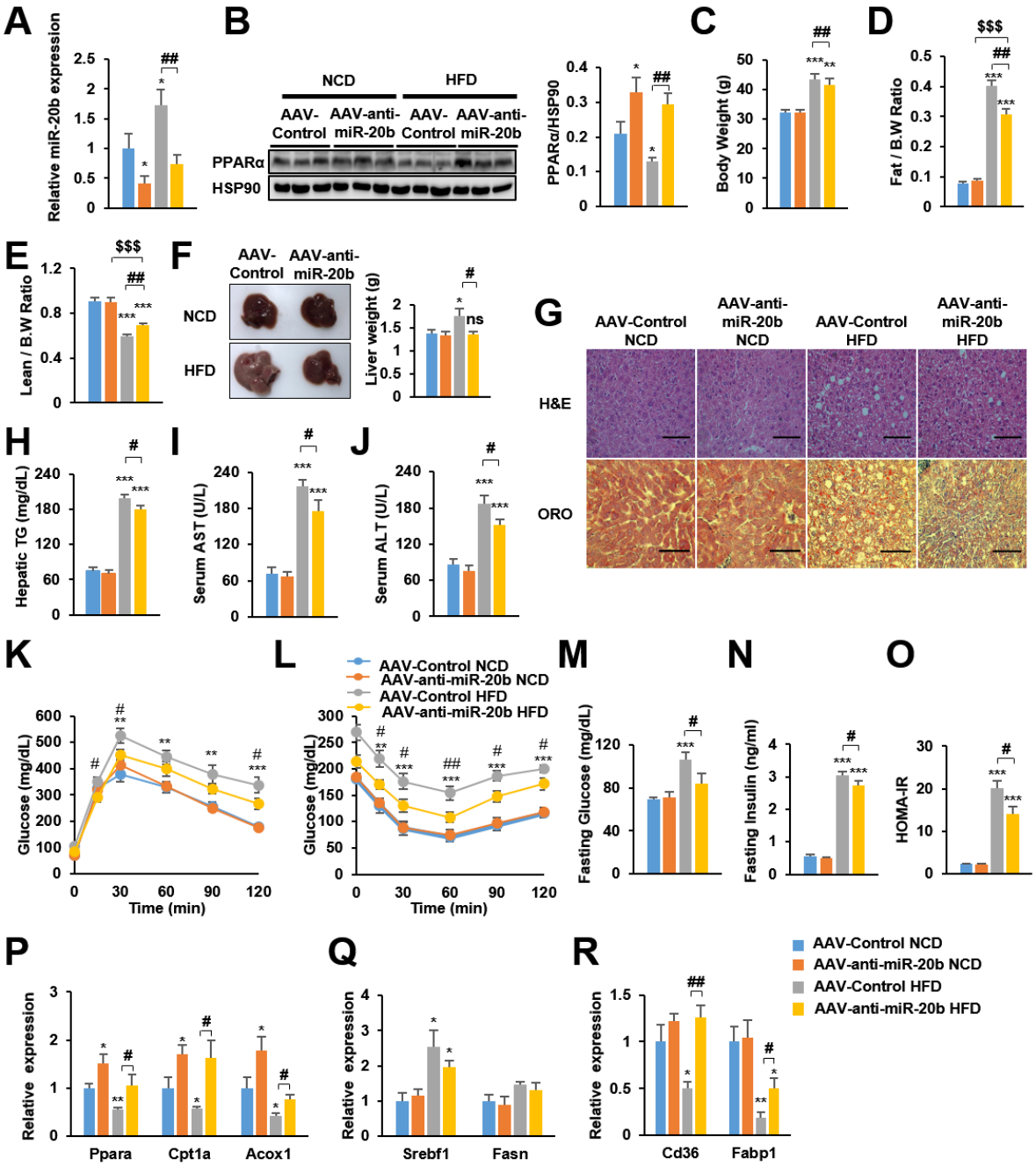

FIGURE 5. Inhibition of miR-20b alleviates hepatic steatosis in HFD-fed mice.

C57BL/6J mice were a NCD or a HFD for 12 weeks with administration of indicated AAV (n = 5 per group). Hepatic miR-20b (A) and PPARα expression (B), body weight (C), the ratio of fat mass to body weight (D), the ratio of lean mass to body weight (E), representative images of liver and liver weight (F), representative images of H&E staining and Oil Red O staining of liver slides (G), hepatic TG (H), serum AST (I), serum ALT (J), glucose tolerance (K), insulin tolerance (L), fasting glucose (M), fasting insulin (N), and HOMA-IR (O) were analyzed in indicated mice. Scale bar is 100μm. Genes related to FA β-oxidation (P), lipogenesis (Q) and FA uptake (R) were determined by quantitative RT-PCR. Relative values are normalized to AAV-Control NCD. Values represent means ± SEM (n = 5). ns, not significant, $^{*}P < 0.05$, $^{**}P < 0.01$, $^{***}P < 0.001$ *vs* AAV-Control NCD. $^{\#}P < 0.05$, $^{\#\#}P < 0.01$ *vs* AAV-Control HFD. $^{\$\$\$}P < 0.001$ *vs* AAV-anti-miR-20b NCD.

Figure 5-figure supplement 1. The weight of peripheral tissues with AAV-anti-miR-20b

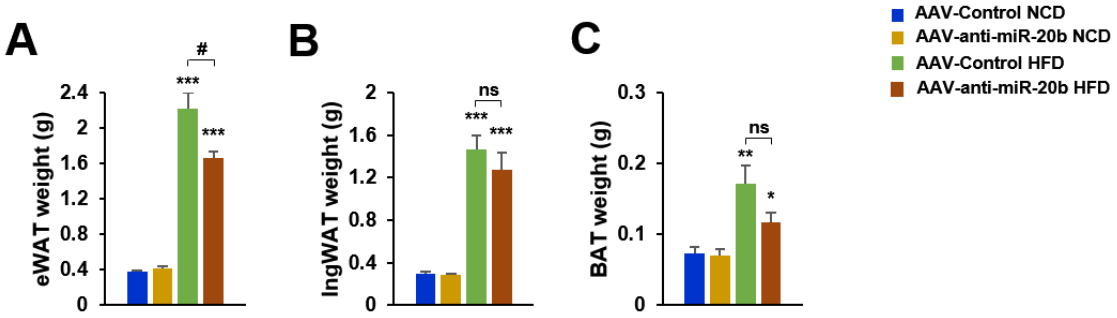

834

835 **Figure 5-figure supplement 1. The weight of peripheral tissues with AAV-anti-miR-20b.**

836 C57BL/6J fed on normal chow diet (NCD, n = 5 per group) or high fat diet (HFD, n = 5 per group) for
837 12 weeks with administration of indicated AAV. All tissues were harvested at the same time. Wet
838 weight of epididymal white adipose tissue (A), inguinal white adipose tissue (B), and brown adipose
839 tissue (C) in AAV-Control or AAV-anti-miR-20b injected mice. Values represent means ± SEM (n = 5).
840 ns, not significant. *$P < 0.05$, **$P < 0.01$, ***$P < 0.01$ *vs* AAV-Control NCD. $^{\#}P < 0.05$ *vs* AAV-Control
841 HFD.

Figure 6. The effects of miR-20b are mediated by PPARα.

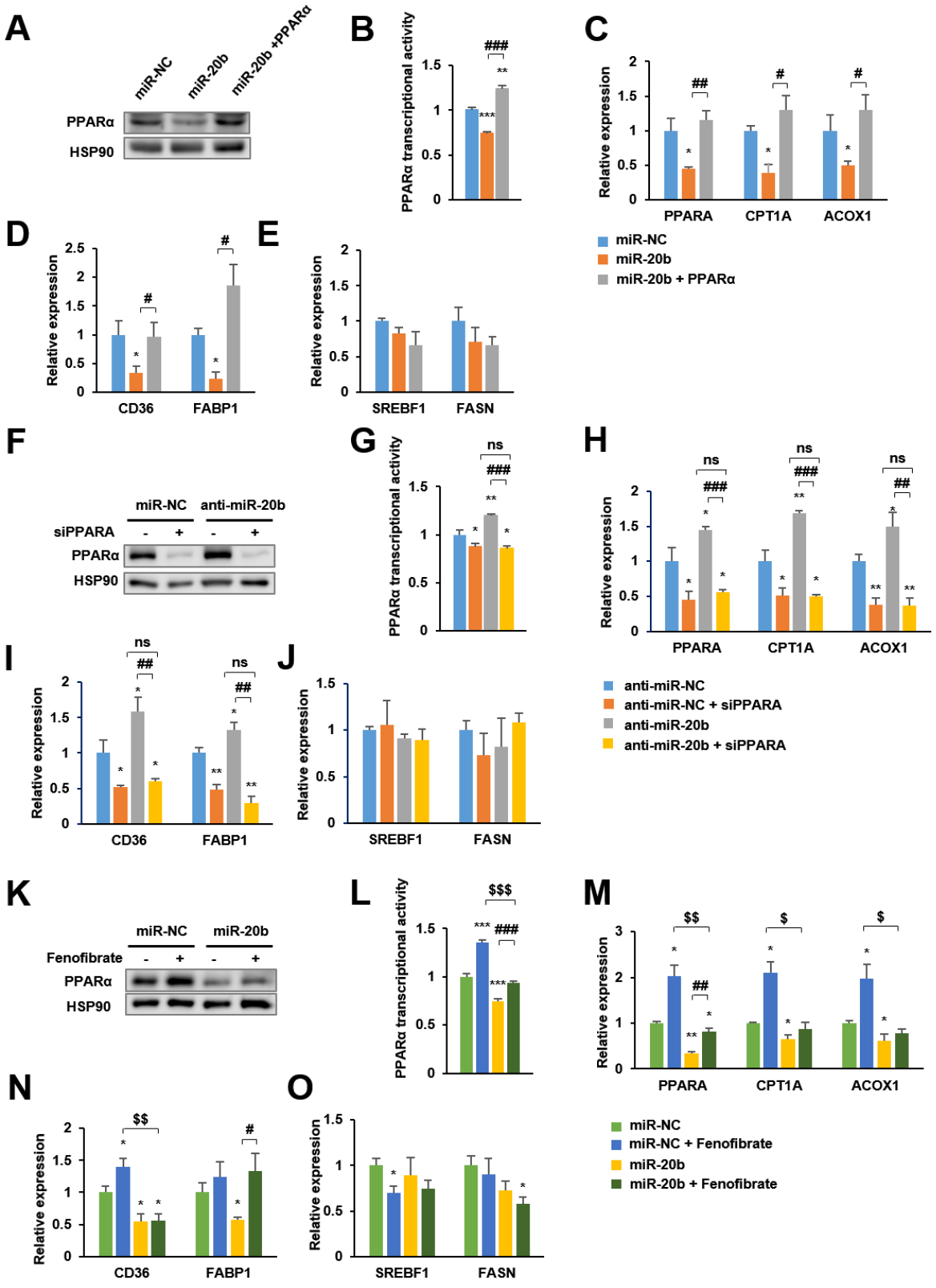

FIGURE 6. The effects of miR-20b are mediated by PPARα.

HepG2 cells transfected with indicated miRNA, siRNA, or PPARA expression vector. Western blot analysis of PPARα (A, F). Luciferase activity using the luciferase reporter DNA constructs containing PPRE (PPAR response element) was transfected in HepG2 cells. Luciferase activity was normalized to renilla activity (B, G). mRNAs level of FA β-oxidation, FA uptake, and lipogenesis were analyzed by real-time qPCR (C-E and H-J). After transfected with miR-NC or miR-20b, HepG2 cells were treated with fenofibrate (100 μM). Protein level of PPARα was analyzed by western blot (K). The transcriptional activity of PPARα was measured (L). Genes involved in of FA β-oxidation, lipogenesis and FA uptake were determined by real-time qPCR (M-O). Relative values are normalized to miR-NC. Values represent means ± SEM (n = 3). $^{*}P < 0.05$, $^{**}P < 0.01$, $^{***}P < 0.001$ *vs* miR-NC. $^{\#}P < 0.05$, $^{\#\#}P < 0.01$, $^{\#\#\#}P < 0.001$ *vs* miR-20b. $^{\$}P < 0.05$, $^{\$\$}P < 0.01$, $^{\$\$\$}P < 0.001$ *vs* miR-NC + Fenofibrate.

Figure 7. The effects of fenofibrate are limited in miR-20b-introduced mice.

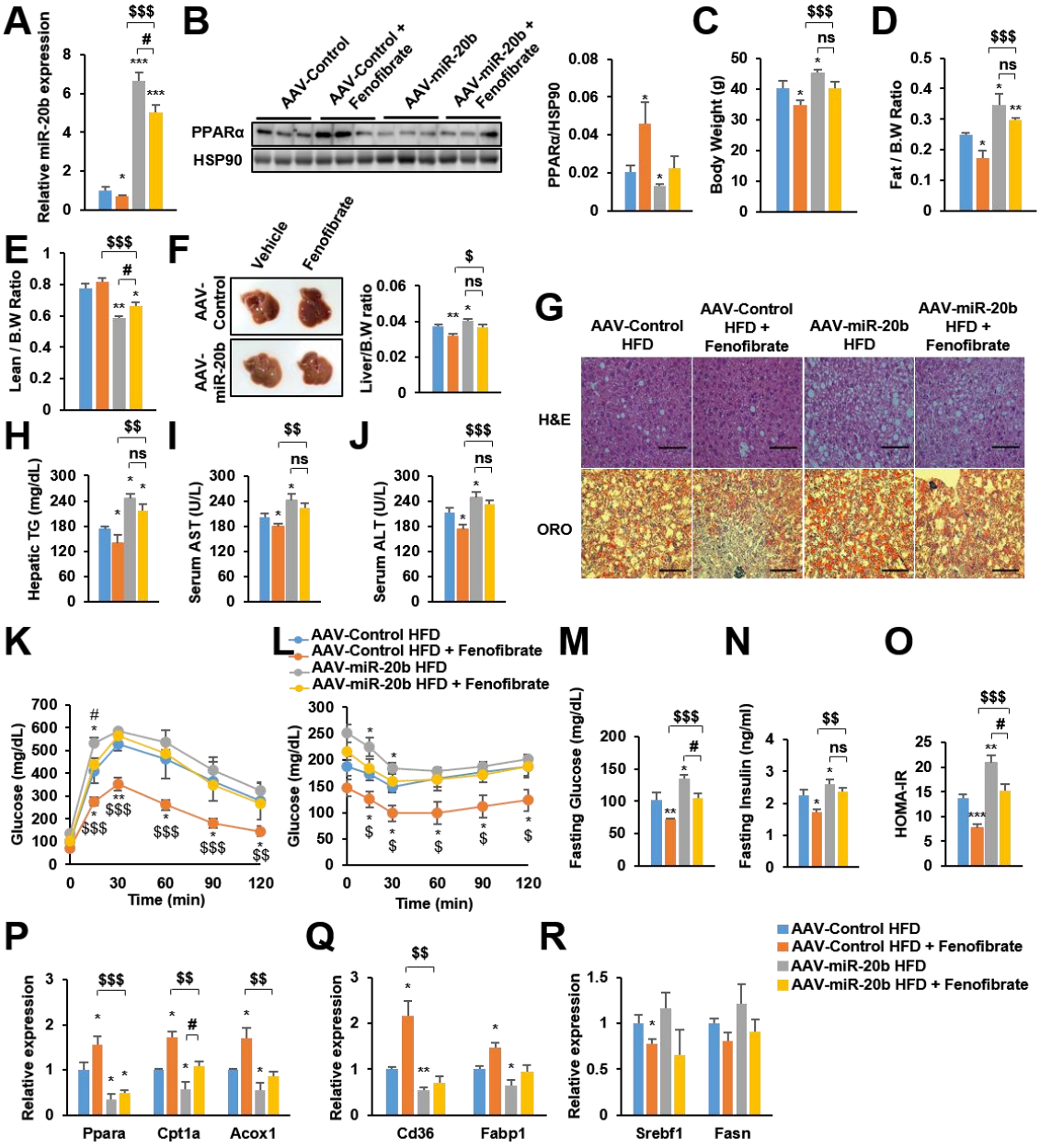

855

856

857 **FIGURE 7. The effects of fenofibrate are limited in miR-20b-introduced mice.**

858 C57BL/6J mice were fed a NCD or a HFD for 12 weeks with administration of indicated AAV (n = 5
859 per group). Then, mice injected with vehicle or fenofibrate (100 mg/kg) for 4 weeks. Hepatic miR-20b
860 (A) and PPARα expression (B), body weight (C), the ratio of fat mass to body weight (D), the ratio of
861 lean mass to body weight (E), representative images of liver and liver weight (F), representative
862 images of H&E staining and Oil Red O staining of liver slides (G), hepatic TG (H), serum AST (I),
863 serum ALT (J), glucose tolerance (K), insulin tolerance (L), fasting glucose (M), fasting insulin (N), and
864 HOMA-IR (O) were analyzed in indicated mice. Scale bar is 100μm. Genes related to FA β-oxidation
865 (P), FA uptake (Q), and lipogenesis (R) were determined by quantitative RT-PCR. Relative values are
866 normalized to AAV-Control HFD. Values represent means ± SEM (n = 5). *$P < 0.05$, **$P < 0.01$,
867 ***$P < 0.001$ vs AAV-Control HFD. ns, not significant, $^{\#}P < 0.05$ *vs* AAV-miR-20b HFD. $^{\$\$}P < 0.01$,
868 $^{\$\$\$}P < 0.001$ *vs* AAV-Control HFD + Fenofibrate.
869
870

Figure 8. miR-20b promotes liver inflammation and fibrosis in MCD-Fed Mice.

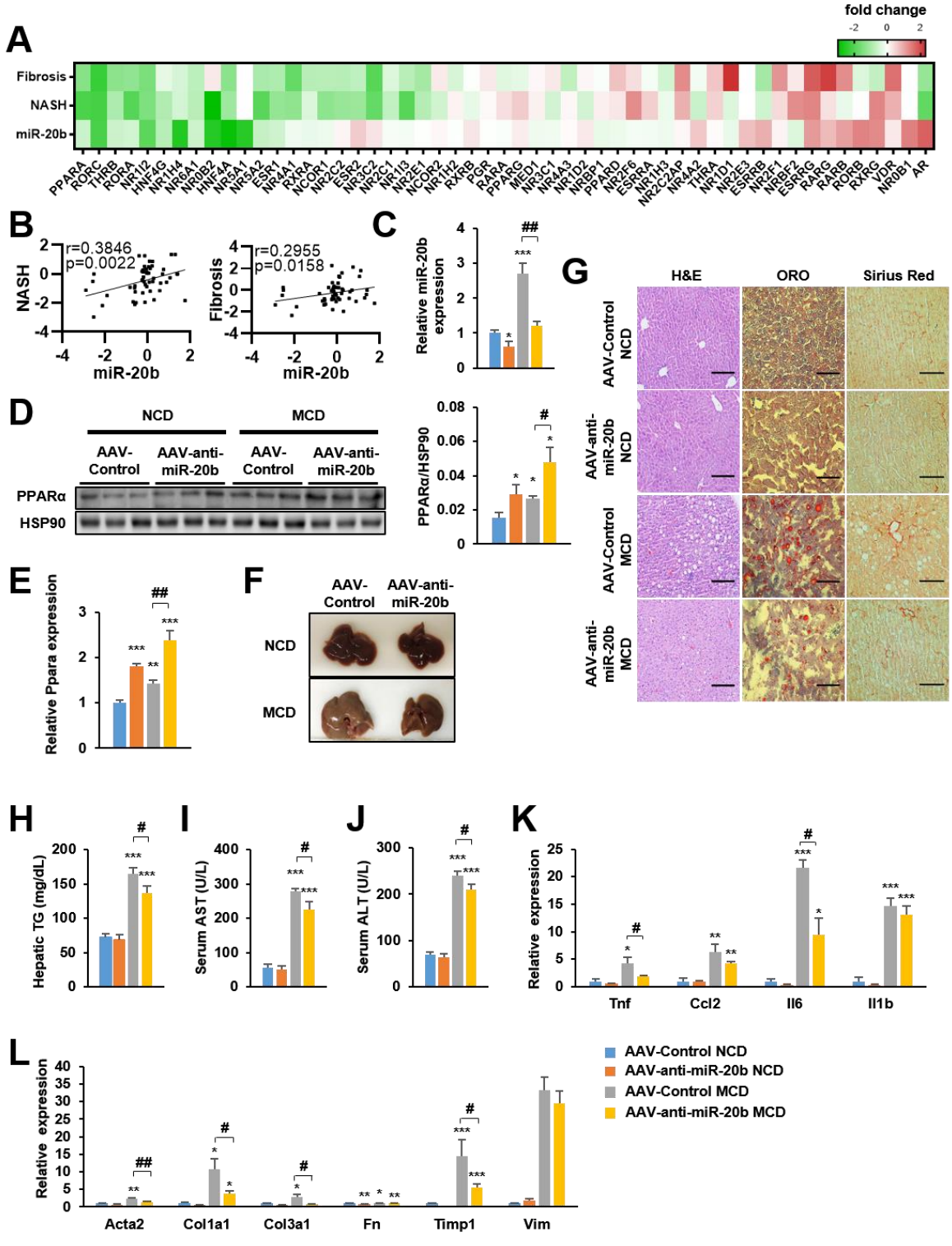

873 **FIGURE 8. miR-20b promotes liver inflammation and fibrosis in MCD-Fed Mice.**

874 Heatmap (A) and correlation (B) of hepatic nuclear receptor gene expression in RNA-seq (Figure 2)
875 with public databases of liver fibrosis or NASH patients. The values are fold change compared to
876 each control samples. C57BL/6J were fed a NCD or a MCD for 4 weeks with administration of
877 indicated AAV (n = 5 per group). Before 1 week of MCD challenge, mice were injected with AAV-
878 Control or AAV-anti-miR-20b. Hepatic miR-20b (C) and PPARα expression(D, E), representative
879 images of liver (F), H&E staining, Oil Red O staining, and Sirius Red staining of liver slides (G),
880 Hepatic TG (H), serum AST (I), and serum ALT (J) were analyzed in indicated mice. Scale bar is
881 100μm. Genes related to inflammation (K) and fibrosis (L) were determined by quantitative RT-PCR.
882 Relative values are normalized to AAV-Control NCD. Values represent means ± SEM (n = 5).
883 $*P < 0.05$, $**P < 0.01$, $***P < 0.001$ *vs* AAV-Control NCD. $^{\#}P < 0.05$, $^{\#\#}P < 0.01$ *vs* AAV-Control MCD.
884

Figure 9. E2F1 is upregulated in both NAFLD patients and mice model

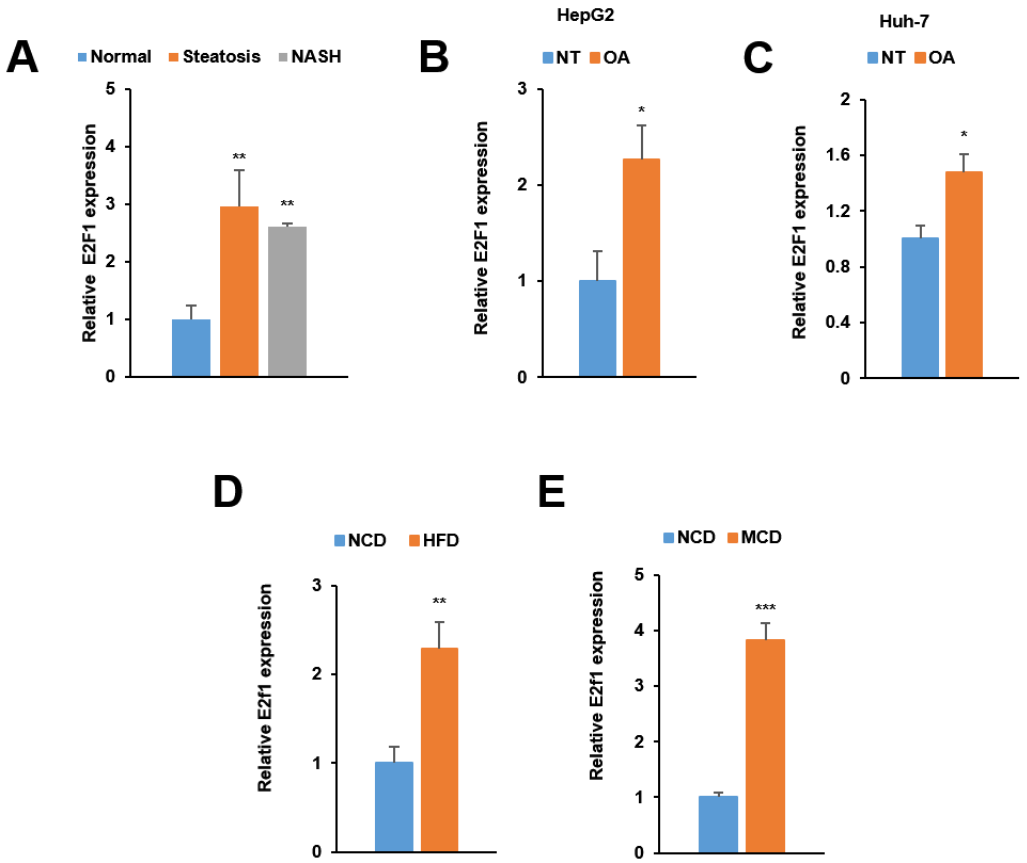

885
886

887 **Figure 9. E2F1 is upregulated in both NAFLD patients and mice model**

888 The expression of *E2F1* was analyzed by quantitative RT-PCR. Hepatic *E2F1* expression levels of
889 steatosis or NASH patients were normalized to those of normal patients. **P* < 0.05 and ***P* < 0.01 *vs*
890 normal patients (A). *E2F1* expression levels from HepG2 cells (B) and Huh-7 cells (C) treated with OA
891 for 24 h were normalized to no treatment (NT). Hepatic *E2f1* expression levels from C57BL/6J mice
892 fed a HFD (D) and a MCD (E) were normalized to NCD. Values represent means ± SEM (n = 3-5).
893 **P* < 0.05, ***P* < 0.01, ****P* < 0.001 *vs* NT in cells or NCD-fed mice, respectively.
894

Key Resources Table				
Reagent type (species) or resource	**Designation**	**Source or reference**	**Identifiers**	**Additional information**
Genetic reagent (*Mus. Musculus*)	**C57BL/6JBomTac**	DBL		
cell line (*Homo sapiens*)	HepG2	ATCC	HB-8065	
cell line (*Homo sapiens*)	Huh7	Dr. Yoshiharu Matsuura; originally from Japanese Collection of Research Bioresources Cell Bank	JCRB0403, RRID:CVCL_0336	
Antibody	Anti-PPARα	abcam	Cat# ab24509	WB 1:1000
Antibody	Anti-HSP90	Cell Signaling Technology	Cat# 4877S	WB 1:1000
Sequence-based reagent	miR-20b (miR-20b mimic)	GenePharma	N/A	Sequence: CAAAGUGC UCAUAGUG CAGGUAG
Sequence-based reagent	anti-miR-20b (miR-20b inhibitor	GenePharma	N/A	Sequence: CUACCUGC ACUAUGAG CACUUUG
Sequence-based reagent	PPARα siRNA	GenePharma	N/A	Sequence: CGGCGAGG ATAGTTCT GGAAGCTT T
Sequence-based reagent	Primers for qPCR	This paper	N/A	See Materials and Methods
Recombinant DNA reagent	psiCHECK-2-PPARα-WT (plasmid)	This paper	N/A	

Recombinant DNA reagent	psiCHECK-2-PPARα-Mut (plasmid)	This paper	N/A	
Recombinant DNA reagent	pOTTC385-pAAV CMV-IE IRES EGFP-miR-20b	This paper	N/A	
Recombinant DNA reagent	pOTTC385-pAAV CMV-IE IRES EGFP-anti-miR-20b	This paper	N/A	
commercial assay or kit	Dual-Luciferase kit	Promega	Cat# E1910	
commercial assay or kit	RNeasy mini kit	Qiazen	Cat# 74004	
commercial assay or kit	QuickChange II Site-Directed Mutagenesis Kit	Agilent	Cat# 200521	
commercial assay or kit	AAVpro® Purification Kit	Takara Bio.	Cat# 6675	
commercial assay or kit	B-hydroxybutyrate assay Kit	abcam	Cat# ab83390	
Chemical Compound, drug	Oleic acid	Sigma-Aldrich	Cat# O1008	
Chemical Compound, drug	Fenofibrate	Santa Cruz biotechnology	Cat# sc-204751	- HepG2 cells were treated with fenofibrate (100 µM) - mice injected with fenofibrate (100 mg/kg)

895

Figure 1. miR-20b significantly increases in the livers of dietary obese mice and human.

A

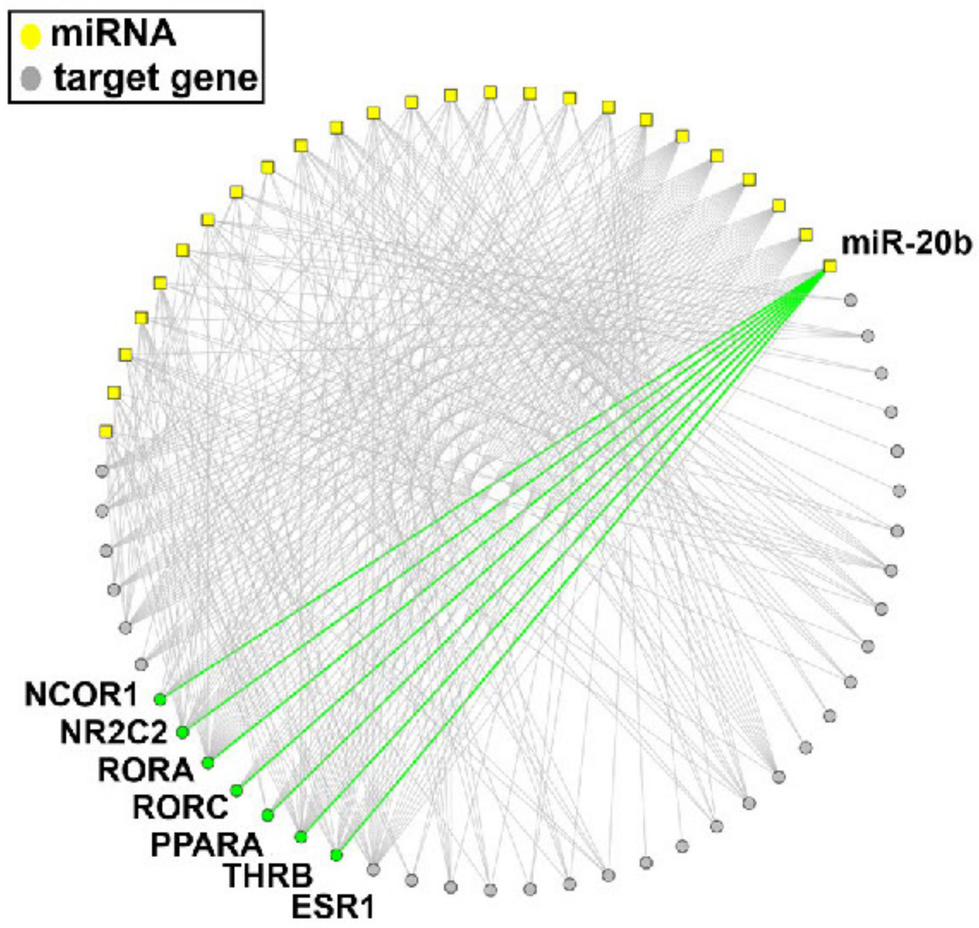

Rank	microRNA	adjusted *p*-value
1	hsa-miR-129	0.0120
2	hsa-miR-219a	0.0158
3	hsa-miR-4782	0.0158
4	hsa-miR-6766	0.0158
5	hsa-miR-20b	0.0474
6	hsa-miR-20a	0.0474
7	hsa-miR-106a	0.0474
8	hsa-miR-106b	0.0474
9	hsa-miR-17	0.0474
10	hsa-miR-519d	0.0474

B

microRNA	Fold change	adjusted *p*-value
hsa-miR-20b	1.226639893	0.0080
hsa-miR-106a	1.078651094	0.0894
hsa-miR-129	1.031414803	0.3217
hsa-miR-106b	0.982514098	0.3020
hsa-miR-519d	0.935426862	0.1644
hsa-miR-17	0.923967423	0.0079
hsa-miR-219a	0.919478183	0.0504
hsa-miR-20a	0.553090004	0.0002

C

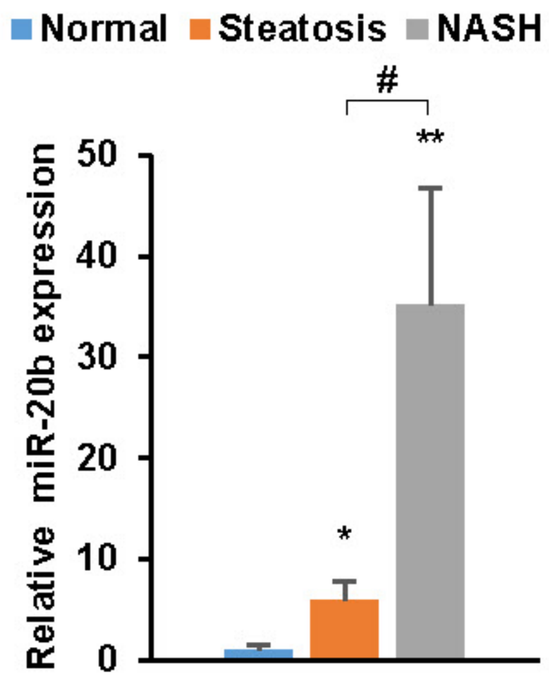

D

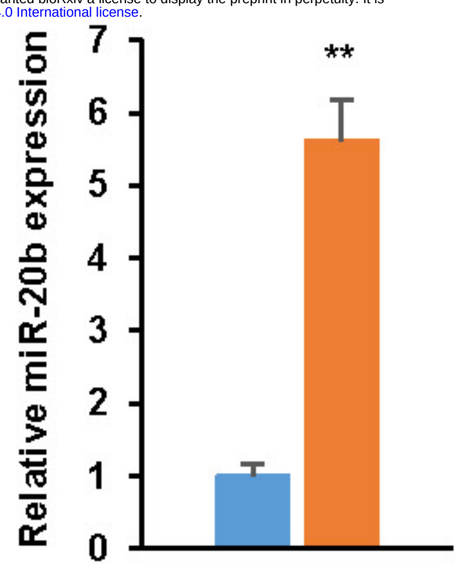

E

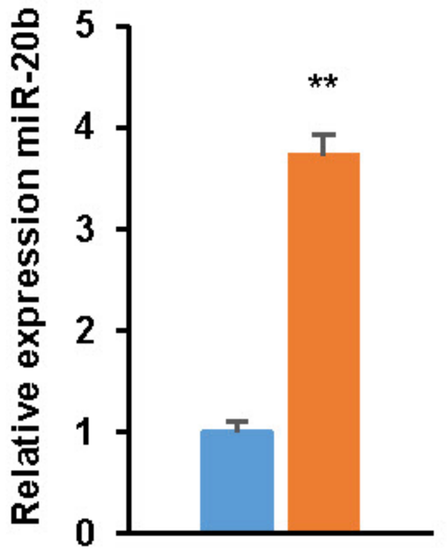

F

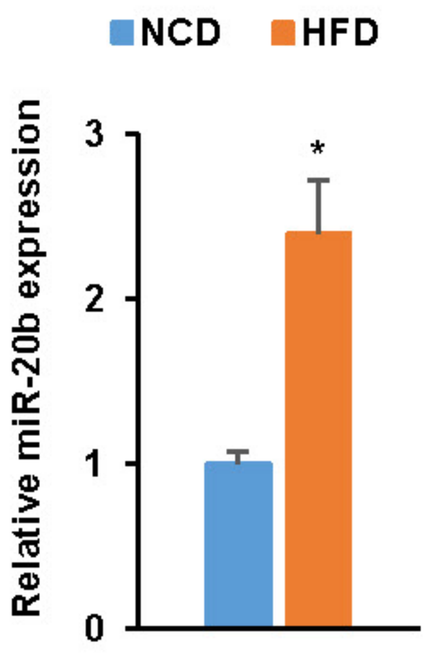

G

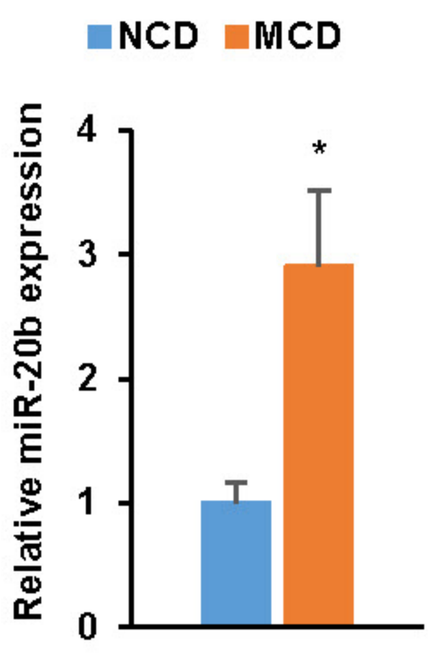

H

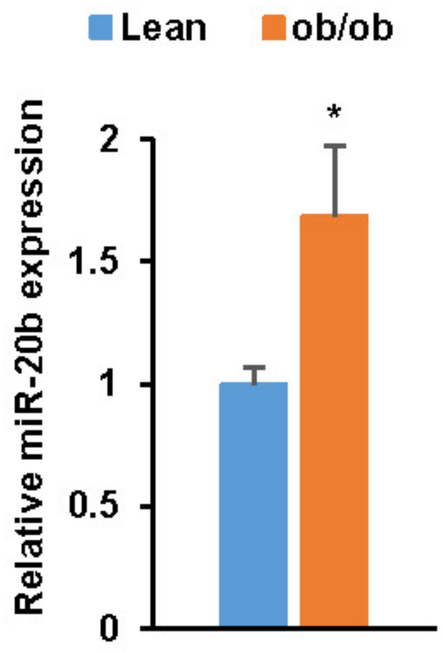

Figure 1-figure supplement 1. Clinical characteristics of patients with control individuals (N=5), steatosis (steatosis > 50%, N=4) and NASH patients (N=4).

Patients	Normal					Steatosis				NASH			
Age (years)	54	45	41	59	58	58	72	54	70	61	67	71	68
Gender	F	M	F	M	M	M	M	F	M	M	M	M	F
Weight (kg)	60.5	67	66.15	73.75	51.1	59.1	70.1	54.91	62.5	73.5	58.7	58.7	65.16
BMI	26.39	22.65	24.33	27.22	18.2	23.92	25.29	21.97	22.98	24.7	21.02	23.5	27.34
AST (IU/L)	26	13	26	28	18	20	23	28	20	31	58	20	64
ALT (IU/L)	30	38	20	28	20	33	23	9	16	35	32	21	31
GGT (IU/L)	30	N/A	33	31	26	26	34	11	38	110	136	37	158
ALP (IU/L)	47	60	73	74	93	62	70	63	68	99	77	63	88
Billirubin (mg/dL)	0.9	0.9	1.1	1.1	0.7	0.6	1	0.7	0.4	0.7	0.5	0.5	0.9
INR	0.97	1.06	1	1.03	0.97	1	0.93	1.07	1	1.01	0.97	1.09	1
Total Cholesterol (mg/dL)	203	88	179	162	178	171	115	169	148	238	161	260	258

Figure 2. PPARα is a direct target of miR-20b.

Figure 2-figure supplement 1. Analysis of PPARα related pathway in RNA-seq of miR-20b overexpressed HepG2 cells.

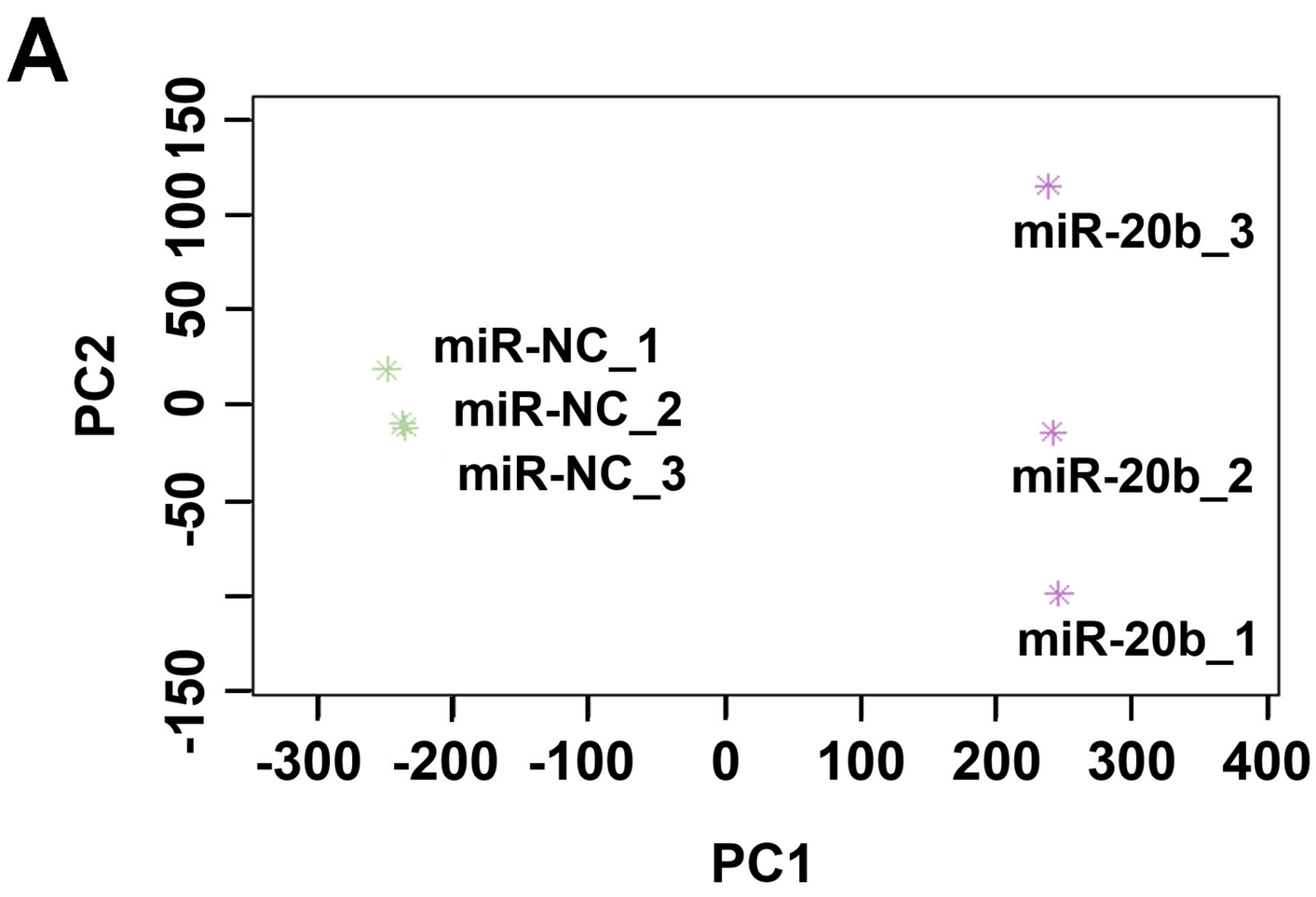

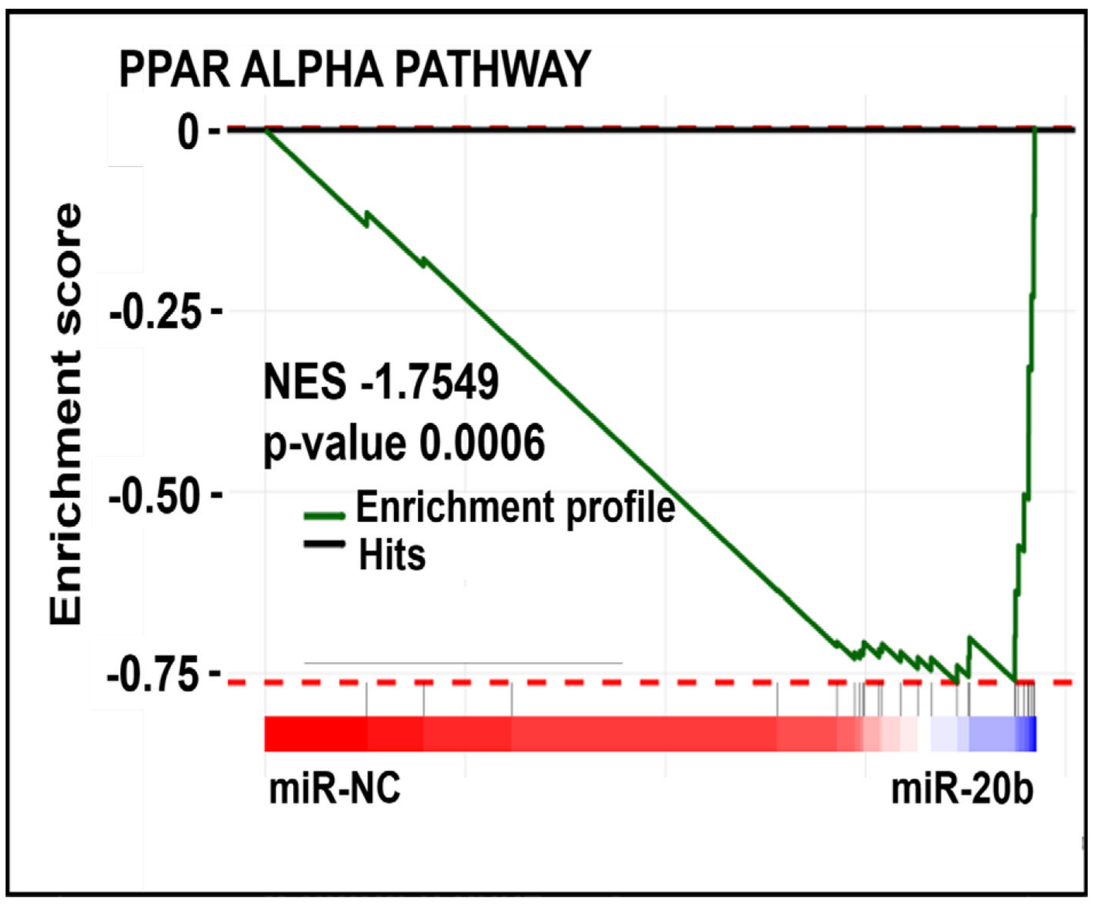

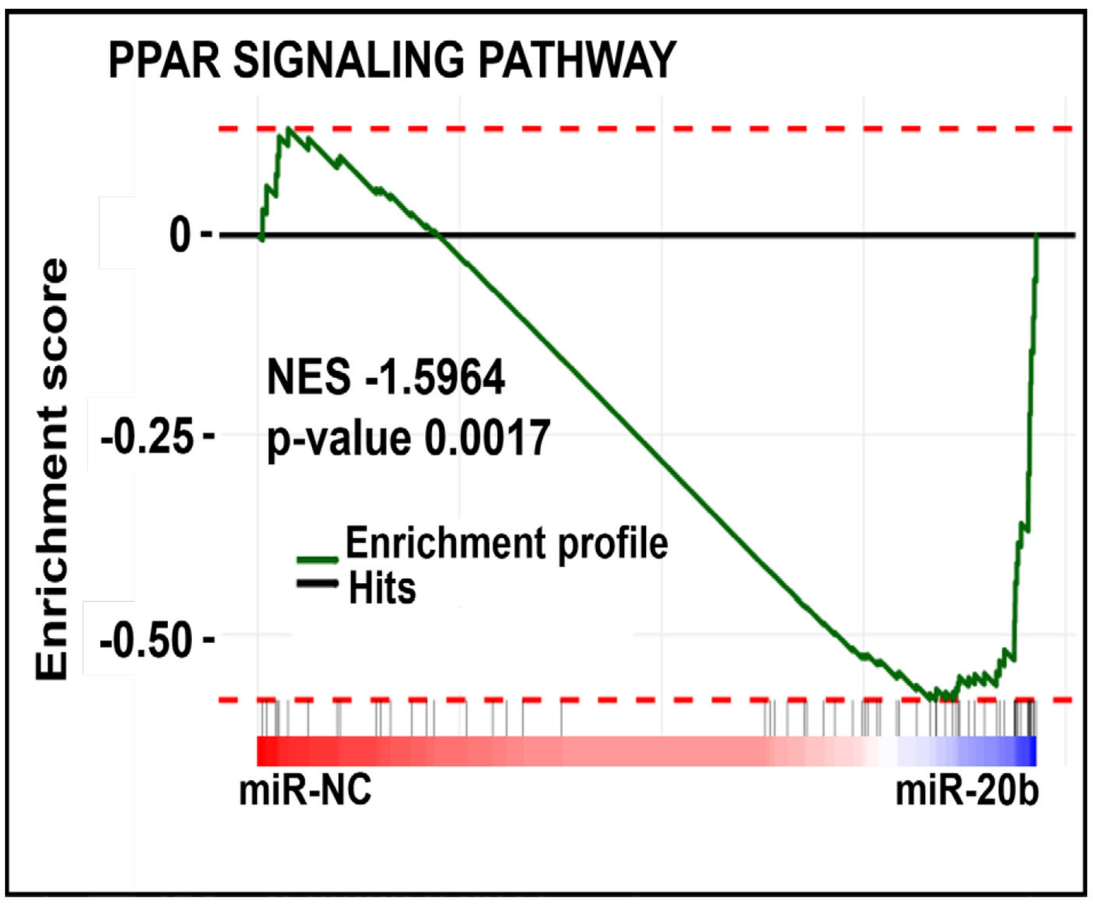

Figure 2-figure supplement 2. PPARα is the primary target of the overlapped candidates.

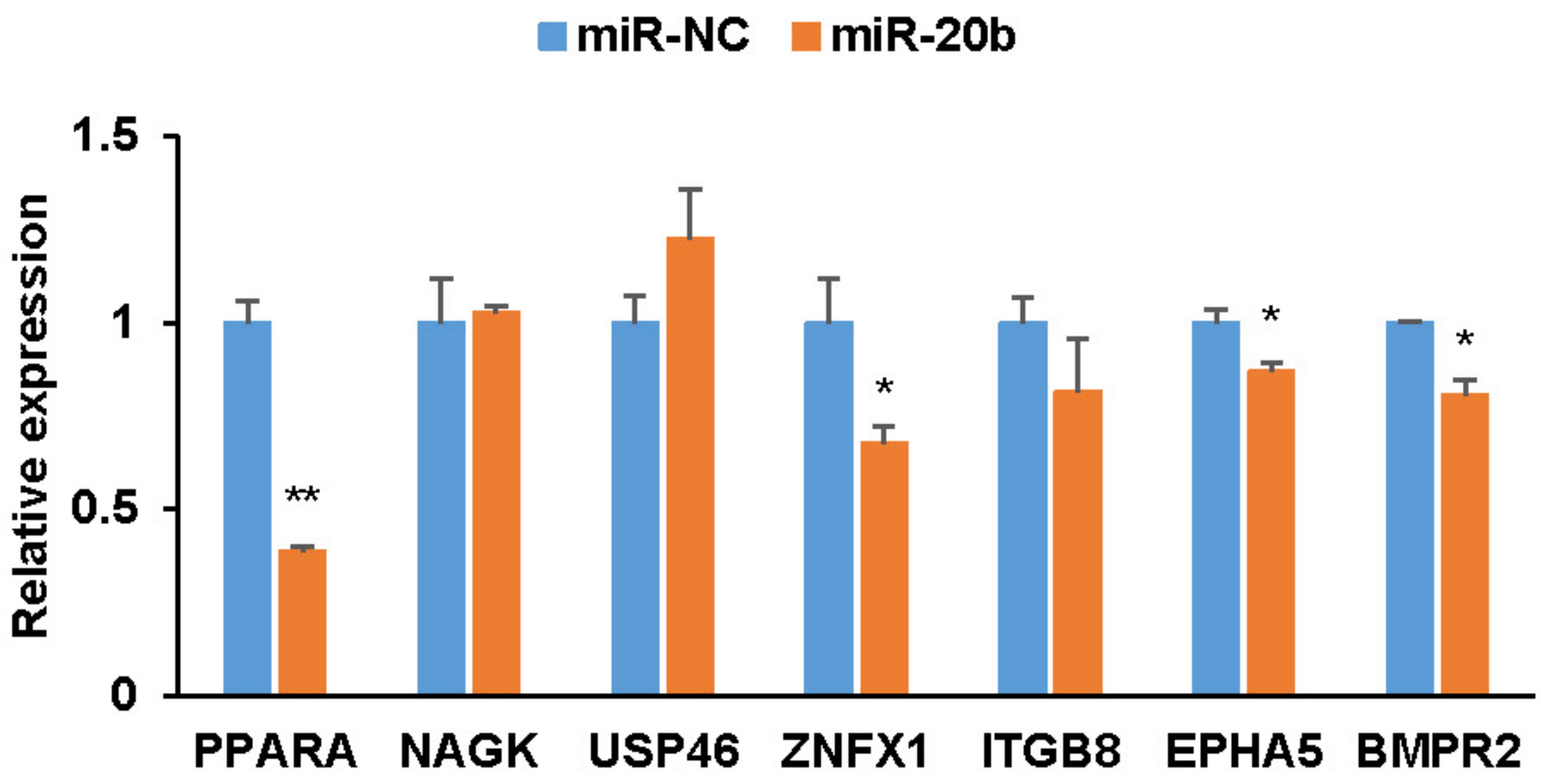

Figure 3. miR-20b regulates fatty acid metabolism.

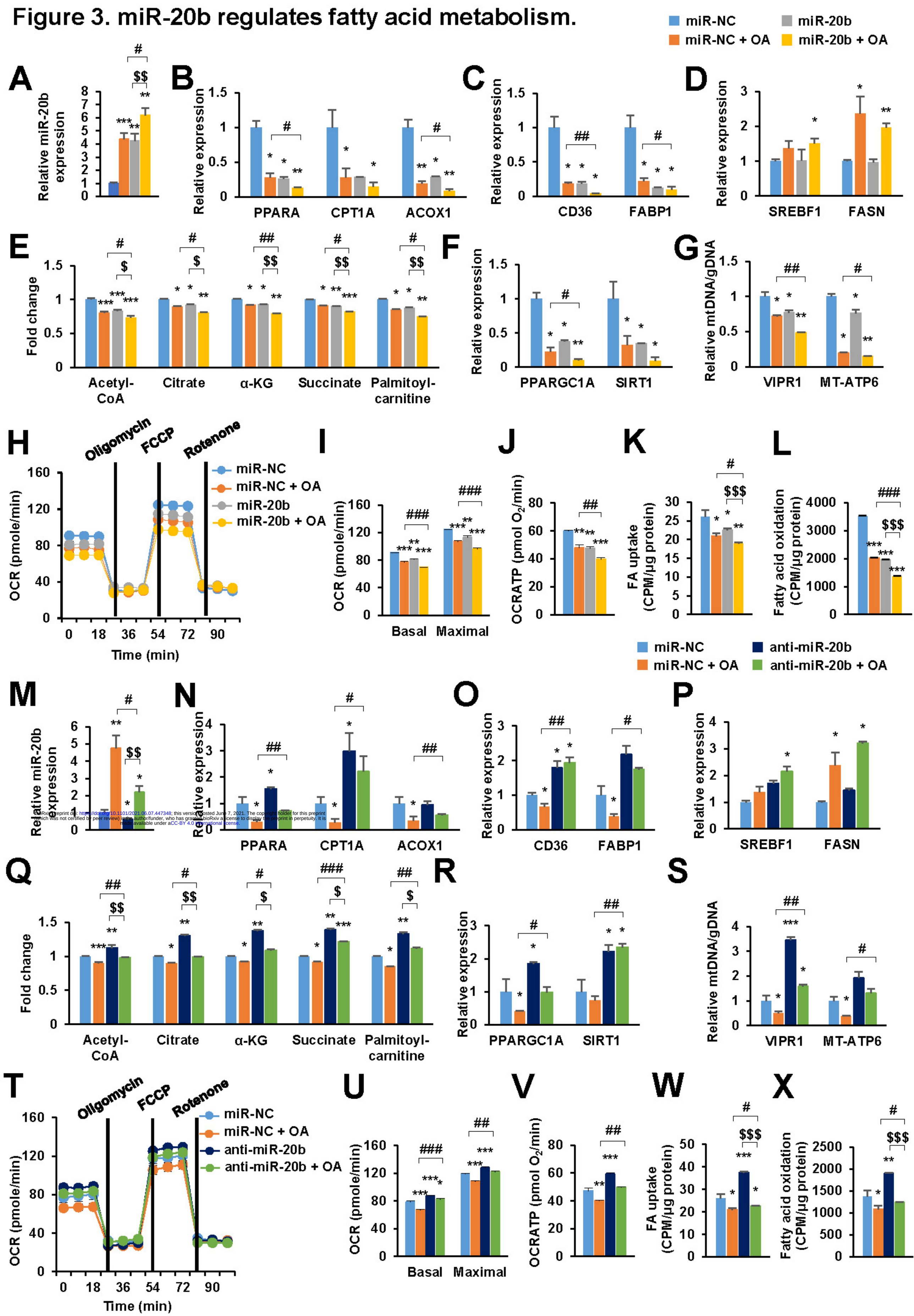

Figure 3-figure supplement 1. The expression of PPARα is regulated both in human and mice.

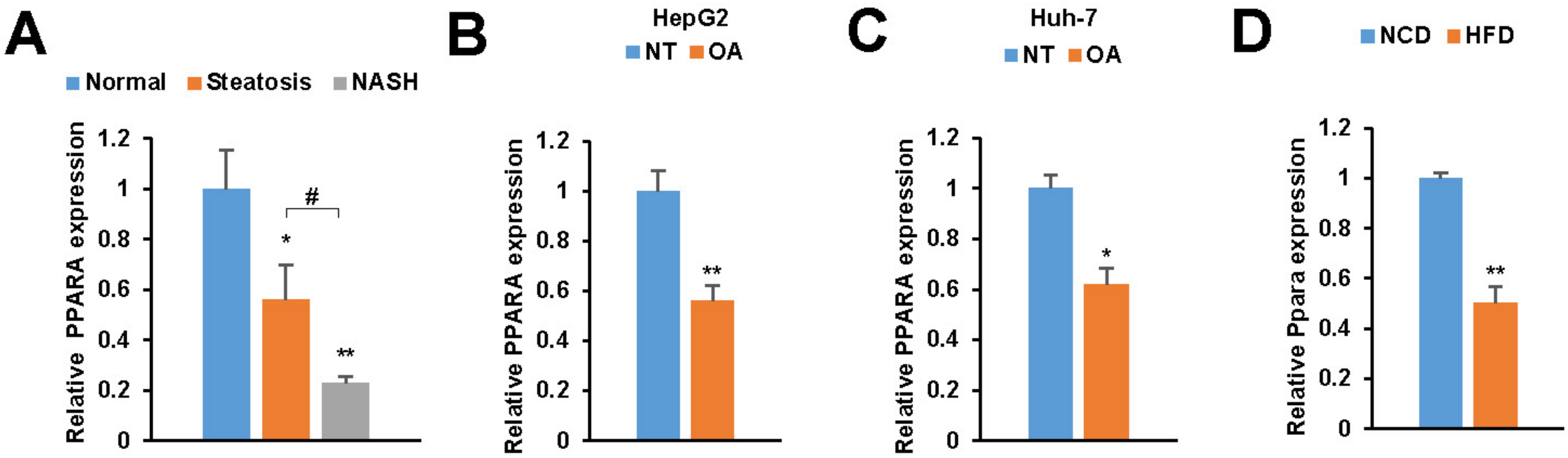

Figure 3-figure supplement 2. miR-20b induces hepatic steatosis in primary hepatocytes

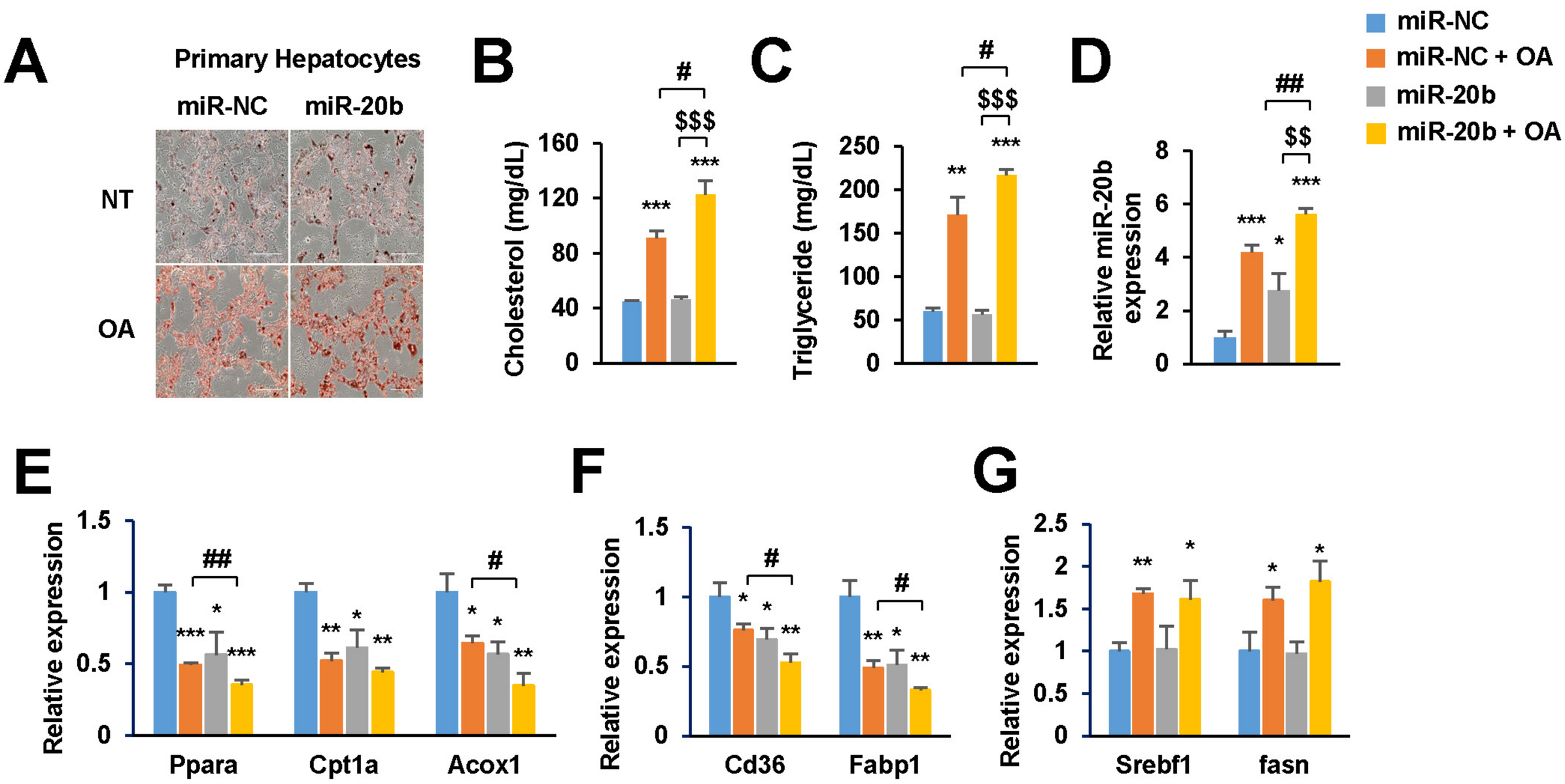

Figure 3-figure supplement 3. Ketogenesis is not regulated by miR-20b in HepG2 cells.

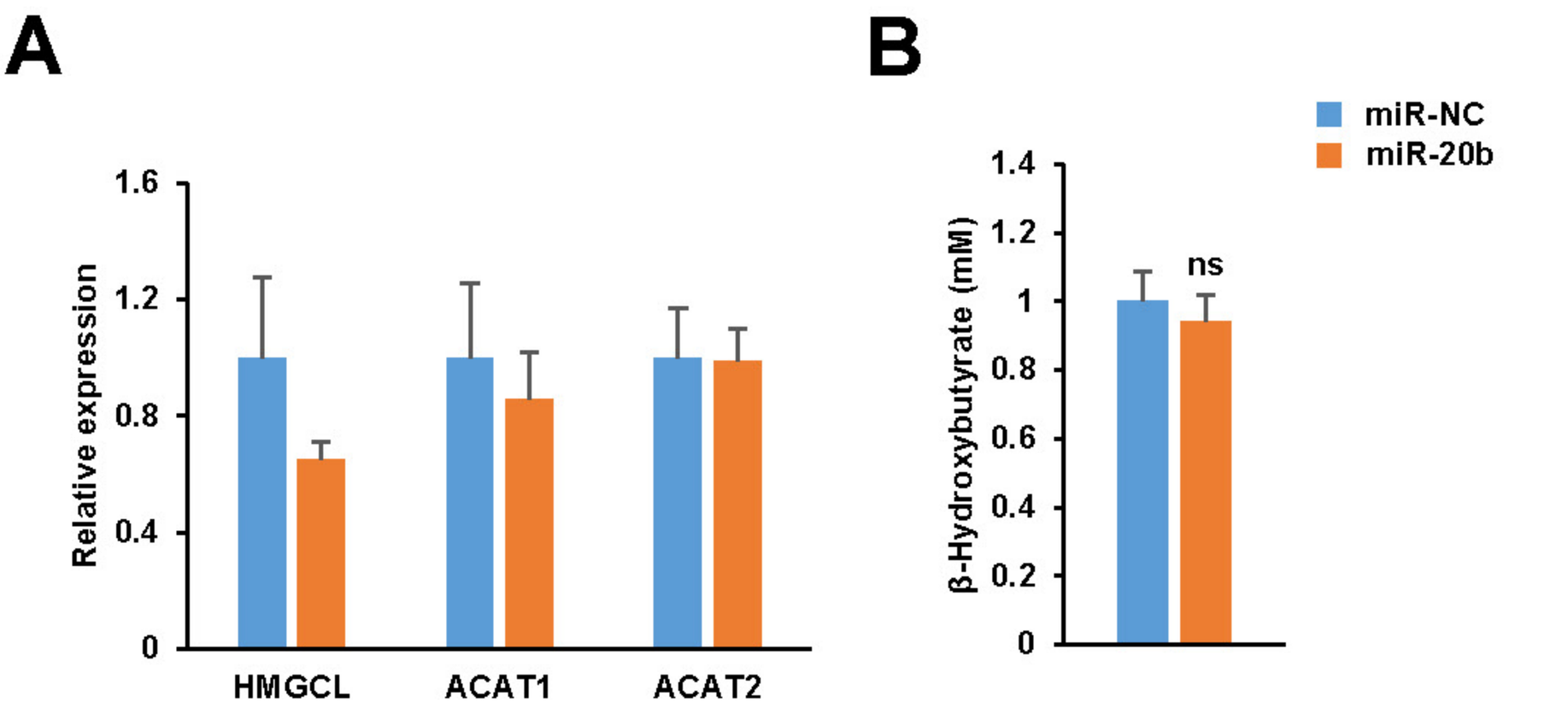

Figure 3-figure supplement 4. Inhibition of miR-20b alleviates hepatic steatosis in HepG2 cells.

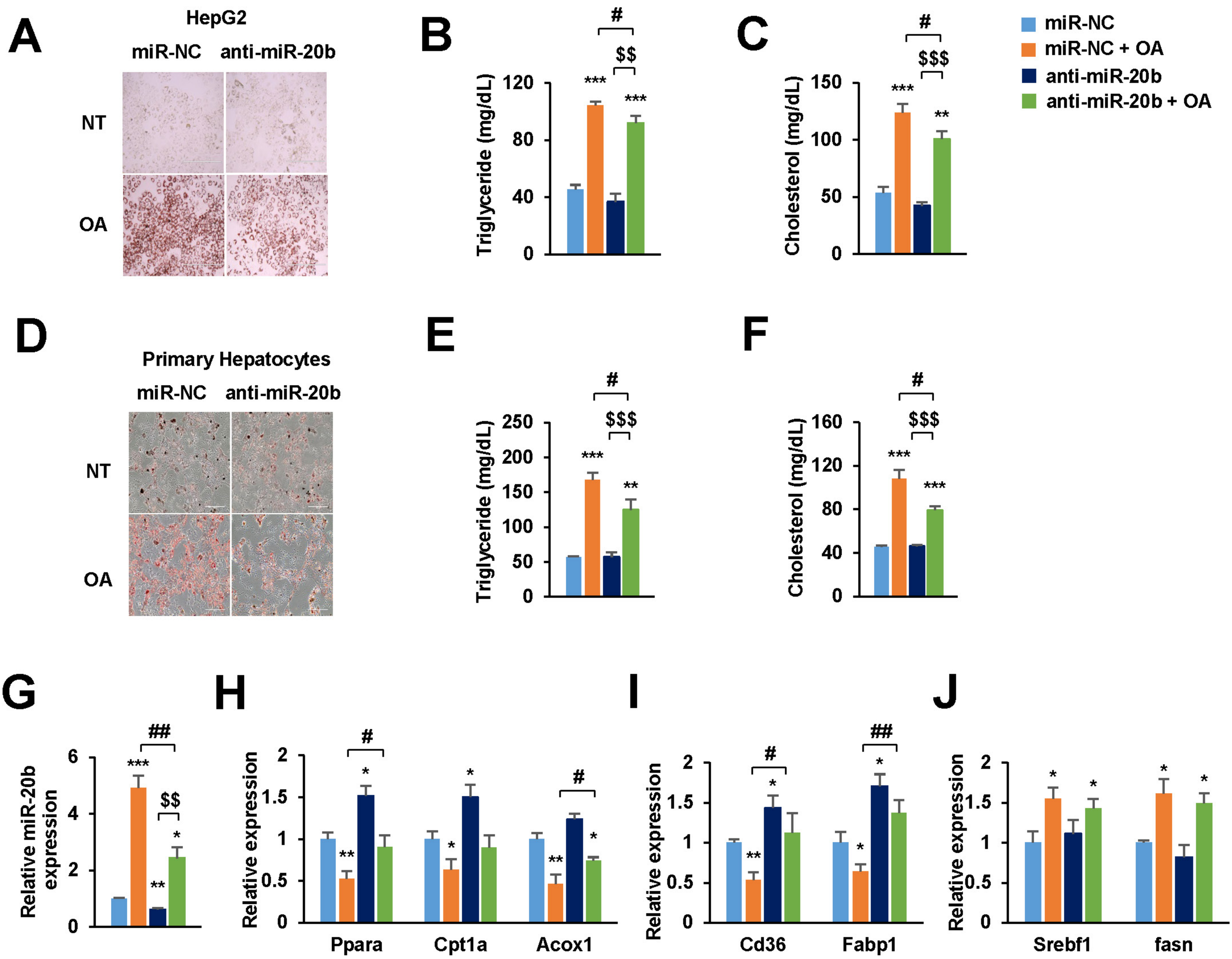

Figure 4. miR-20b promotes hepatic steatosis in HFD-fed mice

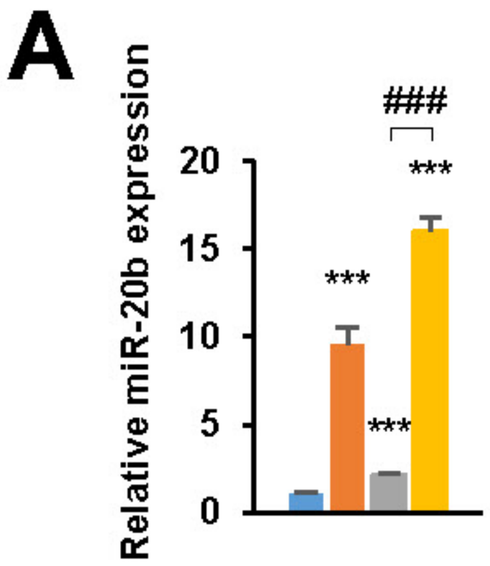

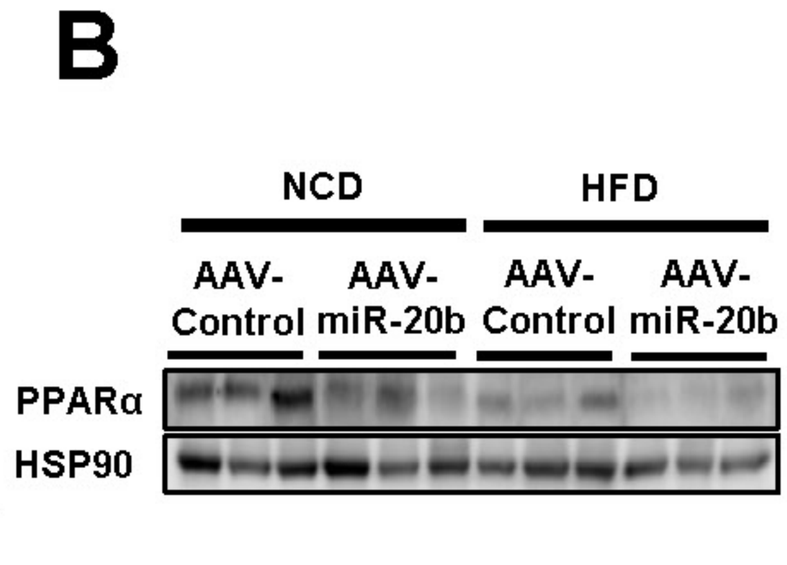

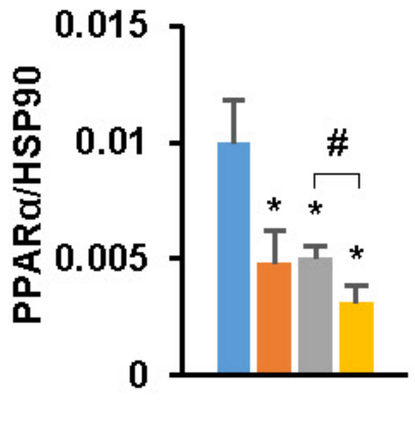

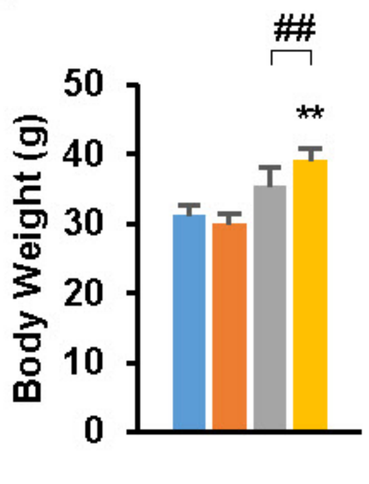

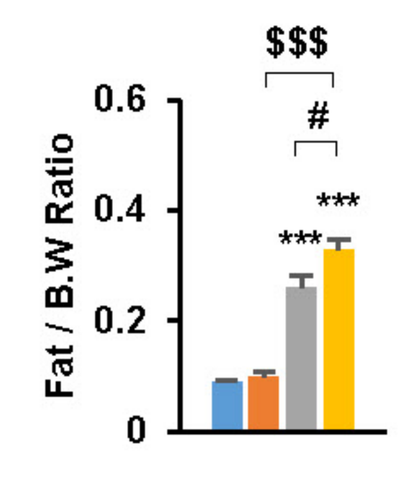

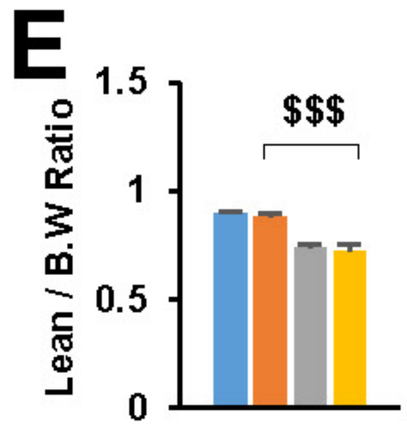

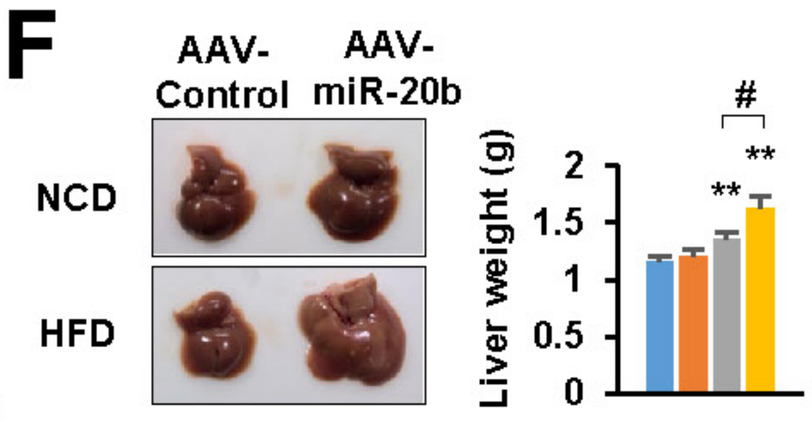

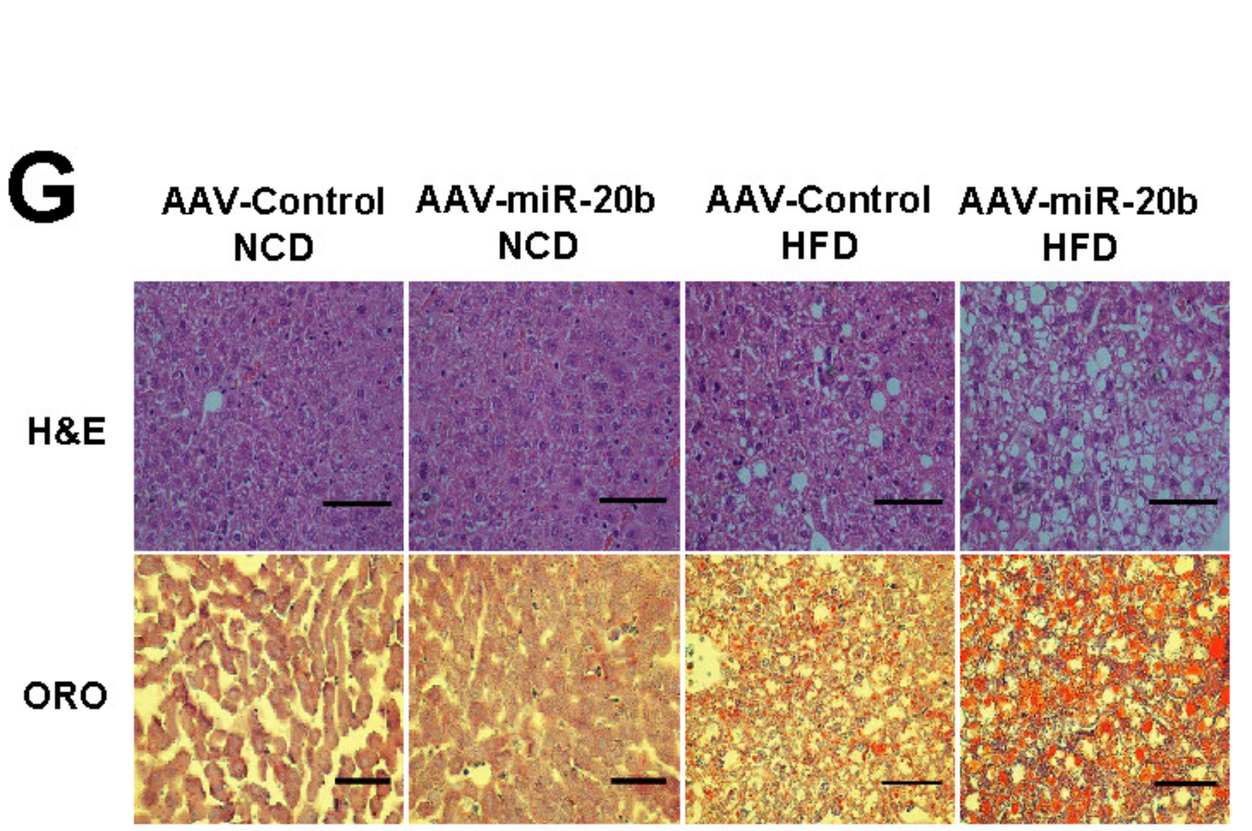

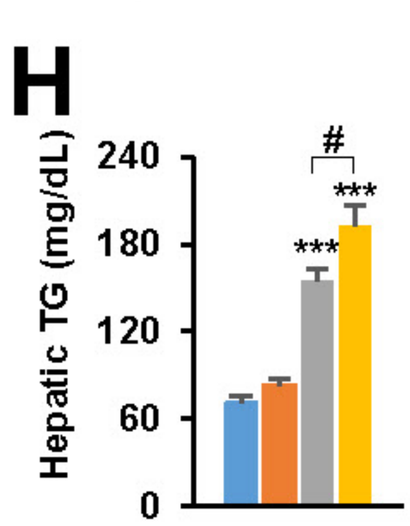

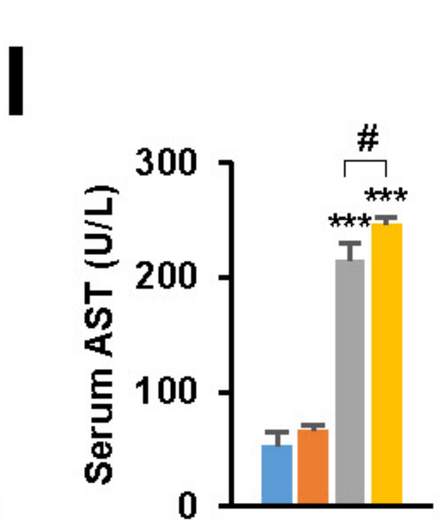

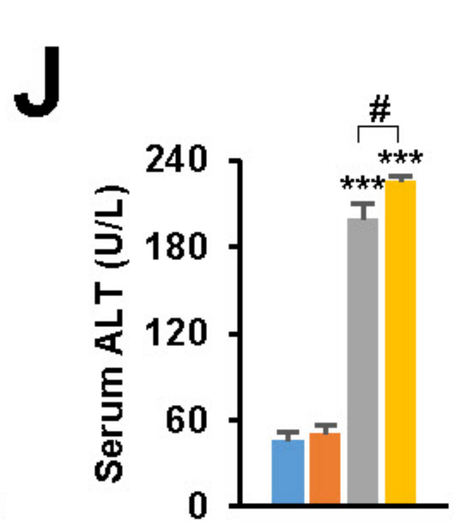

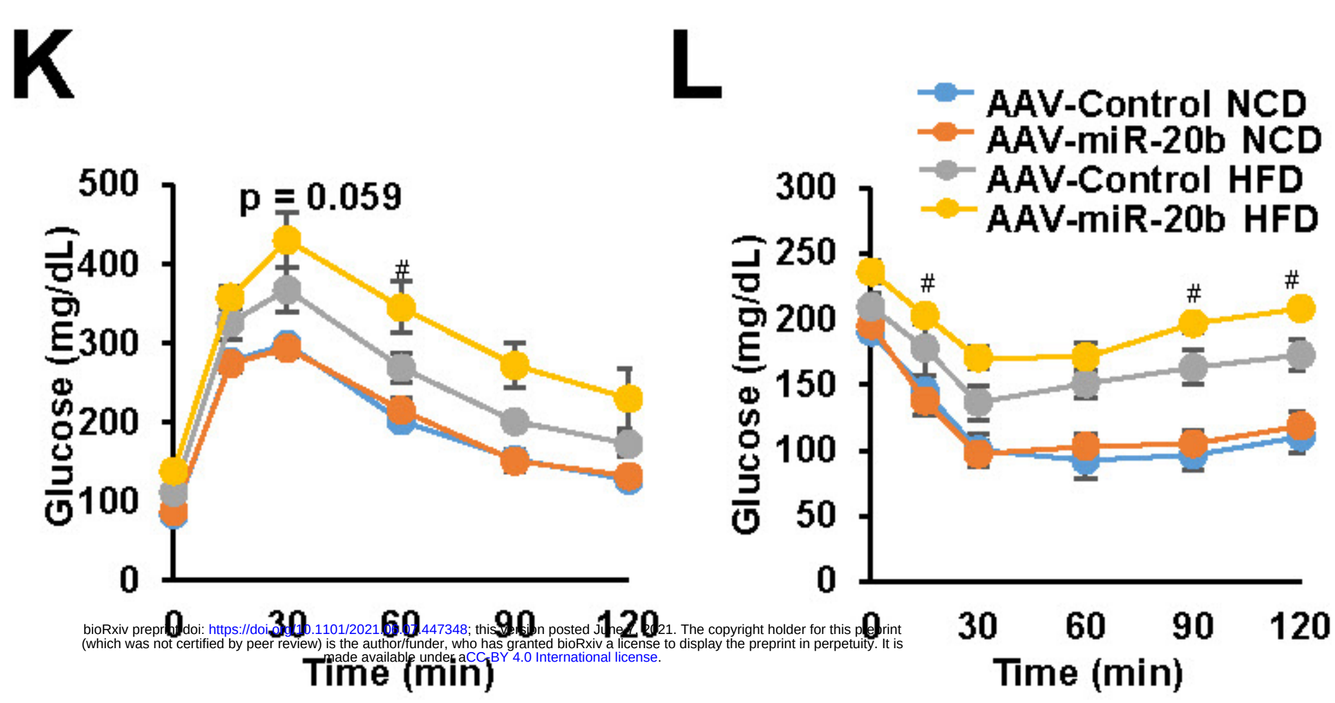

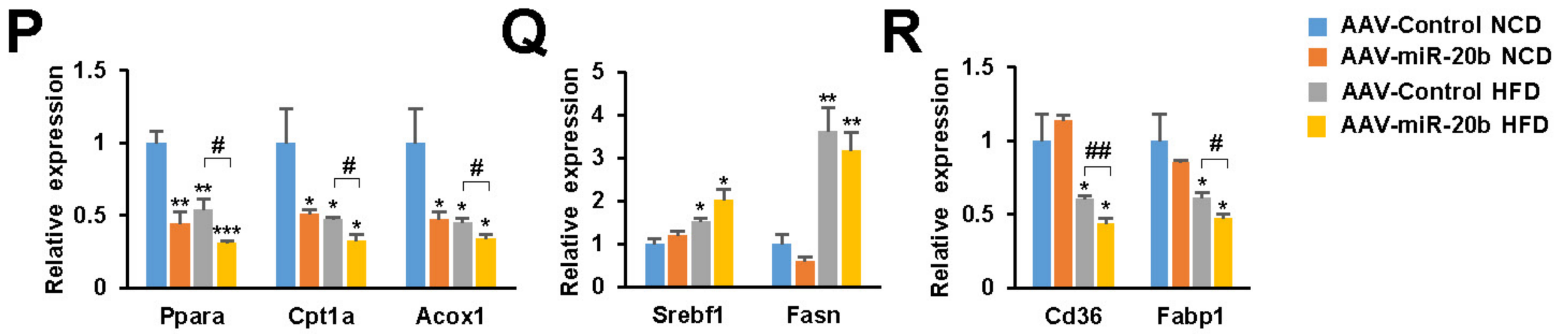

Figure 4-figure supplement 1. The expression of miR-20b in peripheral tissues.

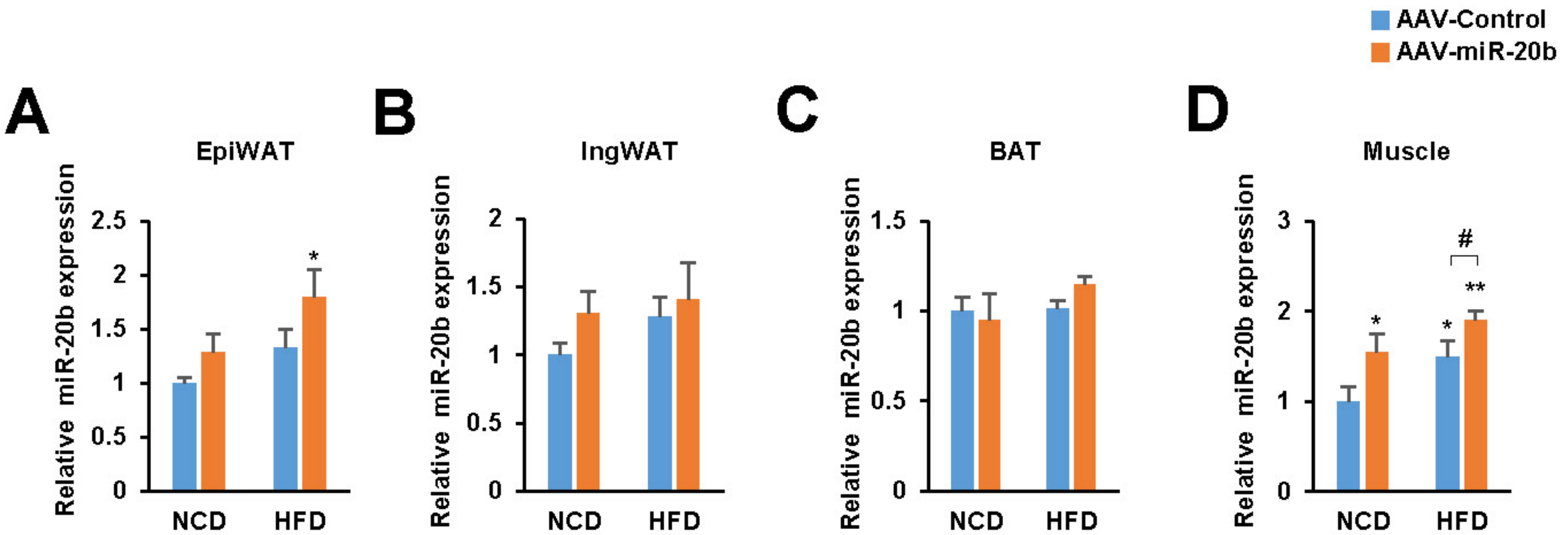

Figure 4-figure supplement 2. The weight of peripheral tissues with AAV-miR-20b

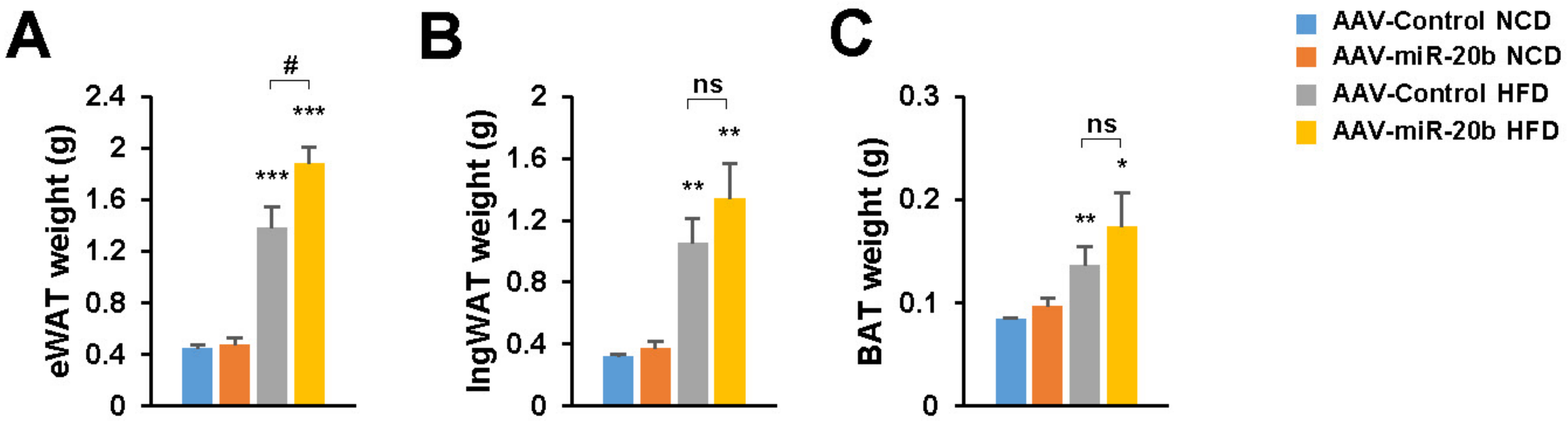

Figure 5. Inhibition of miR-20b alleviates hepatic steatosis in HFD-fed mice.

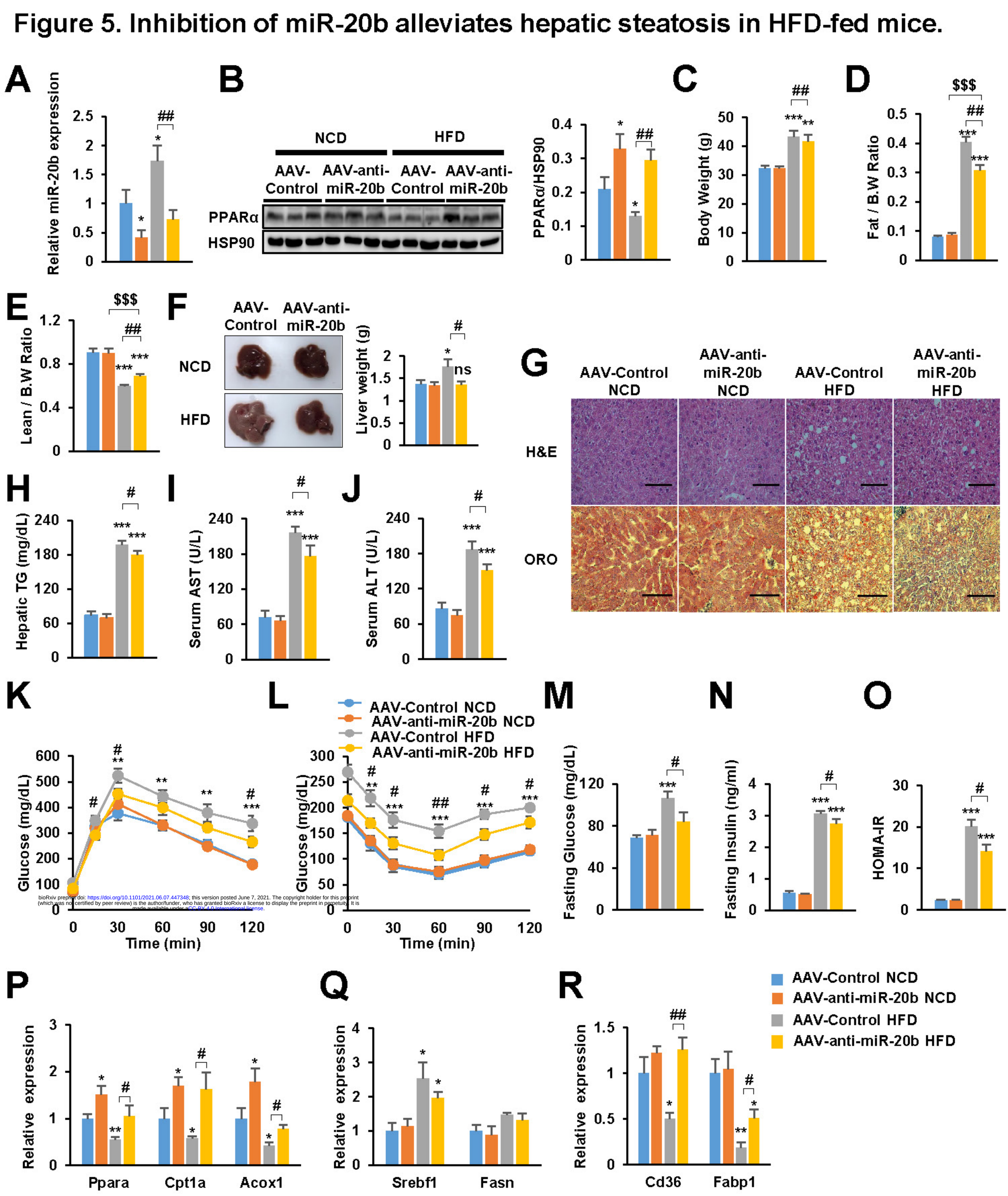

Figure 5-figure supplement 1. The weight of peripheral tissues with AAV-anti-miR-20b

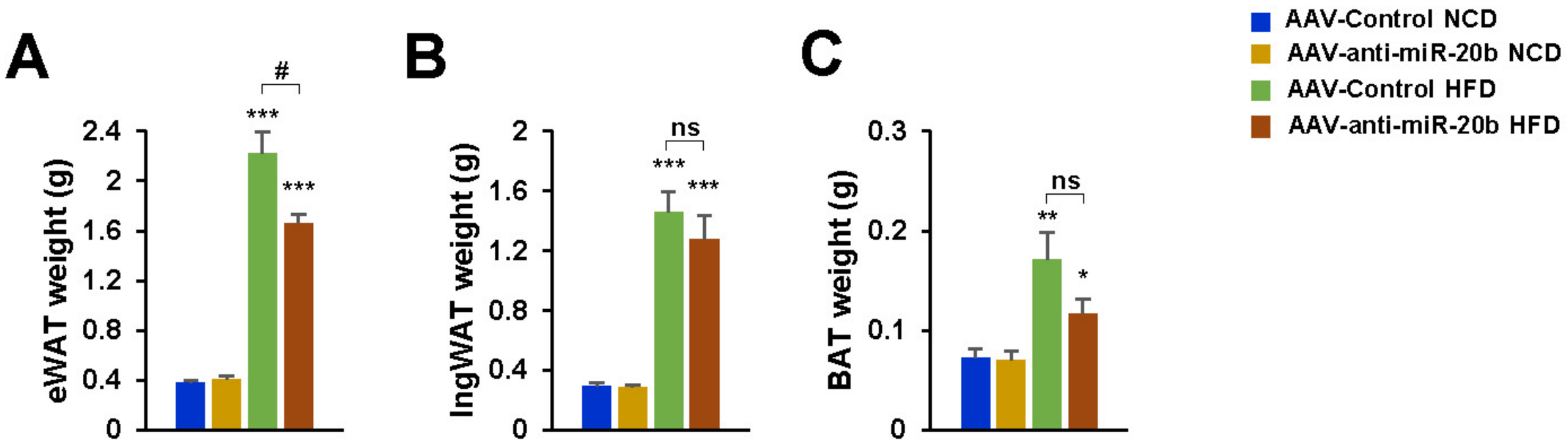

Figure 6. The effects of miR-20b are mediated by PPARα.

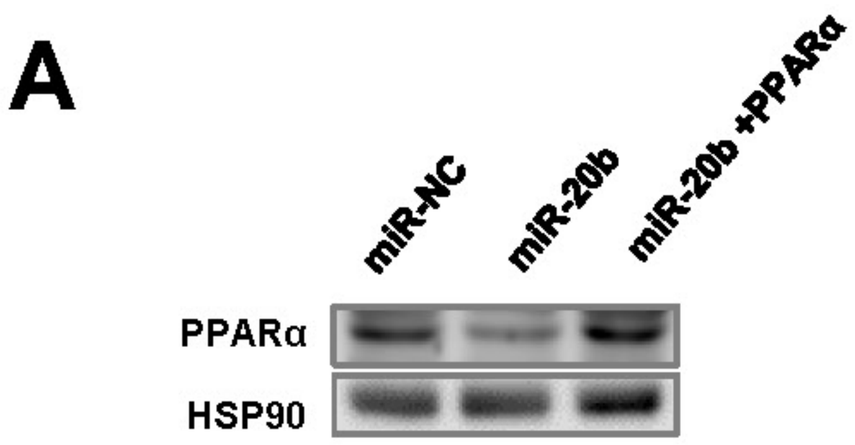

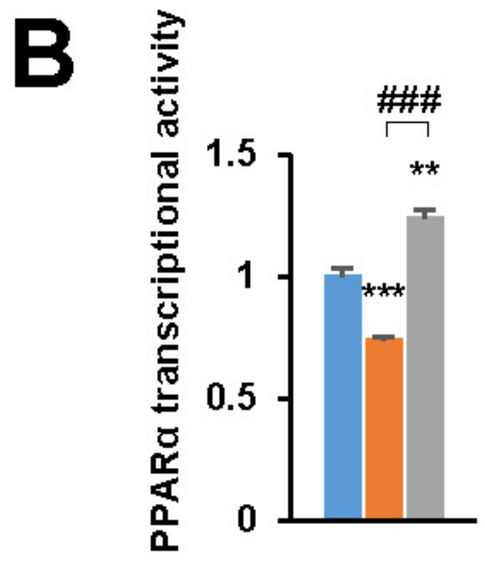

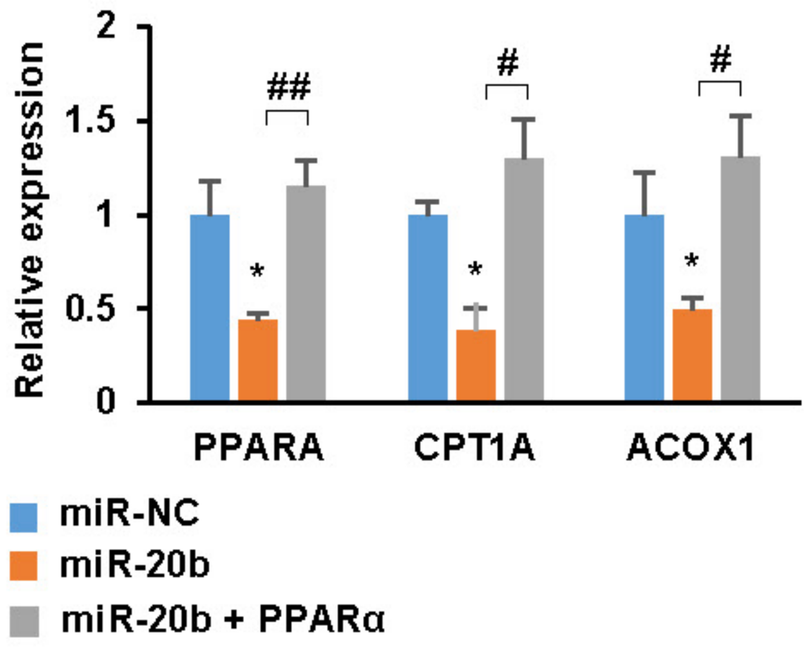

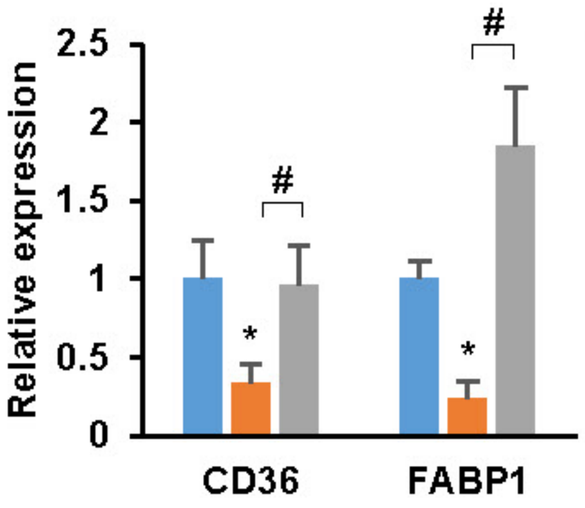

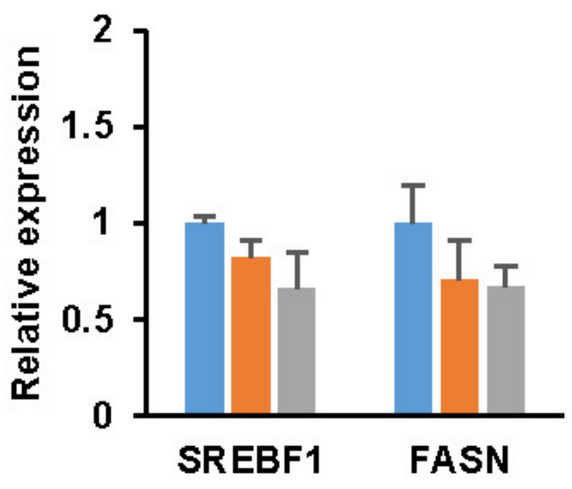

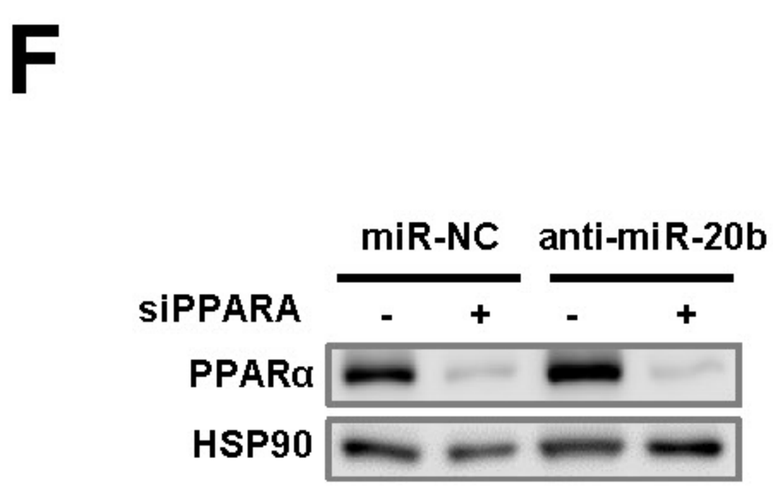

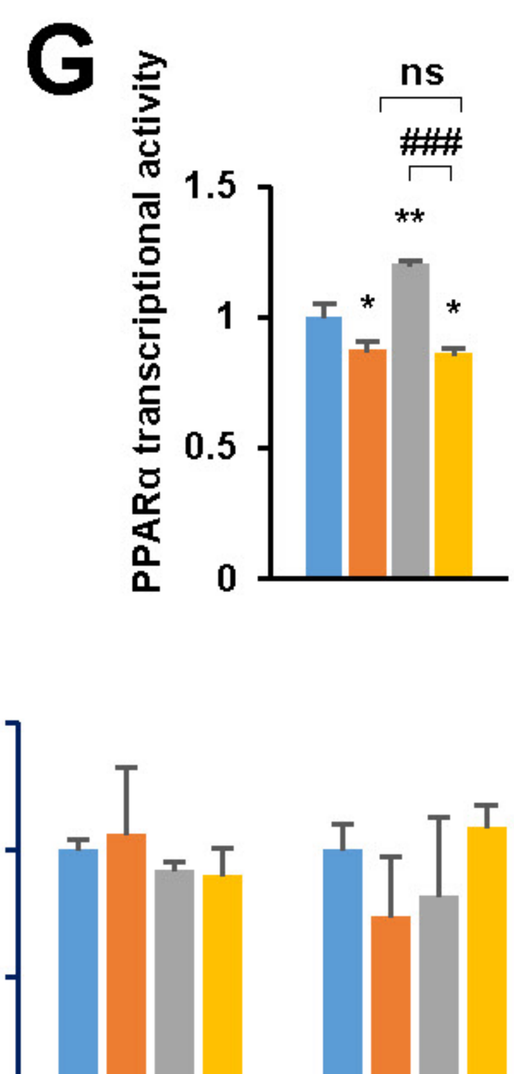

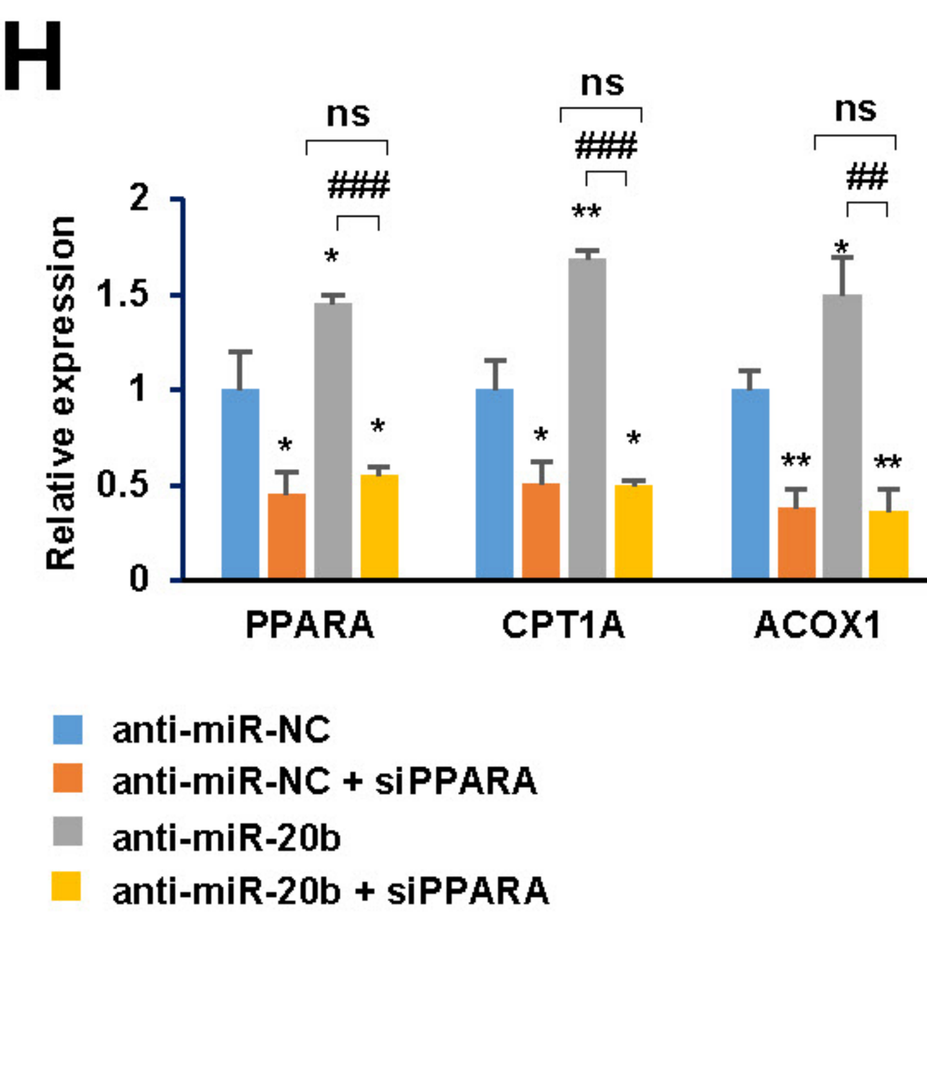

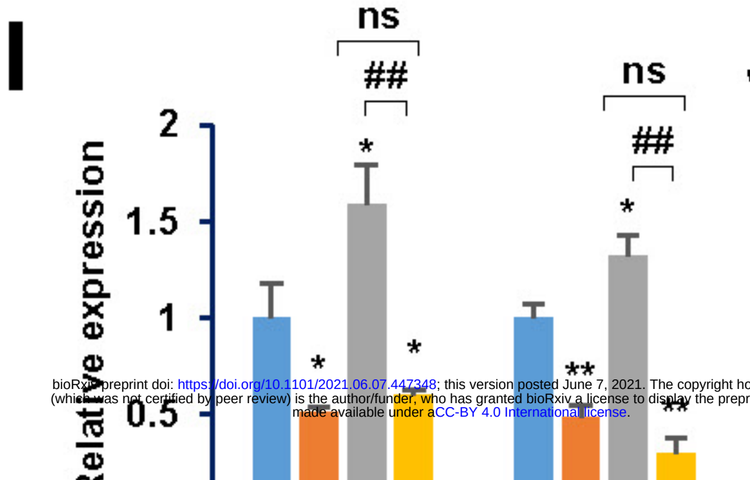

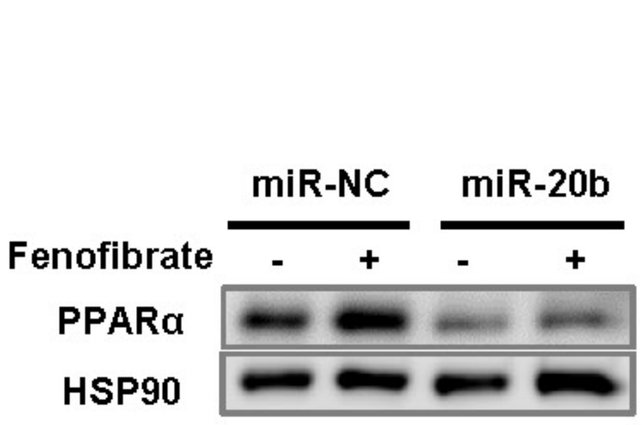

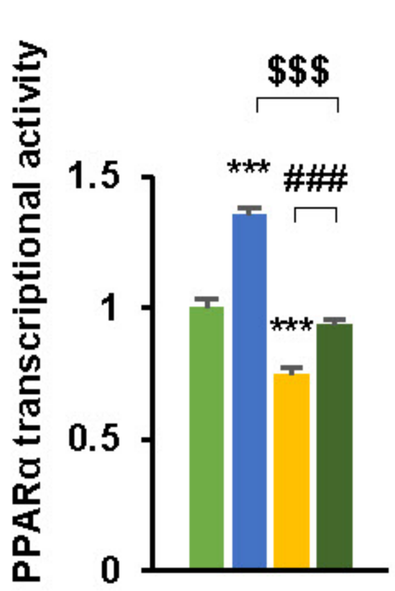

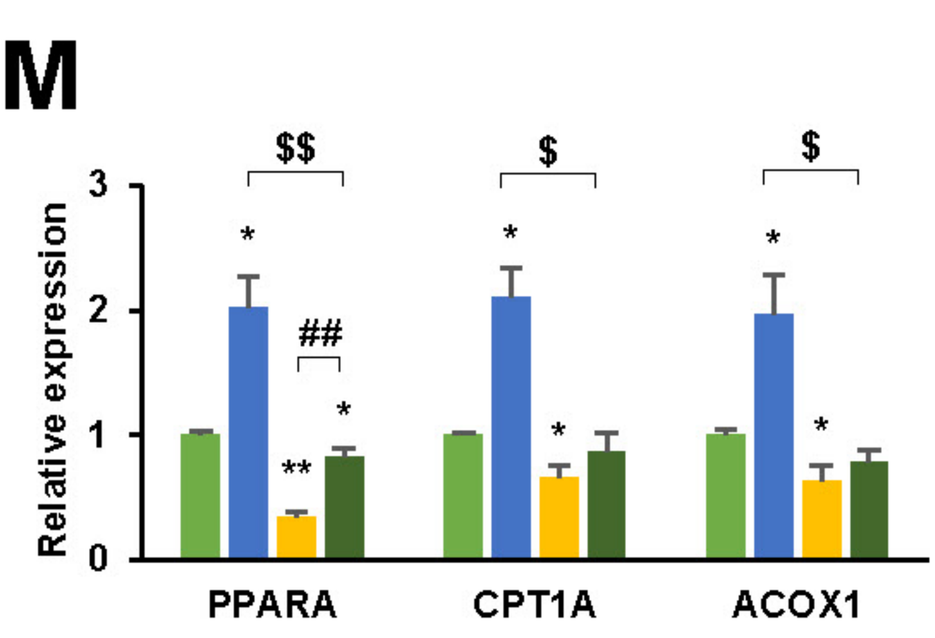

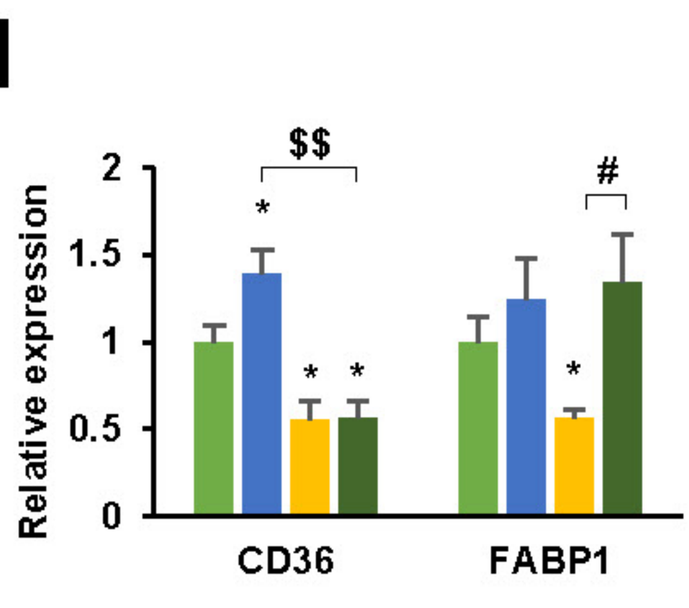

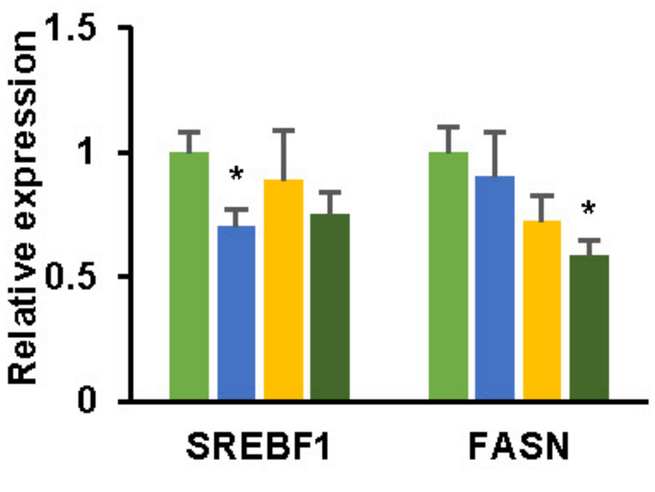

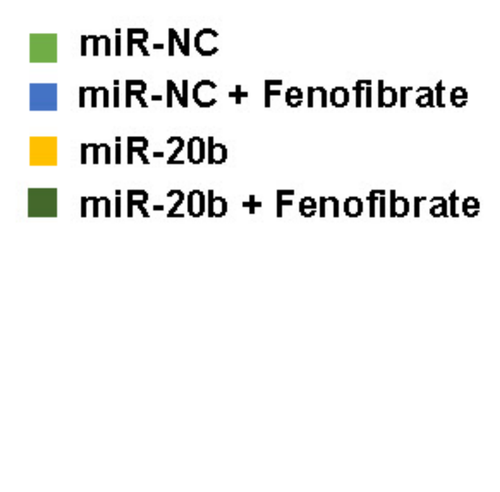

Figure 7. The effects of fenofibrate are limited in miR-20b-introduced mice.

Figure 8. miR-20b promotes liver inflammation and fibrosis in MCD-Fed Mice.

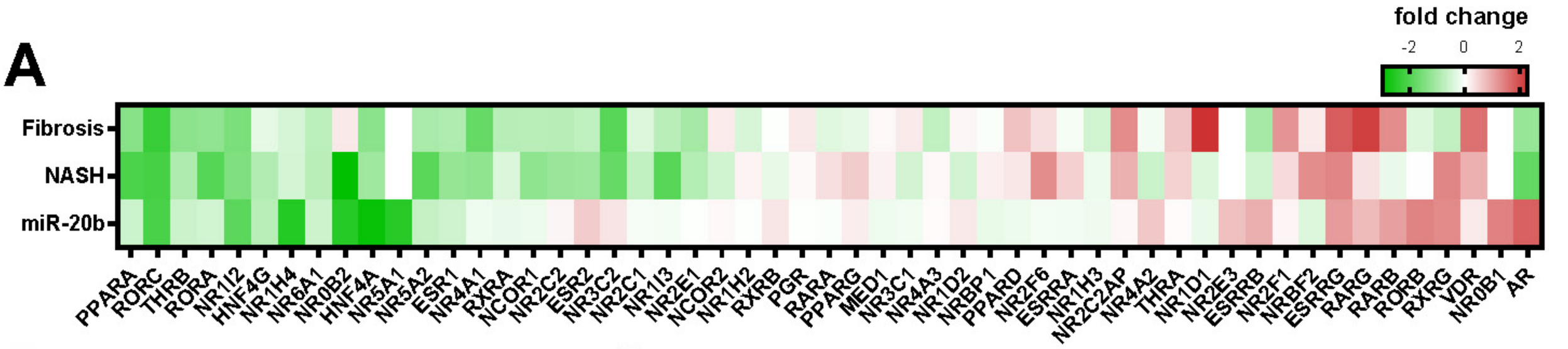

Figure 9. E2F1 is upregulated in both NAFLD patients and mice model